FUNDAMENTAL STUDIES OF INTERFACIAL FORCES ACTING ON THIN FILMS

A Dissertation
Submitted to the Graduate Faculty
of the
North Dakota State University
of Agriculture and Applied Science

By

Timothy John Twohig

In Partial Fulfillment of the Requirements
for the Degree of
DOCTOR OF PHILOSOPHY

Major Department:
Physics

October 2021

Fargo, North Dakota

NORTH DAKOTA STATE UNIVERSITY

Graduate School

Title

FUNDAMENTAL STUDIES OF INTERFACIAL FORCES ACTING ON THIN

FILMS

By

Timothy John Twohig

The supervisory committee certifies that this dissertation complies with North Dakota University's regulations and meets the accepted standards for the degree of

DOCTOR OF PHILOSOPHY

SUPERVISORY COMMITTEE:

Andrew B. Croll, Ph.D
Chair

Erik K. Hobbie, Ph.D

Yongki Choi, Ph.D

Chad Ulven, Ph.D

Approved:

11/4/2021
Date

Sylvio May, Ph.D
Department Chair

ABSTRACT

A thin film is a material that is many orders of magnitude thinner than it is long or wide. They are commonly found in many forms and have been adapted to a wide variety of uses. The art of origami uses thin films(sheets of paper) and precise folding to create complex, three-dimensional shapes out of flat, quasi two-dimensional sheets, and has emerged as a unique way to solve problems in engineering and science. As technology and devices are scaled to smaller sizes new understanding of origami methods are required to work at these small scales.

The interactions between thin films and liquids, substrates that films exist on, and other thin films is the focus of this dissertation. Capillary interactions are used to manipulate and fold thin films that are too thin to be actuated with hands or everyday tools. The relation between the macroscopic and the microscopic interactions at the point where the capillary liquid and the film meet is explored. We show how films can be manipulated by capillary drops and how exactly the force is applied to the film.

The adhesive interactions of the film were studied as a method of precisely placing folds for elastic film origami. The capillary peel of a film from a substrate drove folds to desired locations. Adhesion of a film to itself was used to lock these bends in place in lieu of the permanent creases commonly used in plastic systems such as paper. The combination of these two methods enabled the creation of stable, multi-step origami systems from reusable elastic films.

This research culminates in the discussion of fundamentally new origami-like designs that rely only on adhesion of the film to itself, which we call kuttsukugami (sticky+paper from Japanese). This new form allows for the creation of shapes that are nearly impossible to create with traditional origami methods such as loops, tubes, and cones. Advances made in capillary and adhesive thin film studies allow for kuttsukugami shapes to be scaled down to microscopic sizes for a huge array of applications including drug delivery, thin electronics, encapsulation, and more.

ACKNOWLEDGEMENTS

Graduate Teaching Assistant lines also provided both funding and the opportunity to explore the value of teaching during my time at NDSU.

DEDICATION

This thesis is dedicated to those who have been closest to me and always supported me throughout the years. Most importantly, my amazing wife Elizabeth Twohig. Her support of me perusing my passions has been nothing short of amazing. My cats Nova and Nellie who were always happy to see me and offer encouragement in exchange for pets. To my parents and siblings who have always believed in me and thought I could be a scientist. Finally, Dr. Catherine Twohig who was steadfast in pushing and encouraging me in my academic journey.

TABLE OF CONTENTS

LIST OF TABLES

LIST OF FIGURES

xiv

1. BACKGROUND

In every branch of science there are certain topics of inherent interest. These are subjects that even an outsider could point to and know that there must be some interesting phenomena happening that deserves study. Some of these topics of interest include the extremes of a particular behavior or trend, the beginning or ending of an event, exploration of the limits and behaviors of a completely new phenomena, phase changes, turnover points, or single events that cause an instability to develop in a structure leading to a catastrophic collapse. One thing that is certain is that the boundaries involved in any system will always require study, and will often contain some of the most interesting features. Whether the boundary separates two phases of matter, temperature thermoclines in a body of water, a planet's atmosphere from the surrounding space, a cell from its outside environment, or each individual layer of a stratified rock formation the boundary itself is worth closer study because of what it has to say about not only the two (or more) regions being separated, but also how transitions can occur between other, related, media. Of particular interest to the field of materials science are the boundary interactions that involve thin sheets, which are often approximated as entirely surface, and surface energy interactions, which act to minimize boundaries between phases of high energy in favor of lower energies.

1.1. Thin Films

Thin films can be ubiquitous in the natural world and are found in everywhere from a graphene sheet that is a single layer of atoms thick,[83, 74] to fabric,[72, 75] rolled out pasta dough,[121, 4] sheets of paper,[14, 104] sea ice sheets,[123, 124, 125] and tectonic plates.[99, 43, 62] These examples can be seen buckling and folding like newspaper if the right stresses are applied. This means that a basic understanding of how thin sheets behave can apply to a multitude of length scales from the sub-nanometer to many kilometers. Certain properties, like the weight of the sheet, may be of importance at the biggest scales and will gradually affect the system less and less. Whereas forces that would be insignificant at the kilo-scale, such as adhesion and surface energy dominate thinner systems. Many of these unique attributes seem to appear at smaller (thinner) scales because the surface properties of these films (adhesion, surface tension) are unchanged as the thickness is decreased, but the bulk properties (weight, bendability) decrease proportionally to the

1
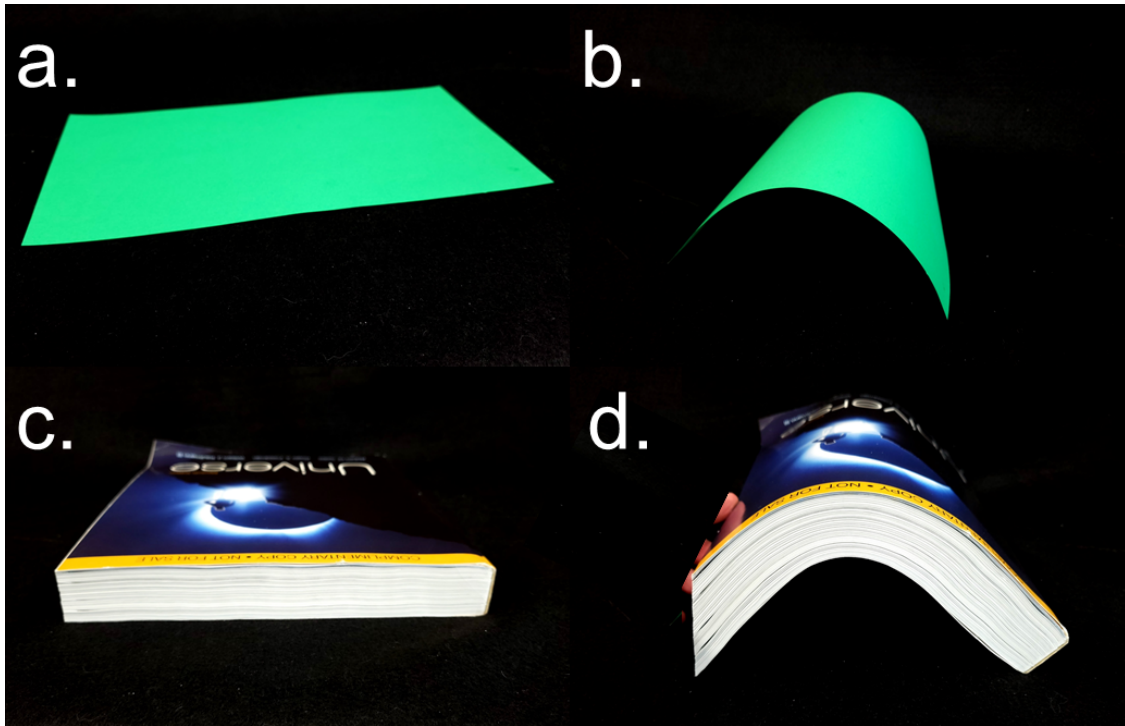
Figure 1.1. a.) A sheet of paper can be easily bent. b.) Bent sheet of paper is not irreversibly deformed, and the weight of an individual sheet has little effect on the overall shape. c.) A book acts more as a bulk made of many sheets of paper joined together. d.) A bent book illustrates much of the sheer between individual sheets as the bulk is bent. In a continuous material, sliding between layers cannot occur and the stress is built into the bent material. The weight of a book is not insignificant and must be considered when determining the overall shape of a bent book. The book will not remain freestanding in the bent configuration due to its large weight.

decrease in thickness. Since sheets (Fig. 1.1a,b) have a much greater proportion of surface area to volume compared to even somewhat thicker objects (Fig. 1.1c,d), these surface affects play a much larger role in governing the interactions of the object. This can be when seen comparing a thick softcover book to a single one of its pages, like in Fig. 1.1. The boundary between the macroscopic and microscopic interactions of sheets represents an important area of study in a world where technology is always pushed to be smaller, lighter, and more robust. As our traditional techniques for creation and manipulation of microscopic technology become more difficult at smaller scales, we must embrace the incorporation of overlooked interactions into manufacturing processes by using these properties of thin sheets to our advantage instead of seeking to avoid all of the possibilities that an understanding of thin films could unlock.[93, 94, 9, 42, 96]

A thin material may act in a way that does not match for how a bulk sample of that material may behave. For example, consider a material which has a density that is greater than water, so
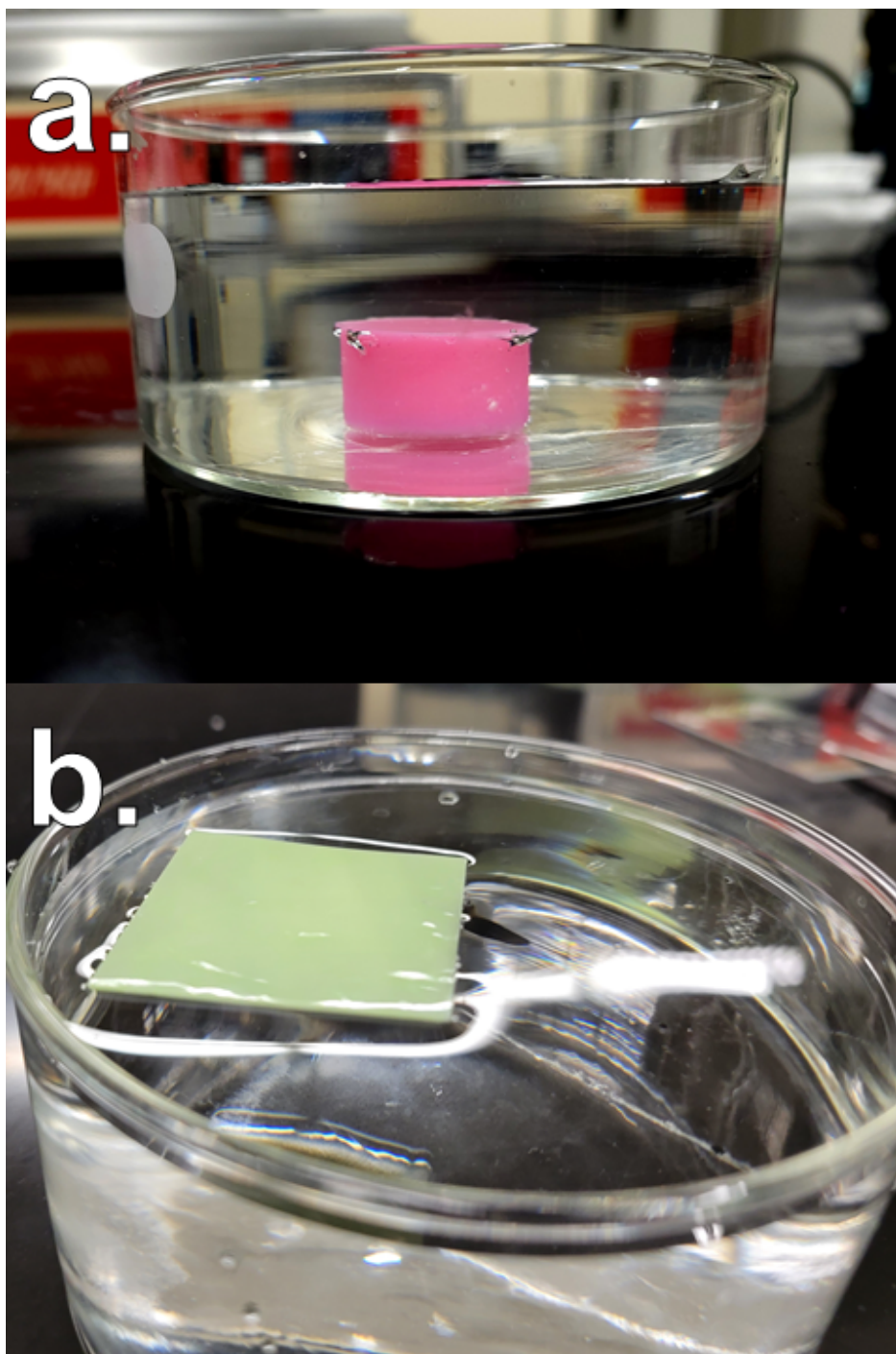
Figure 1.2. a.) A slug of denser than water polyvinylsiloxane sinks in water. b.)A denser-than-water polyvinylsiloxane film floating on water due to the surface energy of the water being in a lower energy state with the film at the water's surface.

when a solid sphere of that material is added to water it will sink. However, if this same sphere

is flattened into a thin sheet the surface forces (which remain unchanged) are now applied over a
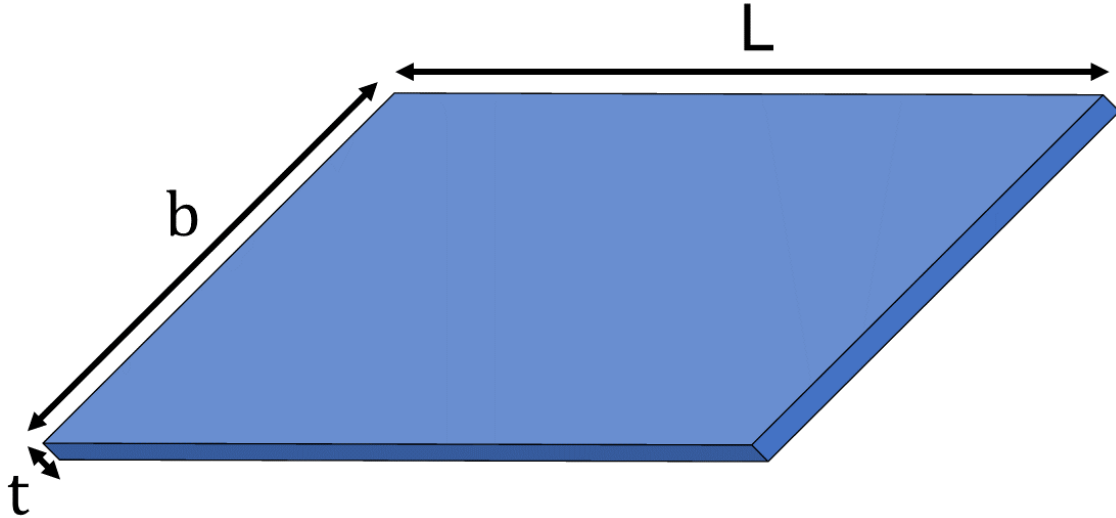
Figure 1.3. Thin sheet with dimensions of length (L), width (b), and thickness (t). The thickness of the film is orders of magnitude smaller than the length or width.

much larger area. This film can then be placed onto the surface of a water bath and it will float due to the upward force of the surface tension as seen in Fig. 1.2b. The importance of the bulk property of weight or density is minimized while the affect of the surface property of surface tension is maximized.

An understanding of the behavior of thin films can first be drawn from a familiar source; a sheet of paper. By definition, paper is a thin film: it is orders of magnitude larger in two if its dimensions (length and width) than it is in its third dimension (thickness).[128] This is covered generally in a schematic in Fig. 1.3 giving variables and their layouts for a rectangular sheet. An example, is a sheet of computer printer paper with a thickness of around 0.1 mm, a length of 279 mm and a width of 216 mm, making it at least 2,000 times wider than it is thick.

Paper is a relatively inelastic material, meaning that it does not easily stretch and then relax to its original length. Instead, paper will usually rip if a large strain is applied. A strain is a comparison of a material's dimensions in its relaxed state and in its compressed or stretched state and can be quantified with

$$\epsilon = \frac{\ell - L}{L} = \frac{\Delta\ell}{L} \tag{1.1}$$

where ϵ is the calculated strain, L is the equilibrium length of the material in a given dimension, ℓ is the dimensional length after the compression or stretching, and $\Delta\ell$ is the difference in these

Table 1.1. Failure strain of some common materials.

Material	Failure Strain
10:1 PDMS[25]	1.4
Polystyrene[88]	0.01-0.02
Aluminium[126]	0.12-.017
Paper[130]	0.01-0.06

two lengths. This means that a compression will yield a negative strain and a stretch will lead to a positive strain. Many materials have an elongation failure strain at which point the material will break. Failure strain values of some common materials are presented in Table 1.1.

These numbers are often citing the tensile, or stretching, strain and are often similar whether the tensile strain tests are performed on a sheet or on a larger bulk sample in which all dimensions are of a similar magnitude.

It can be useful to think of an elastic material as a spring that will resist a compression or elongation proportionally to the distance of this change. Materials that behave in this linear regime can be referred to as Hookean, referring to Hooke's Law where the force applied to a perfect spring is directly proportional to the stretching or compression of that spring (x) times the spring constant (k): $F = kx$. The force (F) which creates a deformation in a three-dimensional material divided by the cross sectional area that is deformed (A) is known as the stress (σ).

$$\sigma = \frac{F}{A} \tag{1.2}$$

The area referenced depends on the mode of deformation. Consider again the solid shown in Fig. 1.3. Here the area might be $A = bt$, shown in Fig. 1.3 for a stretch or compression along the L dimension. Putting Eqns. 1.2 and 1.1 together gives a measure of the elastic strength of a material, or rather how hard it is to deform that material. This measure is called the Young's modulus (E), often referred to as just "modulus" and is one of the most commonly cited characteristics of a material. This is relation was developed by Euler and is stated in Eqn. 1.3.[38]

$$E = \frac{\sigma}{\epsilon} \tag{1.3}$$

Knowledge of what creates a certain modulus can be used to tune materials for specific purposes.

When a material is stretched or compressed, its volume will also adapt to account for the change in length. Similar to when a piece of gum is stretched and the middle becomes thin and stringy. The Poisson ratio ν is a measure of how stretching or compressing a material in one dimension affects the cross-sectional area of the other dimensions.[101]

$$\nu = -\frac{d\epsilon_i}{d\epsilon_j} \tag{1.4}$$

where i is an orthogonal axis of j, and j is the axis the strain is applied to. Intuitively, one would imagine that stretching a material would cause the cross-sectional area of the other dimensions to decrease, like what is seen in gum, and this is normally the case. However, some materials can expand when stretched and reduce their cross-sectional size when compressed. These materials have a negative Poisson ratio, at least in one dimension. The Poisson ratios of several of the materials commonly used in the research presented in this paper are presented in Table 1.2.

This brings the discussion to applications of these variables used in experimental tests. The force required to stretch a material along its length is often used in many experiments to determine the modulus of the material in a tensile strain test. This force can be derived from the Hooke's Law. An elastic material's modulus and cross sectional area are related to the spring constant, but the total length of the elastic material (spring) needs to be taken into account as well. This leads to an analogous spring constant of $k = \frac{EA}{L}$. The area is further broken down into the thickness and width of the film ($A = bt$). The deformation length ($\Delta\ell$) is the same as it would be for a spring. Combining these values gives a force required to stretch (or compress) a material, presented

Table 1.2. Poisson ratios of materials used in this work and other interesting materials.

Material	ν
PDMS[126]	0.49
Polystyrene	0.34[85]
Polycarbonate	0.42[85]
Polyvinylsiloxane[126]	0.49
Glass[85]	0.3
Printer Paper[104]	0.33
Sea Ice[125]	0.33-0.42

as $F_{stretch}$. This can be found by rearranging the stress equation (Eqn. 1.2) to give

$$F_{stretch} = A\sigma \tag{1.5}$$

then rearranging the modulus equation (Eqn. 1.3) to make a substitution for σ

$$F_{stretch} = AE\epsilon \tag{1.6}$$

substituting the strain equation (Eqn. 1.1) for ϵ and $A = bt$ for the area gives the force to stretch a rectangular sheet of elastic material in mostly directly measurable terms.

$$F_{stretch} = bt\frac{E\Delta\ell}{L} \tag{1.7}$$

A material that is stretched or compressed will store elastic potential energy in the same manner that a spring stores potential energy. The total elastic energy stored in a material can be found by integrating the stretching force equation over the length of deformation.

$$U_{elastic} = \int_0^\ell \frac{bE\Delta\ell t}{L} \; d(\Delta\ell) = \frac{1}{2}\frac{btE(\Delta\ell)^2}{L} = \frac{1}{2}\frac{EA(\Delta\ell)^2}{L} \tag{1.8}$$

1.1.1. Bending

Compressing a sheet to the point where it bends instead of absorbing the compression is where the major divergence from bulk properties begins to become apparent. As with a piece of paper resting on a table, pushing the two opposite ends toward one another will not cause the paper to get thicker. Instead, the paper will easily arc away from the table into the vertical (z) coordinate. This is known as bending. Bending will continue until the two ends of the sheet contact each other. A sheet of printer paper is likely to form a continuous loop at this point, but a much longer sheet may form wrinkles with a regular wavelength as the ends are pushed towards one another. If the compression continues, these wrinkles will begin to merge and localize into larger deformations, eventually creating bends that cannot support themselves and will collapse. Energy is applied to the sheet in the form of moving the two ends closer together. This energy is stored in the bend the sheet.

7

In order for a bend to be created, like in Fig. 1.4a, a flat sheet needs to be deformed into an arc. The position along the length of the arc (s) and the change in the slope of the arc (ds'') are the two important mathematical features that describe the arc. If this ark is a smooth bend it will have a constant curvature (κ) that will equal the change in the slope of the arc ($\kappa = ds''$). Sharp bends have a high curvature due to rapidly changing slope of the arc, and gentle bends have a lower curvature with relatively small changes in the arc's slope. The curvature of a bend is related to the radius of curvature (R) of the bend by $\kappa = \frac{1}{R}$. A circular bend, like the bend pictured in Fig. 1.4 has a constant radius of curvature that is equal to the radius of the circle traced through the center of the bend in Fig. 1.4b. The circular bend is an approximation that is often sufficient for most applications. Approximating a bend as circular is often the only way to analytically solve an expression.

Fig. 1.4c gives a good representation as to where the energy in a bent sheet actually goes. The outer radius (R_{out}) of the bend is larger than the radius of curvature, and the inner radius (R_{in}) is smaller. So the energy goes towards stretching the material on the outer part of the bend and also to compressing the material on the inner part of the bend. The middle line of the bend is assumed to neither stretch nor compress and is known as the neutral axis. Measurements are taken using the neutral axis, including the film's position (s). The distance away from the neutral axis of the film's surface is defined as $\pm\frac{t}{2}$, where $t = 0$ is the neutral axis in Fig. 1.4b. The strain of any radial segment of a sheet bent along its long axis (in the direction of $\Delta\ell$) is given by:

$$\epsilon_{bend} = \frac{t}{2R} \tag{1.9}$$

where the interior portion of the bend represents negative t-values. Multiplying Eqn. 1.9 by the material's modulus and taking into account the Poisson ratio gives the bending stress:

$$\sigma_{bend} = \frac{tE}{2R(1 - \nu^2)} \tag{1.10}$$
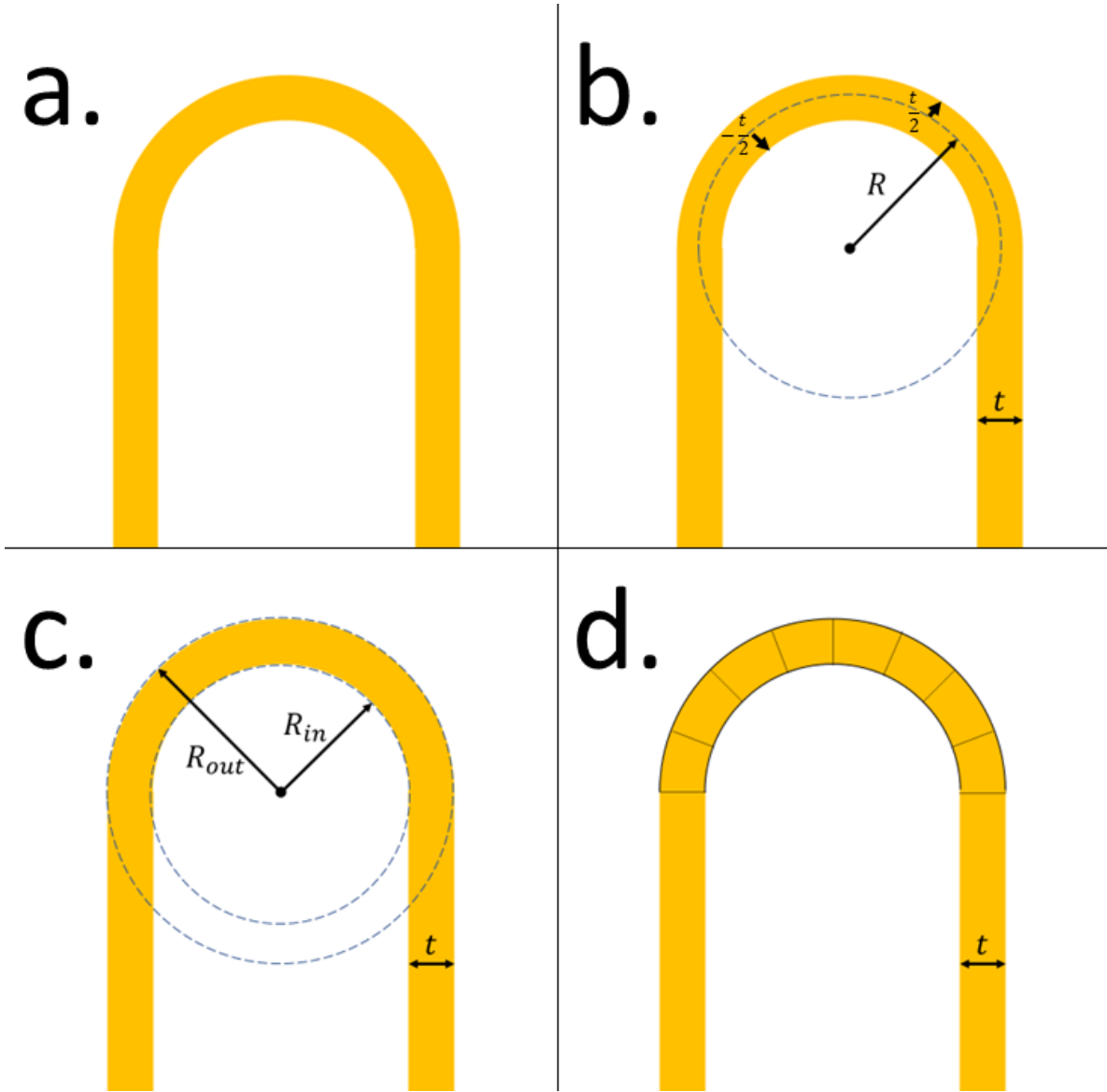
Figure 1.4. a.) Circular bend of a thin film. b.) Radius of curvature is traced over the center line of the bend. c.) The radius of the inner and outer edges of the bend are traced. The inner bend is compressed by the same amount as the outer bend is stretched. d.) Each segment of bent film must balance the moment of the adjacent segment, canceling out any angular moment between sections.

The bending moment (M) required to deform a segment of the film into the circular bend, demonstrated by the individual sections in Fig. 1.4d is given in Eqn. 1.11.

$$M = \frac{Eb}{R(1-\nu^2)} \frac{1}{2} \int_{\frac{-t}{2}}^{\frac{t}{2}} (z)^2 \, dz = \frac{Eb}{12R(1-\nu^2)} t^3 \tag{1.11}$$

For a rectangular beam that is bent in the L-dimension, the moment of inertia (I) is defined as $I = \frac{t^3}{12(1-\nu^2)}$, so

$$M = \frac{EI}{R}b \tag{1.12}$$

gives the bending moment for a singly, tiny segment of the bend. Each segment in a bend with a single curvature will have this same moment.

The beam equation was developed by Euler and allows for the bending energy of a bent beam (or one-dimensional sheet) to be found by integrating Eqn. 1.13 over the length of the curved bend.[38, 127]

$$U_{bend} = \int_0^L \frac{1}{2}EI(ds'')^2 \, ds \tag{1.13}$$

In the case of Fig. 1.4 the bend is circular over half the circle, so $L = \pi R$ and $ds'' = \frac{1}{R}$.

$$U_{bend} = \frac{1}{2}EI \int_0^{\pi R} \frac{1}{R^2} \, ds = \frac{1}{2}\frac{\pi EI}{R} \tag{1.14}$$

The modulus and moment of inertial are often simplified into a term known as the bending modulus (B), where:

$$B = \frac{Et^3}{12(1-\nu^2)}. \tag{1.15}$$

Simplifying and multiplying by the width of the sheet (b) gives the bending energy of the half-circle bend as:

$$U_{bend} = \frac{1}{2}\frac{B}{R}b. \tag{1.16}$$

Comparing Eqn. 1.8 and Eqn. 1.16 allows one to clearly see why thin sheets are easily bent when a compressive force is applied instead of a compaction process. For example, if a sheet of paper is 0.28 m in length, 0.00005 m thick, and 0.216 m wide, with a modulus of $E_{paper} = 6.9 \times 10^9$ Pa; the energy cost to compress (or stretch) that sheet by 0.102 m is 1,384 Joules from Eqn. 1.8.[14] Meanwhile, the cost to bend the same sheet by compressing the ends toward one another the same amount is given by Eqn. 1.16 as 0.0001 Joules.[104] This is a monumental difference and explains why paper sheets almost always will bend when subjected to a strain, instead of compressing.
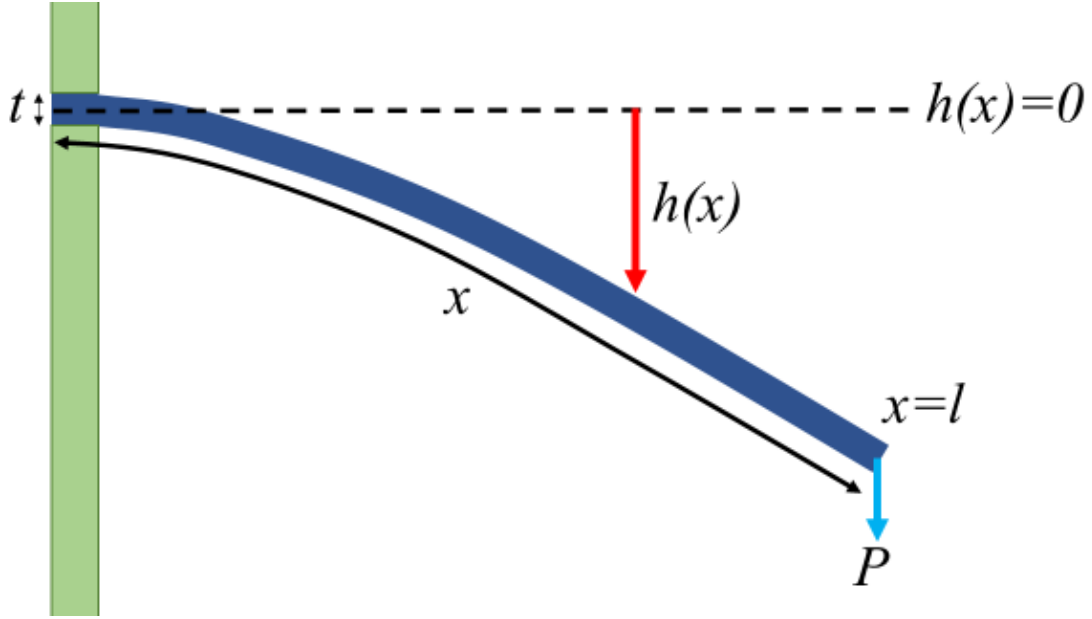
Figure 1.5. Schematic of an unsupported beam. The left end of the beam is attached to a wall with zero height and zero slope. The load is pointing downwards, (gravity) and causes deflection in the downwards direction.

1.1.2. Cantilever Beam

A less simplified example of bending that does not follow a circular bending approximation is the cantilever beam, illustrated in Fig. 1.5. This massless beam of width b is secured to the wall at its left end, corresponding to $x = 0$ with a slope of zero and a height of zero at the wall ($h(0) = 0$). The right end of this beam ($x = \ell$) is loaded with a downward force (P), causing the beam to deflect downwards. The vertical displacement of the beam ($h(x)$) can be calculated from the plate equation (Eqn. 1.17).[128, 73]

$$EIh''''(x) = bP \tag{1.17}$$

Where E is the Young's modulus of the plate and $I = \frac{bt^3}{12(1-\nu^2)}$ is the second moment of inertia of a plate with thickness t and ν is the plate's Poisson Ratio. A delta function, $\delta(x - \ell)$, is added to the end of the beam where the load is applied, and the width of the beam is canceled to give:

$$h''''(x) = \frac{P}{EI'}\delta(x - \ell) \tag{1.18}$$

11

where I' is now the second moment of inertia per width. The boundary conditions are:

$$h'''(\ell) = \frac{P}{EI'} \tag{1.19}$$

$$h''(\ell) = 0 \tag{1.20}$$

$$h'(0) = 0 \tag{1.21}$$

$$h(0) = 0. \tag{1.22}$$

Integrating the plate equation (Eqn. 1.18) and including the boundary conditions give the following solutions:

$$h'''(x) = \frac{P}{EI'} \tag{1.23}$$

$$h''(x) = \frac{P}{EI'}(x - \ell) \tag{1.24}$$

$$h'(x) = \frac{P}{EI'}\left(\frac{x^2}{2} - \ell x\right) \tag{1.25}$$

$$h'(x) = \frac{P}{EI'}\left(\frac{x^3}{6} - \frac{\ell x^2}{2}\right). \tag{1.26}$$

These equations allow the height, slope, and curvature to be found at any point along the beam between $x = 0$ and $x = \ell$. This treatment is often used in this work when calculating the affect of a surface tension acting on a thin film. The tension acts as a point load drawing the film along the surface of the drop. In this approximation, the weight of the drop and interactions with the substrate are neglected.

1.2. Capillary Interactions

Capillary forces arise due to the inherent cost of an interface between a fluid and a different material. This cost leads to a tension at the edge of the fluid that works to cover the surface of the fluid in a material with a lower interfacial cost. The force acting to accomplish this is known as surface tension (γ). However, other materials are also working towards the same goal and have their own surface tensions. In a system where one or more fluids come into contact, the surface tension values and the states of any other materials present will dictate what equilibrium is reached. If a material's surface tension is known, then the capillary energy an area (A) of that material's surface
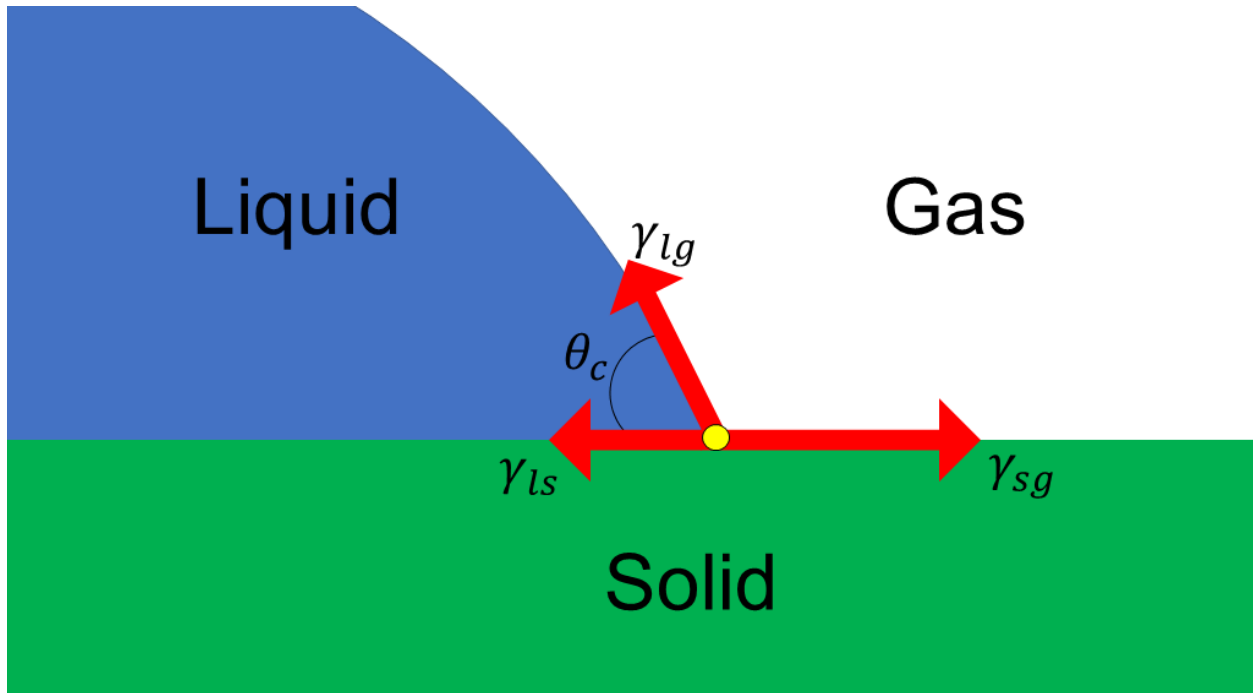
Figure 1.6. A liquid drop on a solid substrate follows the Young-Dupré equation since the upward capillary force of the drop is balanced by the normal force of the solid substrate.

can be calculated.

$$U_{cap} = \gamma A \tag{1.27}$$

A system consisting of multiple materials will always seek the lowest energy configuration. If some or all of the materials are fluids that can move and flow then the system will usually reach this minimum overall energy.

1.2.1. Drop on Solid Substrate

The simplest capillary equilibrium to explain is that of a liquid drop placed onto a solid substrate in an air environment. When represented two-dimensionally, as in Fig. 1.6, the point where these three phases meet is known as the triple point. Each interface has a surface tension that is working to move the triple point along its surface in the way that covers the most area with the lowest energy interface. This means that in Fig. 1.6 the tension from the liquid-gas interface (γ_{lg}) is pulling upwards along the drop, the liquid-solid interface (γ_{ls}) is pulling to the left, and the solid-gas interface (γ_{sg}) is pulling right. Since the substrate that the liquid drop is sitting on is a solid, the vertical forces are all balanced by the normal force of the substrate. So only the horizontal components of each tension need to reach an equilibrium, which simplifies the situation. To find

the horizontal component of the liquid-gas tension, the angle between the solid's surface and the edge of the drop at the triple point must be found. This angle is known as the contact angle (θ) and should be measured from the solid to the surface of the water, within the drop. Assuming that this angle is less than 90° leads to the conclusion that the horizontal components of (γ_{ls}) and (γ_{lg}) are both pointing in the same direction, so (γ_{sg}) must be pointing in the opposite direction. If this assumption were proved wrong, it would not affect the results since the horizontal component of (γ_{lg}) is $\gamma_{lg-horiz} = \cos\theta_c$. Since an equilibrium must be reached, these values can be arranged in the following manner.

$$0 = \gamma_{lg}\cos\theta_c + \gamma_{ls} - \gamma_{sg} \tag{1.28}$$

Rearranging these terms gives the Young-Dupré equation for describing a drop resting on a solid substrate in an air environment.[137]

$$\gamma_{lg}\cos\theta_c = \gamma_{sg} - \gamma_{sl} \tag{1.29}$$

This equation can be quite a powerful tool for finding unknown surface tension values. As long as the contact angle and some of the individual surface tensions can be found, then unknown values can be determined using Eqn. 1.29.

1.2.2. Drop on Liquid Substrate

When a drop is not resting on a solid substrate, but is instead resting on a fluid substrate, surrounded by a third fluid, as shown in Fig. 1.7, the assumption that vertical forces can be neglected is no longer true. This greatly complicates the equilibrium of the fluids around the triple point, since each fluid now has a force vector that can move both vertically and horizontally. Since an equilibrium must be reached for this system, the vertical components and the horizontal components must again add to equal zero. This also means that addition of the vectors themselves will add to zero. The shape formed by graphically representing the addition of the vectors is known as the Neumann Triangle (Fig. 1.8), and should always form a closed triangle for a system in equilibrium.

The system can be solved more easily if a reference horizontal can be found. For example, if the bath that the drop is floating on is flattened by gravity, its surface can be assumed as horizontal. Then 90° from the horizontal is the vertical. The angles between the each vector and these planes
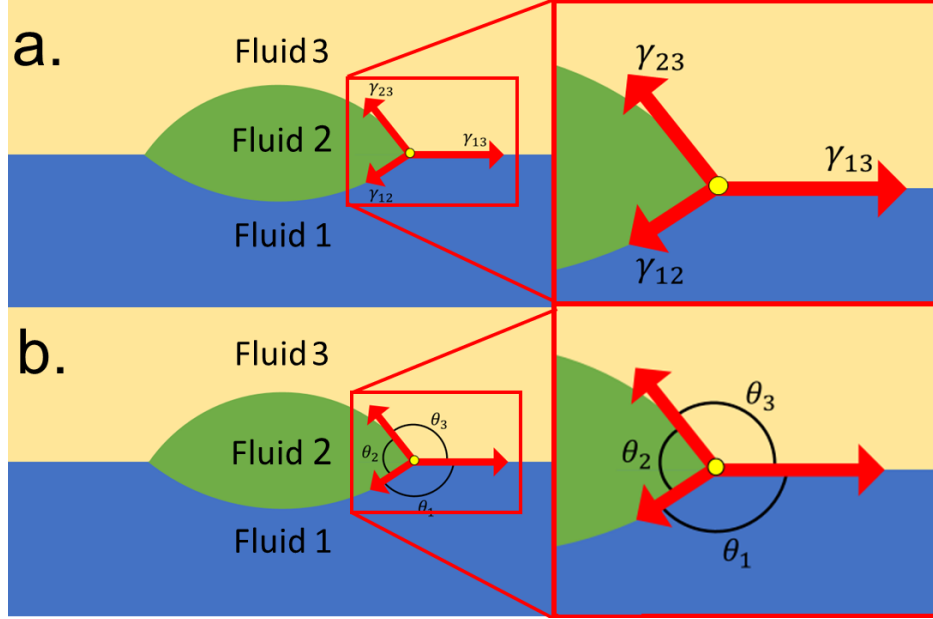
Figure 1.7. Changing the solid substrate to a fluid allows the triple point to wander upwards and downwards. The Neumann triangle relation includes this new free dimension. a.) The force of each surface tension is represented by the length of each vector. The vector's direction is the direction of the force at the triple point. b.) The angles between each vector are used to find the equilibrium of the system.

can then be found and used in a similar manner to the Young-Dupré balance to calculate the equilibrium. If only the angles between each vector are known (as shown in Fig. 1.7a and b), then the following system of equations, known as the Neumann Construction, can be used to find the equilibrium state.[119]

$$0 = \gamma_{23} + \gamma_{12} \cos \theta_2 + \gamma_{13} \cos \theta_3 \tag{1.30}$$

$$0 = \gamma_{23} \cos \theta_2 + \gamma_{12} + \gamma_{13} \cos \theta_1 \tag{1.31}$$

$$0 = \gamma_{23} \cos \theta_3 + \gamma_{12} \cos \theta_1 + \gamma_{13} \tag{1.32}$$

In a similar way to how the Young-Dupré balance could be used to find missing surface tensions, the Neumann Construction can be used to solve for unknown values. Since there are both the vertical and horizontal balance to be found, these equations can possibly work better in systems with less known variables than the Young-Dupré equation.

15
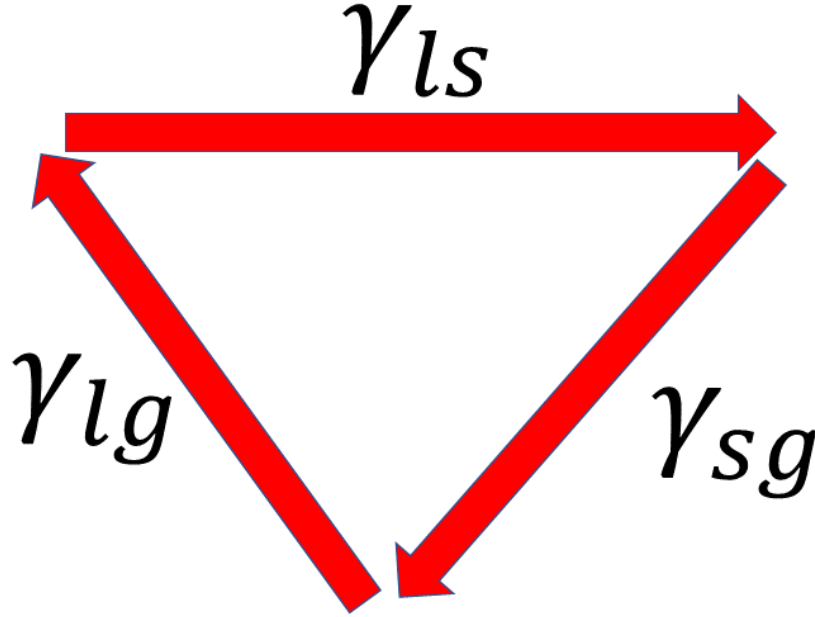
Figure 1.8. Neumann Triangle formed by the addition of the surface tension vectors of a drop floating in a liquid bath system.

1.3. Capillary Origami

Capillary origami is a process by which thin films are moved, bent, and manipulated through the use of high surface energy liquids. These liquids act to minimise their surface energy by covering as much of their surface as possible with the thin film. Usually, high surface energy liquids are used such as water, glycerol, or liquid metals. Liquid metals like mercury and gallium have very high surface energies (about 435.5 and 735 $\frac{mN}{m}$, respectively near room temperature), but are difficult to use safely.[115, 76] Metal solders can be used to manipulate films, but these films need to be resistant to the temperatures at which these metals become liquid.[45, 66, 22] The thin films used are often made of metal films and foils, or silicon. When the solder cools, it solidifies and freezes the films in a particular state. The solid solder drop holds the origami structures rigidly in place indefinitely. Liquid metals can be useful for actuating and holding thin systems, but often come with major drawbacks such as the toxic nature of mercury, or the relatively high temperature that solders need to be at in order to exist in a liquid state.

Water emerged as an ideal capillary fluid for capillary origami systems after a paper was published by Py *et al.* in 2007.[93] This paper showed that when water was placed onto thin elastomeric films, these films would readily bend around the fluid. If the film was cut into specific

shapes before the drop was added, three-dimensional structures could be planned and constructed when the water was added. For example, a film cut into a cross shape would fold roughly into a cube. Pyramids, spheres, and simple envelopes could also be constructed with this method. Structures created with capillary origami remain stable as long as the capillary drop is present. As the drop evaporates, there is no longer tension pulling the film to cover the surface of the liquid. Eventually, the remaining drop is too small to continue to hold the elastic film in a constructed state. The film is released back to its flat state. The water drop continues to dry, and if the water is pure, no residue or damage from the from the drop remains. The ability of water to completely disappear from this process while having quite a high surface tension (72 mN/m) has led to the research of capillary origami for the processes of drug encapsulation, self-assembly of nanostructures, the patterned deformation of floating films, among many other topics.[46, 103, 129, 57, 133, 22, 40, 5, 96, 42]

While studying the effects of water on thin films, many of the advantages of the details that were studied in the works of Py *et al.*[93, 94] started to become hindrances to the overall usefulness of capillary origami. First, the use of water as the capillary fluid is ideal because of the high surface tension and the ability to completely evaporate, leaving a clean surface. However, the property of water to readily evaporate makes detailed study of its interactions difficult. Evaporation causes the capillary drop to change size relatively quickly compared to the equilibration times of these interactions. The changing drop size leads to a moving contact line between the drop and film which greatly complicates any mathematical models that are created to help explain this interaction. To eliminate evaporation, glycerol (often called glycerin) is often used instead of water. Glycerol also has a quite high surface tension (64 mN/m) and is also unlikely to significantly interact with the hydrophobic polymers that are commonly used to create films. Therefore, glycerol can be used in the study of capillary origami, providing a stable fluid that will not complicate the mathematics of the situation. The insights gained from studies using glycerol can be directly applied to applications using water as the capillary fluid. In this dissertation, this useful substitution is used in many situations that require an equilibrium situation to be properly explained.

The interaction of a thin film with its substrate was considered a disadvantage in the early capillary origami experiments.[93, 94, 42] Great care was taken to minimize any bond between the film and its substrate, since this would require additional force from the capillary drop to lift the film. Often a superhydrophibic coating was used in these studies, which can be difficult to procure

and work with. Other surfaces that can be used have little interaction with the film, such as textured paper, but these substrates were not ideal surfaces on which to conduct research.

1.4. Surface Energy

Surface energy is a property of any material that shares an interface with a differing material. There is an energy cost that arises at the edge of the material because atoms there have different interactions than do those in the bulk of the material. Consider a simple lattice model in which each atom interacts with its six neighbors, consisting of two materials (a and b). The energy of two neighboring atoms of the same material is either ε_{aa} or ε_{bb}, and the energy cost of two different neighbors is ε_{ab}. If the sum $\varepsilon_{aa} + \varepsilon_{bb}$ is less than ε_{ab} then the free energy of the system is minimized when the two materials are separated with the smallest possible interface between them. This leads to the surface energy of the interface, or the energy required to maintain a surface area where two materials meet separating the pure bulk portions of each material.

When two surfaces are separated, the work required to accomplish the separation is related to the energy release rate (G) of the crack between the two surfaces. When forces become large enough, the energy release rate reaches a critical value (G_c) at which point the crack begins to grow and the materials separate. The release rate is affected by how quickly the surfaces are separated and if there is any loss during this process due to viscoelastic or fluid movement; where the surfaces are deformed by the process of separation of the two materials. If these materials are separated at an infinitely slow rate and there are no losses from other sources, then the critical energy release rate equates to the work of adhesion of the two surfaces, $G_c = W_{12}$. The interface created by the joining of two materials (γ_{12}) is destroyed when the materials are separated. This also creates two new surfaces (with interfaces between the material and air or some other fluid, usually) which have their own surface energies and tensions (γ_1 and γ_2). The work of adhesion is related to the surface tensions of the materials by the following equation:

$$-W_{12}\delta A = -(\gamma_1 + \gamma_2 - \gamma_{12})\delta A \tag{1.33}$$

where γ_1 and γ_2 are the surface tensions of the materials and γ_{12} is the surface tension of the interface of area A that is destroyed by separating the materials. If a finite amount of work is required to separate the surfaces, then $\gamma_1 + \gamma_2 \neq \gamma_{12}$. Eqn. 1.33 can be a useful tool for measuring

the interfacial energy of a system when γ_1 and γ_2 are known and the work put into the system can be measured.

1.4.1. Elastocapillary Length

One of the recurring themes of these studies is an important length scale that relates the capillary forces to the forces required to bend a film. As presented by Py *et al.* in their 2007 work[93], a length known as the elastocapillary length (L_{ec}) represents a balance between the surface forces of a fluid acting to wrap the surface with film and the bending forces of the film acting to remain in a flat state. The energy for an area of fluid-air interface is $\gamma_{\ell a} A$, where $\gamma_{\ell a}$ is the surface tension of the fluid and A is the area of the interface. The bending energy of a plate is given as $\frac{1}{2} B \kappa^2 A$ where $B = \frac{Et^3}{12(1-\nu^2)}$ and the area is the width of the plate (b) times the length of the plate (L_{ec}). Balancing the two energies leads to the following definition of elastocapillary length:

$$\gamma A = \frac{1}{2} B \kappa^2 A \tag{1.34}$$

$$\frac{1}{\kappa^2} = \frac{1}{2} \frac{B}{\gamma} \tag{1.35}$$

substituting $\kappa = \frac{1}{L_{ec}}$

$$L_{ec}^2 = \frac{B}{\gamma} \tag{1.36}$$

$$L_{ec} = \sqrt{\frac{B}{\gamma}}. \tag{1.37}$$

The elastocapillary length (Eqn. 1.37) is a rough guide for the length of film that a capillary drop can bend and fold. In the extreme, this length represents the radius of a drop that would be completely encapsulated by a thin film with a modulus E and a thickness t. The elastocapillary length can be used as a general guide for which bends and folds are possible with a given liquid. It reveals several "knobs" that can be turned to make certain configurations possible with capillary origami. For instance, a sheet may be folded in half by a water drop effectively doubling the thickness of the sheet. A doubly-thick film results in an elastocapillary length that is $(2.8 = 2^{\frac{3}{2}})$ times the original length, meaning that the surface tension of a drop must be 2.8 times larger to fold the sheet a second time. The modulus of a film can often be tuned as well. The use of a variety of liquids and

mixtures to change the surface tension of these fluids adds a third knob that can be tuned to enable folds of thin films.

The elastocapillary length is used extensively throughout the studies presented in this dissertation. Often the possibility of an experiment's success is estimated in terms of the elastocapillary length. The elastocapillary length is also used as a standard to describe other phenomena. If the relation between length scales or energy balance of a system can be normalized by the elastocapillary length, then the relation becomes universal and data collapses onto a master curve.

1.4.2. Adhesion

Adhesion is a catch-all term for the forces that hold objects together, or more directly the force required to separate two surfaces. These forces can be produced from van der Waals forces, interatomic forces, intermolecular forces, hydrogen bonds, and many more effects that are beyond the scope of this dissertation. Needless to say, when two surfaces are brought into contact with one another there is usually a nonzero force required to separate these two materials. Adhesion is normally explained as a product of surface energies, but certain situations can arise where a more nuanced approach is needed. When two materials are adhered together such that the work required to separate the materials is greater than the sum of the energy of the two created surfaces, then the resulting total energy of the system will be a negative value. This is the interfacial work of adhesion, given in Eqn. 1.38. The force required to separate these two surfaces is the common definition of the adhesive force. The adhesive force (F) per width of the crack (b) is then related to the surface tension values by:

$$\frac{F}{b} = \gamma_1 + \gamma_2 - \gamma_{12}. \tag{1.38}$$

1.5. Materials and Methods

The methods that were commonly used to create and test experimental samples are briefly outlined in the following sections. This is done to avoid repetition later in this dissertation when the topic of sample preparation and experimentation are brought up. The chemicals and materials that are used in experimental study are also given in this section.

1.5.1. Coating and Release Methods

A key component of experimental studies of thin films is to ensure that pure films can be readily and repeatable created with a uniform thickness. After these films are created, they need

to be released from the substrates that they were created upon. Several methods were used in the process of the research covered in this paper to accomplish each of these goals. These coating and release methods are covered in detail in the upcoming sections. Many of these procedures require the use of purified water, it should be noted that MilliQ purified, filtered water (MilliQ, Millipore Inc.) was always used in for these experiments.

1.5.1.1. Spin-Coating

Spin-coating is the method used in these research projects to create the thinnest films studied. These films could be as thin as tens of nanometers thick for the thinnest polystyrene films created, to a few hundred micrometers thick for the thickest polydimethylsiloxane films created. Spin coating works through the action of the angular acceleration of the sample which causes the liquid to flatten and spread outwards. Excess liquid is flung off the sides of the sample. The surface tension of the liquid means that there will always be a portion of the liquid attached to the sample substrate, as it would increase the surface energy of the system to completely separate the liquid from its substrate. The liquid's surface tension also works to flatten the film, since bumps in the film would create more surface. The rapid spinning also acts to quickly evaporate any volatile solvent in which a solid had been dissolved, leaving behind a solid film.

The instrument used was a Laurell Technology Model WS-400BZ-6NPP/Lite (Fig. 1.9), which has controls to set the maximum angular speed that the sample would spin at and for the acceleration to get to that angular speed. In a general sense, increasing the number of revolutions per minute decreases the thickness of the film created. Increasing the acceleration increases the area that a liquid drop would spread over on the sample substrate. After these variables were set, the substrate was attached to the spin coater's central post and a vacuum and air supply were turned on. This allowed the vacuum of the spin coater to be activated, securing the substrate to the machine. At this point, the liquid was placed onto the substrate. Then the spin function was activated and ran for 1 minute to allow time for the excess liquid to leave the surface. This setup with a slide placed onto the spin-coater and drops of solution placed onto the slide is shown in Fig. 1.9.

Polymers dissolved in solvent required a different coating procedure than two part elastomers. The polymer solutions were usually polystyrene dissolved in toluene or polycarbonate dissolved in chloroform. The concentration of the solution was another variable that could possibly
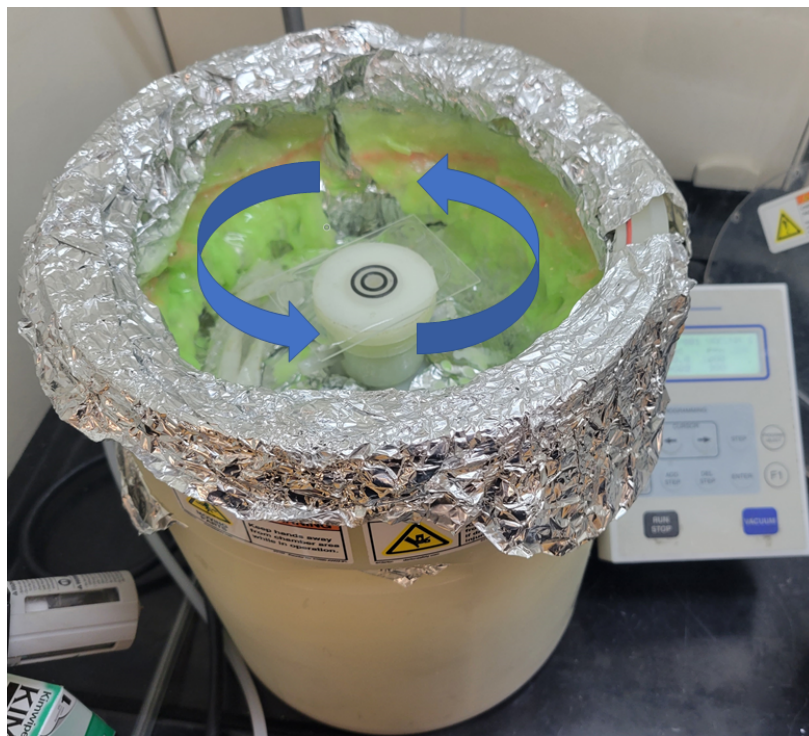
Figure 1.9. Spin-coater with a slide attached to the chuck. The direction of spin is indicated by the curved arrows.

affect the thickness of the films, with more concentrated solutions leading to thicker films with all other variables the same. After the solutions were made, 4-20 drops were placed into the center of the substrate before the spinning was started, depending on the area of the substrate desired to be covered. As quickly as possible after the drops were placed onto the substrate, the spinning was started to prevent the forming of a film around the edges and top of the drop. The spinning removed excess solvent and evaporated the rest, leaving behind a solid film that was ready for annealing and removal from the substrate. This process was used to create films of thickness of tens of nanometers up to tens of microns from solution.

Two-part elastomers were prepared and placed onto the substrate after it was attached to the spin coater. Instead of placing a series of drops in the center of the substrate, the entire surface was covered with the liquid elastomer. Due to the high viscosity of these mixtures (5100 Cp), it is difficult to get them to spread over significant distances on the substrate. This also means that longer spinning times are often used with elastomeric films, usually less than three minutes total. These films were ready for curing after the spinning process. The thinnest elastomeric films created
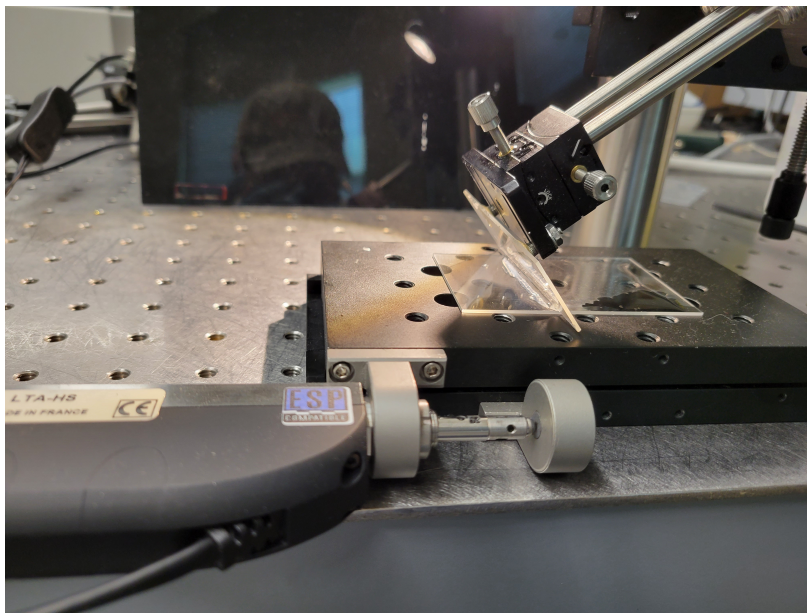
Figure 1.10. Flow-coater used to create films of polymers dissolved in solution. The glass blade remains stationary while the stage moves the sample under it, spreading a thin film.

were tens of microns thick. Films thinner than this were nearly impossible to keep from crumpling upon themselves after removal from the substrate.

1.5.1.2. Flow-Coating

Flow coating is a process where a fluid is spread across a substrate by a blade placed a small distance above the substrate. It is used to crate films of a medium thickness, on the order of tens of microns to hundreds of microns in thickness. The blade pushes the drop as it moves along the substrate, leaving a thin liquid film behind that will become the solid film after the solvent evaporates. This process is similar to butter being spread onto the surface of bread, or even paint spread by a brush-albeit the brush is acting as a much softer blade.

This process was only used in to create films from solution for the work covered in this writing. The flow-coater used was built in the lab using a motion-stage to hold the sample/substrate, and an angled glass slide as the blade. The blade was positioned above one end of the substrate. Several millilitres of solution were spread along the leading edge of the blade. As quickly as possible, the stage the substrate was placed upon was moved so that the blade spread the liquid over the entire surface, or until there was no fluid left to spread, whichever came first. As long as the stage moves at a constant rate and the blade does not move, the film will be quite regular in thickness. Care must be taken to not stop the stage when there is still a drop along the blade, otherwise the

liquid will flow under the blade. This creates a puddle near the blade that is of uncontrollable thickness, thereby ruining much of the sample film. Thinner films can be created by using a less concentrated solution, setting the blade closer to the substrate, or moving the stage at a faster rate. Since the area behind the blade remains a thin liquid for a time any bumps are able to smooth before the film dries to a solid. After the film dries, it is ready for annealing and removal from the substrate.

1.5.1.3. Drop-Casting

Drop-casting (or drop coating) is a method of creating thin films, where a liquid of either dissolved polymer or uncured elastomer is poured either onto a surface or into a container and allowed to harden. This method was used in experiments to create the thickest films used, from hundreds of microns in thickness up to several centimeters thick.

Coating onto a flat surface means that the only constraint on the liquid spreading outward and leaving behind a thinner film is the liquid's surface tension and viscosity. Since these liquids were not rapidly solidified, the viscosity was usually not a factor in the overall thickness.

Elastomeric liquid solutions were poured onto the substrates so that the substrate would be mostly covered. The elastomer/substrate system was allowed to rest on a flat surface so that any bumps or unevenness could self-level. Elastomeric coatings were then placed into an oven to cure. Creating elastomeric films on flat substrates yielded a somewhat limited range of thicknesses, so thicker films were created by drop-casting into a dish with raised sides was utilized to prevent spreading of the liquid. The procedure for these was similar, except the elastomer liquid was poured into a polystyrene dish until the dish had filled to the desired thickness of the film. The dish system was allowed to settle and then cured on a flat surface. Creating these films in a polystyrene dish did not require a release layer or mica sheet. The elastomers were thick enough and strong enough to readily peel from the plastic surface.

Polymer solutions were also poured onto a substrate, covering most of the surface. These were then placed onto a flat surface in a chamber whose atmosphere was saturated with the solvent. This was done to slow the evaporation process of the solvent from the film, as too rapid evaporation could cause an uneven surface to develop on the film. This was allowed to sit for 3-5 days until the solvent had evaporated from the system. The film was then ready to be annealed and removed from the substrate. The thickness of the films could be adjusted by changing the concentration of

the solutions used in the drop-casting process. Since the solvents used to dissolve polystyrene and polycarbonate to create these solutions would also dissolve the polystyrene dishes used to create thicker elastomeric films, glass dishes would sometimes be used to create films from solutions. This was done in a similar manner to the procedure for elastomers.

1.5.1.4. Annealing

The creation processes of thin films build stress into the sample. This can be due to surface effects from the substrate or from uneven evaporation throughout the bulk of the sample. A film with a large amount of stress built in will spontaneously curl if given the chance. This is most often seen in polystyrene and polycarbonate films that are created from a solution. The molecules that make up elastomeric films are allowed enough movement that they can usually relax to an unstressed state on their own without annealing as a separate process. Removing this built in stress is an important step in preparing films for scientific testing, since any stress from an outside source could possible change results and observations made during a test.

Annealing is the process by which built in stresses are removed from a thin film through the heating of the substrate to above its glass transition for a period of time. The films were created through the various processes detailed above, and left on the substrates throughout the annealing process. This provided stability to the films, forcing them to stay in a flat state. A small hot stage (Linkam Scientific LTS-420) was used to anneal the majority of the thin films created using glass slides. The samples were annealed by heating the film to ~ 30 °C above each material's glass transition and hold it there for for 1.5-2 hours.

Larger films did not fit into the hot stage, so a hot plate was used to anneal these films. The film was placed onto the hot plate and a glass container was placed over the sample to limit air movement. The film was closely watched until a shimmer was noticed on the surface of the film. This signified that the glass transition had been crossed and that the shimmering area had liquefied. The heat was lowered at this stage and the film was watched until the entire test area had achieved this shimmering effect. The sample was then removed from the heat to a warm area so as to not shock the film as it re-solidified. Extreme care must be taken to monitor the film temperature during this process because the film would scorch and turn a brownish hue if it was allowed to climb much above the point where shimmering was noticed.

After the annealing process, films were ready to be removed from their substrates.

1.5.1.5. Coating on Mica

Mica is a silica-based material that forms naturally into very smooth sheets, or can be grown in a lab or by a manufacturer. Mica is useful for film coating purposes in a lab setting due to its extremely flat surfaces, ability to separate from thin films, insolubility with the vast majority of common solvents, and ability for a sheet to be readily cleaved into two fresh and pure mica sheets. A cleaved sheet of mica can be used as a substrate for almost any coating process mentioned in this work, and can also stand up to heating, annealing, and bending giving added functionality that other film preparation substrates may not offer.

The first step to prepare a mica sheet (Ted Pella, Inc.) for coating is to cleave a single sheet into 2. This reveals 2 new mica faces that have not been exposed to atmosphere and are therefore uncontaminated. Cleaving is accomplished by forcing two layers apart with either a razor blade or a sharp tweezer. This is easiest when initiated at the corner of a sheet. Once the crack has been started, it is spread through the rest of the sheet by gently pulling the two new sheets apart with two sets of tweezers. The two separated sheets can usually then also be cleaved and separated, giving between 6 and 12 pure faces to use as substrates per mica slide from the manufacturer. These sheets are then placed pure side up onto a glass slide to provide stability. Often a fraction of a drop of water is placed onto the glass slide before the mica sheet is placed to help adhere the mica sheet to the glass. The water spreads out under the drop and the surface tension of the water resists allowing the mica to peel from or move around the glass. The glass/mica system is then used as the substrate for the various coating methods described in this paper.

1.5.1.6. Floating from Mica

After the polymer films have been annealed or dried onto the mica substrate, the film surface is gently scored with a razor blade cutting the film into the desired shape. Then the film/mica/glass slide system is then held together with a tweezer and slowly dipped into a bath of MilliQ water. The water travels along the score marks, penetrating under the film and spreading through capillary action (Fig. 1.11a). This separates the film from the mica due to the water's surface energy preferring a water-film surface to a water-air surface. This action is continued by dipping the coating system further into the water as more of the film detaches from the mica substrate (Fig. 1.11b). Occasionally, a segment of the film will stick to the mica even after the
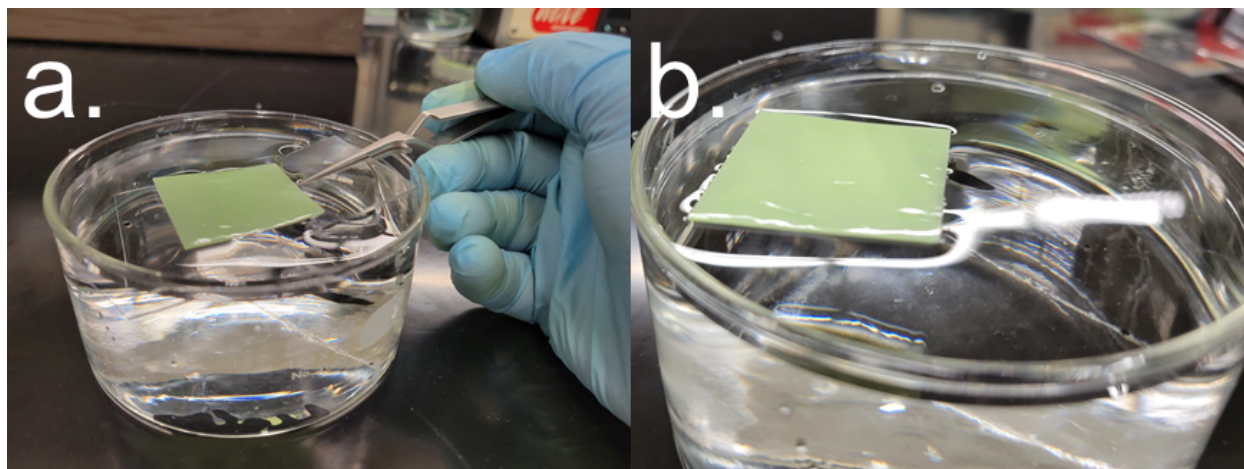
Figure 1.11. The process of floating a film from a mica substrate. a.) a film coated on a mica substrate is scored and dipped into the water bath, beginning to peel the edge of the film. b.) Slowly submerging the entire slide into the bath progresses this separation until the entire film is separated and freely floating on the water.

water has released the surrounding area. When this happens, a second tweezer is used to gently poke this region to free it. Continuing this process eventually frees the entire film, allowing it to float on the water's surface.

Films with a relatively large thickness were directly removed from the water bath by picking them up with tweezers and placing the films on a kimwipe (Kimberly-Clark Cooperation) in a covered container to dry for at least 24 hours. The thinnest films used would crumple in on themselves if they were removed this way due to the remaining water drops clinging to the film acting to cover their surface with film in a process that could be described as unplanned capillary origami. These films were removed from the surface of the water by being "fished" out of the water with a flat kimwipe. A kimwipe was submerged in the water under the film and pulled flat, parallel to the film. The kimwipe was then gently raised so that is was partially submerged and moved into contact with the film. Further raising of the kimwipe drew the film from the water surface and onto the flat kimwipe. Care was taken to not wrinkle the film once on the surface of the kimwipe. The kimwipe-film system was then placed in a covered container onto dry kimwipes to dry for approximately 2 days. The dry films could then usually be lifted from the kimwipes and used in experiments. The thinnest films, however, were too thin to be directly handled and needed to remain placed on the dry kimwipe until they were placed directly into their experimental position by inverting the

kimwipe onto the desired substrate and pressing the film into contact through the kimwipe. The kimwipe was then gently peeled from the film.

1.5.1.7. Coating on Polyacrylic Acid

Polyacrylic acid (PAA) is a relatively safe, water soluble polymer that is useful as a release layer in many coating processes. This is because polyacrylic acid can be dissolved in a water solution and applied to a surface as a flat coating through a variety of methods, such as spin-coating, flow-coating, or drop casting. After the polyacrylic acid coating has dried, it provides a stable substrate for the coating of polymers dissolved in organic solvents such as polycarbonate in chloroform or polystyrene in toluene or two part elastomer-binder materials such as polydimethylsiloxane or polyvinylsiloxane. After these polymers have been coated, polyacrylic acid release layer acts as a simple method of removing these films from their coating substrate in a water bath.

The method for creating the polyacrylic acid release layer used in this study involved creating the water-polyacrylic acid solution, creating a thin flat substrate of polyacrylic acid on the surface of a glass slide, coating the desired polymer onto this surface, and dissolving the polyacrylic acid release layer. The first step was to create a 1:1 solution of polyacrylic acid (Aldrich Chemistry) and MilliQ water by weighing equal amounts of each liquid into a small glass vial and shaking vigorously for one minute. This was done so that the liquid applied to surfaces later would flow more easily than the pure chemical from the manufacturer, making the coating process easier. The mixture was then allowed to further mix for at least 24 hours before use. The mixture was again shaken for 10-15 seconds before each subsequent use to ensure that the two liquids were still in solution. A glass slide was placed onto the spin coater and accelerated to 2000RPM and cleaned by spraying MilliQ water at the slide while the slide was rotated. Water was sprayed over the entire spinning radius for approximately 10 seconds. The slide was spun at 2000RPM for approximately 30 more seconds to dry the cleaned surface. The slide was then placed clean side up on the counter and 8 drops of the water-polyacrylic acid solution were placed on the center of this slide. A second cleaned slide was then placed clean side down onto the drop and first slide. This caused the liquid solution to spread between the two slides, coating the entire cleaned surface of each slide. The slides were then separated and individually placed coated side up onto the spin coater and accelerated to 2000RPM at 2000RPM/s. This spinning flung off excess solution and evaporated much of the water remaining on the glass, leaving behind a solid and thin film of polyacrylic acid.

These coated slides were used as a substrate in the polymer coating process, the same way as any other solid substrate is used in this document.

1.5.1.8. Floating from Polyacrylic Acid

After the polymer film had annealed or solidified, the polyacrylic acid release layer was dissolved in a bath of water, allowing the polymer film to float to the surface of the water and be removed.

The films coated on the polyacrylic acid release layer were scored with a razor blade into the desired shapes. The coated slides were then submerged in MilliQ water to a depth of 0.5-1cm for at least 4 hours. The scores in the polymer coating allowed water to effectively penetrate the coating and dissolve the polyacrylic acid layer. With the substrate dissolved into the bath solution, the unsecured film drifted freely in the bath. However, when a part of the film reached the surface of the bath, it would be held there by surface a surface tension. The high energy water surface is in a lower energy state with a polymer film covering part of its surface than with the film submerged. This effect also acted to pull any film still adhered to the substrate to the surface of the water. After a period of at least 4 hours, the majority of the release layer had dissolved, and the film would either be at the water's surface or partially drifting due to some segment having a small attachment to the substrate. In this latter case, a tweezer was used to gently poke at the attached region to release it from the substrate. A tweezer may have also been occasionally used to raise a film to the surface to begin the floating process.

1.5.2. Polystyrene Thin Films

Polystyrene (PS) is a glassy polymer that is commonly used for industrial and academic purposes. Its widespread use means that it is an extremely well characterized material, where knowledge of novel interactions can be used to improve existing technology. Polystyrene has a relatively high modulus, forms a clear solid, and can be formed into very thin films easily through the use of a solvent and a number of coating and forming methods. As a glassy polymer, polystyrene can be elastically bent through small, reversible deformations. There is a range of slightly larger deformations that will plastically and permanently deform a polystyrene solid. Even larger deformations will cause polystyrene to fracture or shatter as a glass.

The method for creating thin polystyrene films requires bulk polystyrene pellets (Aldrich, Mw = 192 kg/mol) to be dissolved into a solvent. The solvent used in each experiment involving

polystyrene was lab grade toluene (Fisher Chemical). A solution was prepared by measuring a mass of polystyrene pellets into a glass vial and adding an appropriate amount of toluene to that vial to create a solution of a desired percentage concentration. All amounts were measured by weight and were generally used to create thicker or thinner films by the coating methods mentioned earlier in this work. Solutions made were between 0.5-10% polystyrene in toluene. These solutions were allowed to sit in a closed vial for at least 24 hours then given a vigorous mixing before use.

Nile Red Dye (MP Biomedicals, LLC) was also sometimes added to the solution to increase the visibility of the polystyrene films. This dye would fluoresce orange when activated with a blue laser and could allow for the finding of both the surface and information about the bulk of a film.

1.5.3. Polycarbonate Thin Films

Polycarbonate (PC) is a plastic polymer that is also commonly used for industrial and academic purposes. Its widespread use means that it is another well characterized material, where knowledge of novel interactions can prove to improve existing technology and profitable. Polycarbonate has a modulus of 3.5 GPa[35], and is one of the toughest commonly used plastics, forms a clear solid, and can be formed into very thin films easily. The toughness of this polymer means that it is often used in safety equipment such as safety goggles and blast shields. Unlike polystyrene, polycarbonate is more likely to plastically deform than to shatter. Small deformations of polycarbonate do remain in the reversable, elastic regime. Larger deformations lead to irreversible plastic deformations. Only extreme deformations cause fracture in polycarbonate films. These features make polycarbonate an ideal material to use in applications where the job is to bend but not break.

The method for creating thin polycarbonate films requires bulk polycarbonate pellets (Scientific Polymer Products Inc., Mw = 60kg/mol) to be dissolved in a solvent. The solvent used in each experiment involving polycarbonate was lab grade chloroform (Acros Organics) or sometimes methylene chloride (Fisher Chemical). A solution was prepared by measuring a mass of polycarbonate pellets into a glass vial and adding an appropriate amount of solvent to that vial to create a solution of a desired percentage concentration. All amounts were measured by weight and were generally used to create thicker or thinner films by the coating methods mentioned elsewhere in this work. Solutions made were between 0.5-10% polycarbonate in solvent. These solutions were allowed to sit in a closed vial for at least 24 hours then given a vigorous mixing before use.

Nile Red Dye (MP Biomedicals, LLC) was also sometimes added to the solution to increase the visibility of the polycarbonate films. This dye would fluoresce orange when activated with a blue laser and could allow for the finding of both the surface and information about the bulk of a film.

1.5.4. Polydimethylsiloxane Thin Films

Polydimethylsiloxane (PDMS) is a silicone-based elastomeric rubber (commonly shortened to elastomer) that is one of the most commonly used silicone rubbers on the market. It has a wide range of uses from kitchen utensils and implements to gaskets and tubing to medical and implantable health devices and because of this is often studies and has well-understood material properties.[36, 133, 25, 34, 79, 53] Polydimethylsiloxane can be bent and stretched to extremes without breaking. This wide variety of uses and environments of application mean that there are always opportunities to increase the understanding of polydimethylsoloxane's interactions with different materials that would be beneficial to a wide swath of the scientific community. The specific polydimethylsiloxane used in our experiments was Sylgard 184 (Dow Corning). This is a proprietary blend of a prepolymer oil and various fillers (which together are called the base) and a binding agent that works to polymerize the base into an amorphous solid.

The preparation process for this elastomer is more involved than the process for the solution-based films due to polydimethylsiloxane's tendency for form bubbles and bumps during the mixing process. These bumps and bubbles need to be removed before studies can be conducted. Mixtures of base and binder were prepared in different ratios according to the manufacturer's instructions and the desired modulus and adhesion of the eventual film. The most common ratio used was 10:1 base to binder, by weight. This ratio led to films with the highest modulus and lowest adhesion values of all the polydimethylsiloxane mixtures used. As the ratio of base to binder became higher, the modulus dropped and the adhesion values rose. Other ratios used were 20:1, 30:1, 40:1, and 50:1. The last of which was close to being a gel and needed to be handled with caution to avoid tearing the films apart.

The base and binder were measured by weight and combined. The combination was then mixed for 10 minutes. During this mixing, bubbles were often dispersed throughout the mixture. The mixture was placed into a vacuum oven and placed under a vacuum of 10-25 inHg for 10-20 minutes. This process caused any bubbles in the bulk of the mixture to expand. This expansion

allowed the bubbles to rise to the top of the mixture where over time they would pop. After a wait, the vacuum was released. The mixture was coated onto the substrates as described elsewhere in this work. After this, the substrates and films were placed into a vacuum oven. The vacuum was cycled between atmospheric pressure and 25 inHg twice. After this the vacuum was held at 25 inHg for 20 minutes. The vacuum was cycled once more back to atmospheric pressure then to 25 inHg. The vacuum was held at 25 inHg and the temperature was turned on, set to 85°C. This was held for 90 minutes, after which the heating was turned off and the vacuum released. The film was allowed to cool for several minutes on the bench-top. After this the films were ready for cutting/scoring and removal from the substrate.

1.5.5. Polyvinylsiloxane

Polyvinylsiloxane (PVS) is a silicone-based elastomeric rubber used in scientific research and for creating rubber moulds of 3-dimensional objects. Polyvinylsiloxane is useful for quickly creating moulds of 2-dimensional objects becasue it can cure to a solid relatively quickly and at room temperature. It can be used to create opaque rubbers with a modulus higher than that of 10:1 polydimethylsiloxane and, but lower adhesion values. Dye is often added to polyvilylsiloxane making it easier to see, and more obvious to the user if the two ingredients are not fully mixed. This will appear as streaks of white binding agent mixed with the colored prepolymer. The surface of polyvinylsiloxane can be treated in an ultraviolet-ozone chamber to oxidize exposed regions. This prevents exposed surfaces from interacting with other elastomers, enabling polyvinylsiloxane to be used as a mould to create elastomeric duplicates of moulded objects. The use of polyvinylsiloxane was limited in in these experiments to acting as a moulding material or as a thin film for demonstration purposes. Thin polyvinylsiloxane films could be made somewhat transparent as their thickness dropped below several hundred microns, but these films were much easier to visualize and image than polydimethylsiloxane films of similar thickness. The material similarities between these two films meant that a demonstration created from polyvinylsiloxane would very accurately recreate actual experimental conditions and observations found from polydimethylsiloxane.

Preparing polyvinylsiloxane (Elite Double 32, Polyvinylsiloxane (A-Silicone) Duplicating Material) for use was a similar but shortened version of the perperation of polydimethylsiloxane. The only ratio used was a 1:1 ratio of the green prepolymer to the white binding agent. These quantities were measured by weight and added together followed my vigorous stirring for 1 minute.

The mixture was then poured into the mould or used with the coating methods mentioned above. Within a few minutes, the elastomer had begun to set. This eliminated the possibility of effective vacuum removal of bubbles within the solid. However, given the 1:1 mixing ratio and the short stirring time, bubbles were not often encountered or a major problem in the creation of either polyvinylsiloxane moulds or thin films. The manufacturer's instructions state that the curing should be complete within 30 minutes of mixing, but to ensure that the curing process was fully finished the elastomer was allowed to cure for at least 2 hours before use.

1.5.6. Ultraviolet-Ozone Treatment

Ultraviolet-Ozone (UV-O) treatment was accomplished using a Jelight Company UVO Cleaner Model No. 42A oven for the experiments covered in this work. UV-O treatments can be used on silicone-based elastomers to modify surface characteristics such as surface energy or modulus.[34] This process creates excess ozone in the oven chamber and breaks many of the bonds in the silicone rubber. Prolonged UV-O treatments change the surface characteristics of these rubbers from hydrophobic elastomers towards hydrophylic glasses more similar to pure silica than to a silicone rubber. Longer treatments can push the effects deeper into the bulk of a material. However, this treatment tends to only affect the uncovered surfaces of materials exposed to both the ultraviolet light and ozone gas. Masks can be created from rubber, plastic, or glass that cover surfaces preventing the ozone and/or ultraviolet light from affecting these areas. Masks can be created through printing a material directly onto a surface, or by cutting out a mask using a Cricut Cutter and applying it to a surface with relative ease. Complex or multilayer masks can be created that affect the surface features and properties of a material in a wide variety of ways. The feature that was used in the experiments covered here was to treat an elastomeric surface so that it would not bond to other elastomers as they cured. This allowed the treated elastomers to act as substrates or moulds used for the creation of other substrates or moulded objects.

The UV-O treatment was also used to polymerize any remaining unpolymerized resin in 3D printed objects. Unpolymerized regions could be easily felt as sticky when handling these objects. 35 minutes in the UV-O chamber effectively polymerizes these regions, while only acting on the surface of the remainder of the rest of the object. Regions that were fully polymerized before treatment would slightly brown from the treatment.

1.5.7. 3D Printing

The ability to design and create objects of virtually any shape and form through 3D printing proved invaluable in the design and prototyping of many parts of the work covered in this paper. Instruments, tools, moulds, and more could be designed, printed, and tested within a few days of a need arising.

The program used to design 3D objects was Google's free online version of SketchUp. This program is ideal for creating relatively simple 3D objects consisting of geometric shapes. Although many of the premium features are disabled in the free version of SketchUp, it is possible to create a multitude of designs built from simpler geometric shapes. 3D objects were saved as .STL files and imported into Formlabs software for preparation for printing. These objects were printed using a Formlabs Form 2 laser-activated photopolymerization 3D printer. The resin used was the Formlabs clear resin, which solidifies to a relatively hard and light material that can be submerged in water, baked in an oven, or have polymer films or mouldings created on its surface without damage. All 3D printed objects were placed in a bath of isopropyl alcohol and agitated two minutes, then rested in the bath for ten minutes. The mould was then allowed to dry in the air for at least 24 hours. 3D printed objects that were to be used as tools or instruments and would not come into contact with a sample were further cured in the UV-O oven for 35 minutes to polymerize any remaining unpolymerized resin, and harden the overall structure. These objects were washed with water and detergent before and after the UV-O oven treatment and were ready for use when dry.

1.5.7.1. 3D Printed Mould Preparation

3D printed objects that would come into contact with polydimethylsiloxane or other experimental polymers needed further treatment, as it was observed that polydimethylsiloxane cured on the resin surface would not cure properly. Photoinhibitors in the resin would leech into the polydimethylsiloxane and prevent the binder from properly reacting with the prepolymer. The following process was used to remove excess photoinhibitor from printed moulds.

Moulds were then soaked in filtered MilliQ water for 2hr, rinsed with MilliQ water, and placed into an oven at 85° C for 24 hours. The moulds were allowed to cool, then washed with detergent and water, rinsed with MilliQ water, and allowed to dry for at least 24 hours. This

process would allow polydimethylsiloxane to be cured against the resin in the same way that poly-dimethlysiloxane can be cured in polystyrene dishes.

3D objects are printed with a slight roughness from the resolution of the laser beam as it polymerizes the resin, so any surfaces that needed to be flat were sanded using a wet-sanding technique. This sanding started at 200-grit sandpaper and was continued up to 5,000-grit sandpaper. The moulds were again cleaned and processed to remove excess photoinhibitor at this point.

Surfaces that were needed to be even smoother than what could be achieved with sandpaper had layers of polystyrene deposited unto the resin surface. A solution of 10% polystyrene in toluene was poured onto the surface of the resin, then the excess solution was poured away. This process was repeated 3-5 times and then examined under a microscope to determine relative roughness of the surface. The desired smoothness would show as 100% adhered to a polydimethylsiloxane film draped onto the surface, the above process was repeated until this was achieved.

1.5.8. Moulding

Moulds were often used as 3D negatives to produce repeatable objects from polydimethyl-siloxane. Since polydimethylsiloxane is not easily shaped once it it cured, the use of moulds offers a direct path to create a wide range of 3D shapes from polydimethylsiloxane.

1.5.8.1. Polystyrene Moulds

A patterned glass slide was created by attaching many glass pipettes side-by-side onto a slide using epoxy. When the epoxy had dried, patterned slide was placed onto the lid of a polystyrene dish so that the patterned part of the slide was against the dish. A 1 kg weight was placed onto the top of the dish, pressing it into the slide. This stack was placed onto a hot plate, with the glass slide in contact with the heating stage, and heated. After a time, the heat was turned off and the stack was allowed to cool. This hot-press created cusps and half-pipe shapes in the polystyrene dish. Polydimethylsiloxane or other elastomers could then be drop cast into this prepared dish to create an elastomer with a surface with rounded features the same size as the pipettes. These were prepared in the same way as the drop cast samples made in dishes (described in section 1.5.1.3) and were ready for use as soon as they were peeled from the dish.

1.5.8.2. Printed Resin Moulds

Moulds created through the 3D printing and preparation process given above could be used directly as a dish in which to drop cast polydimethylsiloxane. These moulds could also be used as a

double-negative mould that would create moulds. Moulds with small features (below 0.5 mm) could not be used with polyvinylsiloxane since its cure time is too short to allow for the use of a vacuum oven to force the elastomer into every region of the mould. Polydimethylsiloxane was poured into the moulds and placed into a vacuum oven. The vacuum was cycled between 0-30 inHg until there were no bubbles present in the mixture. The mould/elastomer setup was then baked as one. The cured polydimethylsiloxane was carefully peeled from the mould and was either ready to be used as a substrate or for further treatment to work as a mould.

1.5.8.3. Polydimethylsiloxane Moulds

Moulds were created either through the 3D printed moulding process described in the previous section, or by directly pouring the uncured elastomer into a closed container around an object. When the object was completely covered, the elastomer was cycled in vacuum between 0-30 inHg, until there were no bubbles present. This was then baked to cure the polydimethylsiloxane.

After curing, the polydimethylsiloxane was removed from the mould or container. The cured polydimethylsiloxane was placed into a UV-O oven and treated for 35 minutes. This oxidized the surface of the elastomer, making it non-adhesive to other uncured elastomers. After UV-O treatment, the polydimethylsiloxane was ready to be used as a mould, in a similar manner as the 3D printed or polystyrene moulds from earlier sections.

1.5.8.4. Polyvinylsiloxane Moulds

Polyvinylsiloxane moulds were created in the same manner as polydimethylsiloxane moulds. The difference is that the decreased cure time of polyvinylsiloxane does not allow for a vacuum to be used to pull liquid elastomer into each crevice of a mould or object. However, polyvinylsiloxane was ideal for quickly creating moulds of objects with relatively large features (above 0.5 mm). These moulds would also be treated in a UV-O oven for 35 minutes to oxidize the surface and make it unable to bond to other elastomers. After this, the polyvinylsiloxane moulds were ready for use to shape polydimethylsiloxane.

1.5.9. Measuring Surface Energies, Contact Angles, and Surface Tensions

Careful measurement of all surface tension values (directly relating to surface energies) is an important step before testing any theoretical model against real experiment, as a small change in any of these variables could drastically affect the predicted outcome. Several methods were used to find the surface tension values of the experimental liquids and surfaces used. The amount of liquid
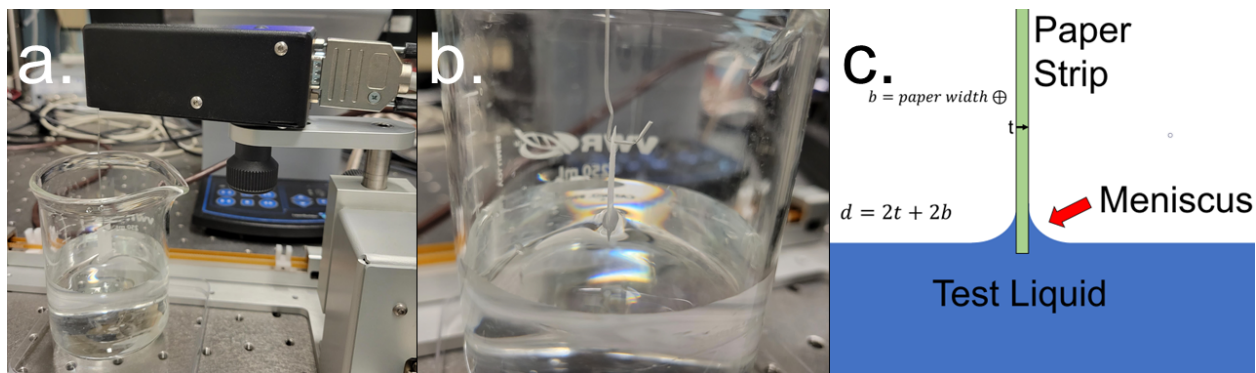
Figure 1.12. a.) Wilhelmy Plate setup showing the force transducer. b.) Closeup of paper strip contacting the test liquid and creating a meniscus. c.) Diagram of the side profile of the plate contacting the liquid. [134]

available and its relative surface tension determined which method would be best for determining surface tension. After surface tension values (air-liquid interfacial surface energies) were found, the tension values of the other interfaces also need to be found. Again, depending on the state of the materials involved there were different tests to choose from. Mainly, if the interface was a liquid and a solid or a liquid and a liquid. If two of the surface tensions and the liquid's contact angle were known in a drop-on-a-solid-substrate system, then Eqn. 1.29 could be used to calculate the final surface tension. This was usually done in order to calculate the surface energy of any solid material used in these experiments. These different methods are covered in the following sections.

1.5.9.1. Wilhelmy Plate Method

The Wilhelmy Plate Method can be used to find the surface tension of a liquid in air. This method relies on the measurement of the weight of a meniscus pulled upwards by a Wilhelmy Plate inserted into a liquid to determine the surface tension in air of that liquid. Wilhelmy Plates need to wet perfectly with the liquid, meaning that the top of the meniscus approaches surface of the plate at a zero degree angle (Fig. 1.12). Plates are often made of platinum or glass, which need to be flame-cleaned before each use. Disposable filter paper can also be used, as long as this paper can achieve perfect wetting with the liquid. The plates used to find the values in this work were found using 1 cm wide filter paper attached to a KSV Instruments Minimicro force sensor, seen in Fig. 1.12.

All containers, dishes, and bowls were thoroughly cleaned and rinsed with MilliQ water before experimentation, as even a small contamination could drastically affect the surface tension

results. A clean filter paper strip was obtained and its width and thickness were measured and recorded to give the plate diameter (d). Then the strip was placed onto the force sensor hook of the KSV Layerbuilder (Fig. 1.12a). The data recorder on the KSV software was started. The paper strip was lowered until only the very end of the paper strip was touching the liquid's surface (Fig. 1.12b). This was allowed to sit for several minutes, enabling the liquid meniscus to climb the paper strip. After the motion of the meniscus stopped, the paper was raised so it was no longer in contact with the liquid. The difference in the force measured when the meniscus had fully formed and when the paper strip was no longer in contact with the liquid was recorded as F in Eqn. 1.39. The measured force and the plate diameter are the measurables required to calculate the liquid's surface tension since the contact angle with the plate is assumed to be zero degrees. This calculation also assumes that the meniscus does not fully wrap around the plate and therefore does not affect the surface tension. This test was repeated several times to get a statistical average for the recorded value of the liquid's surface tension (γ).

$$\gamma = \frac{F}{d\cos\theta} \approx \frac{F}{d} \tag{1.39}$$

The statistical values were calculated along with their respective errors and are presented in Table 1.3. It should be noted that "Used Glycerol" and "Used Water" in Table 1.3 refer to the glycerol (99.9% Fisher Chemical) and water (MilliQ) that had been directly used in an experiment, respectively. During these experiments, these liquids had come into direct contact with polydimethylsiloxane and possibly uncured polydimethylsiloxane oil or binder. These oils are believed to leech into the liquid from the surface of the polymer and act as a surfactant wetting the surface of these liquids. This phenomena was noticed during the work conducted in this dissertation[134, 133], but was also observed by other researchers working in similar circumstances.[117] A test was conducted to verify these results by placing a drop of glycerol onto a polydimethylsiloxane bath. This drop

Table 1.3. Surface tension values for experimental liquids. Found using the Wilhelmy Plate Method.

Liquid	Surface Tension $[\frac{mN}{m}]$	Error $[\frac{mN}{m}]$
Water	73	2
Glycerol	62.3	0.6
Silicone Oil	22.1	0.7
Used Glycerol	45.3	0.8
Used Water	49	2.5
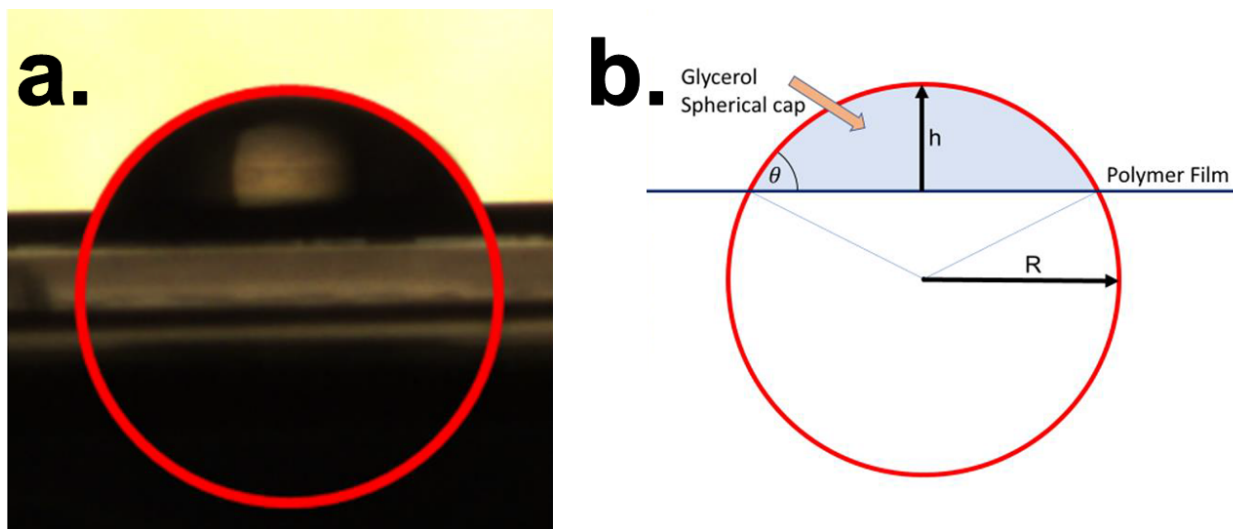
Figure 1.13. Side profile of a low-radius liquid drop on a solid substrate. A circle fit to the profile of the drop, and the drop's maximum height are all that is needed to determine the contact angle.

spread outward and reached equilibrium. When the tension values were measured using a method covered below in the Drop Floating in a Bath section. These values were in agreement with the "Used Glycerol" values presented here.

1.5.9.2. High Surface Energy Liquid on Solid Substrate

After the liquid-air surface tensions have been determined, they can be used to find the values associated with other interfaces, such as the liquid solid interface. In the case where a liquid has a relatively high surface tension, it will often form a small-radius spherical cap when placed onto an ordinary substrate. Such a situation forms a relatively tall drop, like the drop in Fig. 1.13. If low-radius drop can be enlarged enough to be imaged in side profile, then the process of determining the contact angle with the substrate is relatively straightforward.

Silicon wafers were spin coated with a thin coating of a solid, usually polystyrene or polycarbonate. Drops were placed onto these surfaces and allowed to equilibrate for 24 hours. A camera was centered on the plane of the substrate and the setup was imaged from a side profile. This gave an image like Fig. 1.13.

A circle is fit to the drop's profile, as seen in Fig. 1.13b, this gives a drop radius (R). The height from the top of the drop to the substrate (h) is also measured. These two measured variables

Table 1.4. Contact angle measurements for glycerol and used glycerol on polystyrene (PS) and polycarbonate (PC) substrates.

Materials	Advancing Angle [°]	Receding Angle [°]	Average Angle [°]
Glycerol-PS	77±3.6	65±3.2	71±3.4
Used Glycerol-PS	73±5.7	60±14	67±9.9
Glycerol-PC	63±4.2	57±1.9	60±3.1
Used Glycerol-PC	75±9.0	56±3.0	66±6.0

can be used to find the contact angle (θ) of the drop on the substrate using Eqn. 1.40.

$$\theta = \arccos\left(1 - \frac{h}{R}\right) \tag{1.40}$$

Advancing and receding contact angles were measured by adding or removing small amounts of liquid from the capillary drops. Images were taken 10-20 seconds after the addition/ removal of liquid, before equilibration could occur. This was repeated 3-4 times of continuously adding or continuously removing liquid to get a data set. There was a 30 minute wait time after a series was recorded before the following series of angles was started. The next series would be the opposite of the previous, switching from all-addition to all-removal for example. This process was repeated several times to obtain values for advancing and receding contact angles. These measurements were averaged to calculate the average angle. These angles were recorded in Table 1.4.

The values reported in Table 1.4 were slightly lower than the accepted values for these materials. This could be due to the impurities in the system, possibly the fluorescent dyes used for imaging. The equilibrium contact angles were similar between the pure and used glycerol, but the advancing and receding angles varied quite a bit from the pure values and from other used glycerol measurements, represented by the higher experimental errors. This could be due to increased pinning at the edges of the drop causing stick-slip events where the contact angle will hold in one spot for a period (even with changing contact angles) and then abruptly jump to a different spot possibly overshooting the equilibrium contact angle.

1.5.9.3. Low Surface Energy Liquid on Solid Substrate

Liquids with a low surface energy tend to spread when placed upon a surface. The profile of these drops is too low to properly image, so a different method is used to determine the height and radius of these drops. In the experiments covered in this work, polydimethylsiloxane oil was the
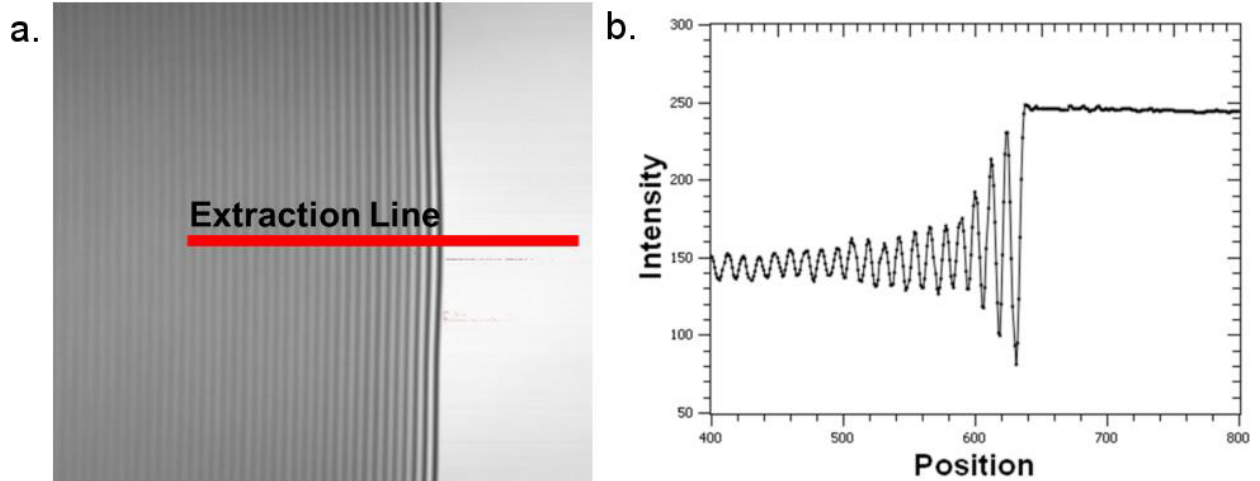
Figure 1.14. a.)High-radius liquid drop on a solid substrate. The bright and dark fringes created from the laser interference can be used to determine the height of the top of the oil drop at each fringe's location. b.)Intensity and position data from the extraction line. [134]

drop. The drop was placed onto a silicon wafer that had been spin coated with either polycarbonate or polystyrene. This drop was allowed to equilibrate for 24 hours, after which no further spreading was observed. At this point, the surface of the oil at the edge of the drop was imaged in three dimensions with confocal microscopy. These three dimensional scans could be processed to find the peak reflectance of each vertical stack of the images. These peak reflectance heights were configured into a plot to give a slope. This slope was compared to the slope of the substrate, and a contact angle was recorded. These contact angles were quite low, and the noise in the maximum intensity height data could often obscure the data.

Luckily, a diffraction pattern developed at the edge of the oil drop from laser light interfering with itself causing light and dark fringes in a recorded image. These fringes are visible in Fig. 1.14a in the oil on the left side of the image. The right side of Fig. 1.14a is the substrate surface.

The dark fringes in Fig. 1.14b were labeled as $m = 0.5, 1.5, 2.5, ...$ starting with the dark fringe at the edge of the drop. The position of each fringe was recorded along the extraction line. The wavelength of the laser (λ) used to image the liquid and the index of refraction (n) of the liquid were needed to calculate the height of each fringe (d) using the following equation.

$$d = \frac{m\lambda}{2n} \tag{1.41}$$

41

Table 1.5. Contact angle measurements for polydimethylsiloxane (PDMS) oil on polystyrene (PS) and polycarbonate (PC) substrates.

Materials	Contact Angle [°]
PDMS Oil-PS	3.2±0.34
PDMS Oil-PC	4.3±0.26

This height, paired with the position of each fringe, was used to find the slope of the liquid wedge at the edge of the film. Comparing this slope to the slope of the substrate gave the contact angle of the fluid on the substrate. These values were recorded in Table 1.5

These recorded values are much lower than what is recorded for familiar liquids such as water and glycerol. The lower contact angle indicated the oil's readiness to spread on these substrates. This can often be a frustrating property of polydimethylsiloxane oil, causing the oil to spread everywhere and be tracked to undesirable places.

1.5.9.4. Drop Floating in a Bath

The contact angle of a drop floating in a bath can also be found using a method similar to the high-radius contact angle measurements. Again, this is typically only possible to use with drops that have a smaller surface tension than the bath. High surface tension drops will act to cover their surface with the bath liquid and will be submerged.

A drop of the capillary liquid was gently placed onto the surface of a liquid bath and allowed to equilibrate for 24 hours. Then the edge of this drop was imaged using laser scanning microscopy (confocal microscopy without using the height dimension). Interference fringes again appear, and the thickness of the liquid wedge at the edge of the drop can again be determined using Eqn. 1.41. The profile of the surface of the bath and the top of the drop were also imaged using confocal microscopy. Combining these measurements gave the profiles of the surfaces of the bath, the top of the drop, and the drop/bath interface (Fig. 1.15a). These profiles were used to calculate the angle swept out by the bath, the drop, and the air at the triple point, shown as $\theta_1, \theta_2,$ and θ_3 in Fig. 1.15b, respectively.

1.5.10. Measuring Film Thickness

Finding the thickness of a film remains a vital step in any experimental process that involves thin materials. A small deviation in the assumed and actual thickness of an experimental sample could mean that a calculated quantity is orders of magnitude from its actual value (see Eqn. 1.15).
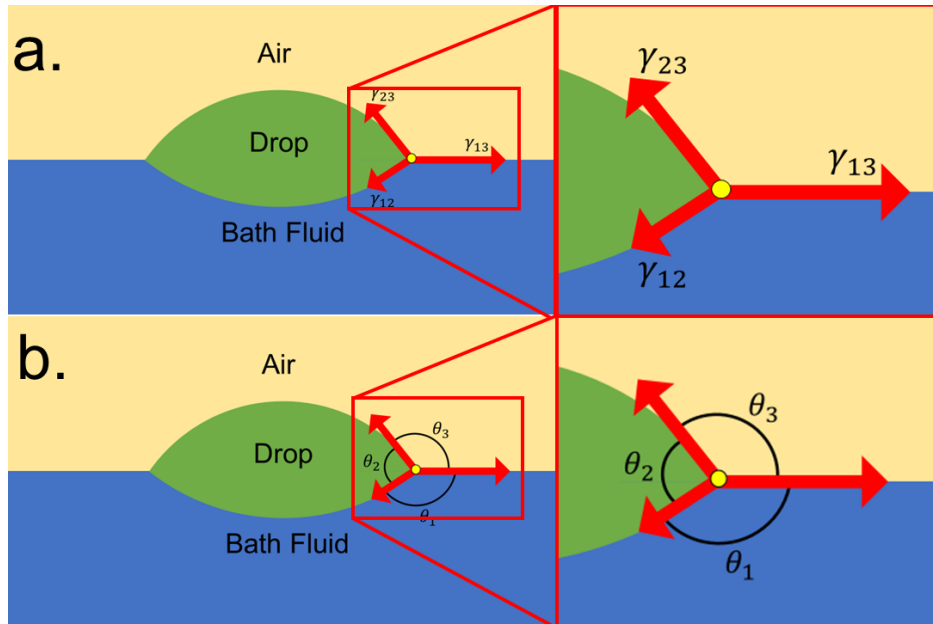
Figure 1.15. a.) A drop floating on a bath in air. The slopes of the surfaces at the triple point (yellow circle) are marked as red arrows. These arrows indicate the direction of each surface tension force. b.) Angles created by the equilibrium of each of these surface forces, in accordance with the Neumann Construction.

Such a mistake could drastically throw off the understanding of a phenomena, or a model created to explain the larger picture. With this in mind, several methods of finding the thickness of films were used to ensure that any thickness measurement was conducted using a process that had the highest likelihood of producing reliable results. The method for finding the film thickness depended on the relative thickness of the film, which was determined during the coating process.

1.5.10.1. Image Analysis

The thickest samples used were above several millimeters in thickness. These samples could have their thickness accurately measured by taking a side-on profile picture of the film and a ruler, to give scale. One such picture is given in Fig. 1.16, where the vertical thickness of the film is measured in three places (red boxes) using ImageJ software (developed by the National Institutes of Health and the Laboratory for Optical and Computational Instrumentation), giving an average height of the film in pixels. This height is converted into real length units by measuring the distance of known measures in pixels. In this case, 1 cm and 2 cm measures are taken from the ruler on the left side of Fig. 1.16, represented by red arrows. These measures were also averaged to create a conversion factor that was multiplied to the average thickness to give the actual thickness.
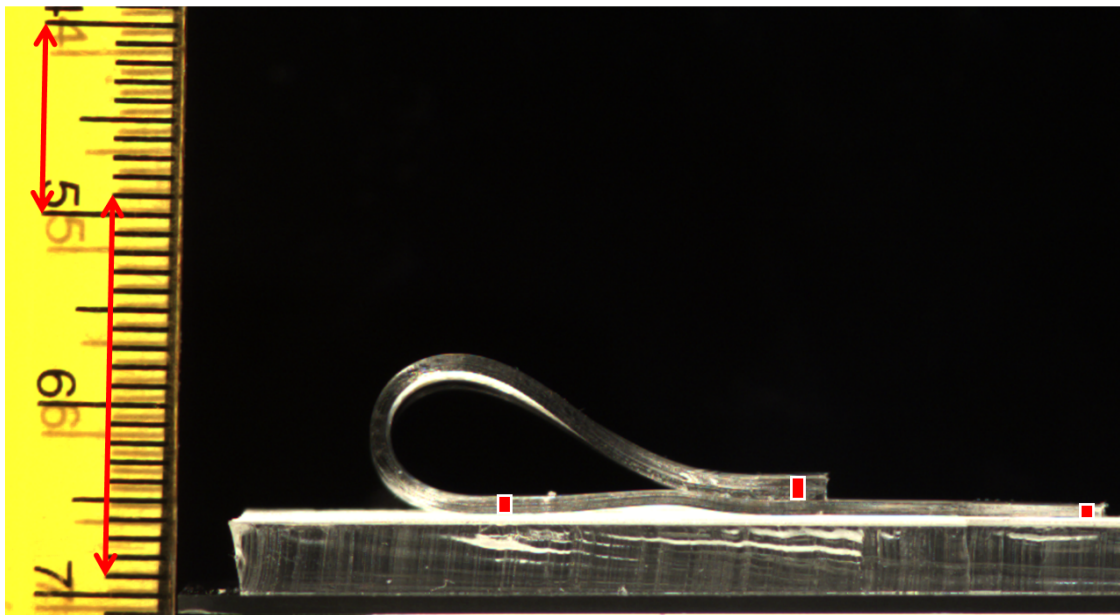
Figure 1.16. Side profile picture of a relatively thick sample and a centimeter ruler. Red boxes indicate where thickness measurements may have been taken. Red arrows indicate where standard lengths were measured to create a conversion factor.

Image analysis was sometimes used to find the thickness of slightly thinner films that had too low modulus to be measured by other methods. For example, polydimethylsiloxane created at a ratio of 40:1 prepolymer to binder would present difficulty when measured with a caliper. The surface would yield when squeezed with a caliper, and no definite thickness would be found. Image analysis eliminates the need to estimate when an instrument actually comes into contact with a soft sample. The thickness of a water drop presents another example of when the material cannot be directly measured. Heights of water drops could be easily and accurately measured in profile using image analysis.

1.5.10.2. Caliper Measurement

Samples that were between 0.1-3 mm thick often had their thickness measured using a caliper (Sylvac Systems-Pro Max). After experimentation, The sample was placed between the jaws of the caliper and the jaws were gently closed onto the sample. This reading was recorded and repeated at least two more times at different locations for each sample. The average of measurements for each sample was recorded as the thickness. Samples with large deviations in thickness were eliminated from the experimental data.

1.5.10.3. Confocal Microscopy

A confocal microscope (Olympus FLUOVIEW FV1000) was used to create 3D profiles of samples that could be used to determine the thickness of samples. This method was used for samples with thicknesses in the range of hundreds of nanometers to hundreds of microns. Measurements were taken at three or more flat areas of a film adhered to a glass slide. Thicker samples (hundreds of microns) were imaged using a 10x magnification lens at an edge of the film. Scans were set up so that both the surface of the glass slide and the film would appear in the same scan along the same focal plane (Fig. 1.17 b). The heights of the top of the film and the top of the glass slide were found by extracting the height voxel (volume pixel) with the highest reflected light intensity for each of these surfaces (Fig. 1.17 a). The difference in these two height measurements was the film thickness. If the surfaces appeared to be at an angle, similar to the surface seen in Fig. 1.17 b, then the equation of the line was found and used to give a height difference of several points which would then be averaged to find the film thickness. A similar method was used to find the height profiles of experimental samples using the confocal microscope. The main difference was that individual data points were not averaged together to create single values for these profiles. Instead, all points along an extracted line were used to create the profile, sometimes with consecutive scans or adjacent points being used to eliminate noise in the data.

Thinner samples were scanned using a 50 times magnification lens (Numerical Aperture 0.95). These scans were through the entire thickness of the sample and slightly into the glass slide. This meant that the intensity values of the reflected light would show a large peak at the height of the top of the sample and a smaller peak representing the height of the top of the glass slide (Fig. 1.17 a). The difference in these two heights (t_{image}) was found and multiplied by the index of refraction of the material (n) to give the actual thickness (t) of the sample (Eqn. 1.42).

$$t = t_{image}n \tag{1.42}$$

Samples that did not have a known index of refraction, could also have their thickness measured using the previous method of scanning a film profile at the edge of the film and comparing the height of the glass slide to the height of the top of the film. Once these values were known, Eqn. 1.42 could be used to find the index of refraction of the material.
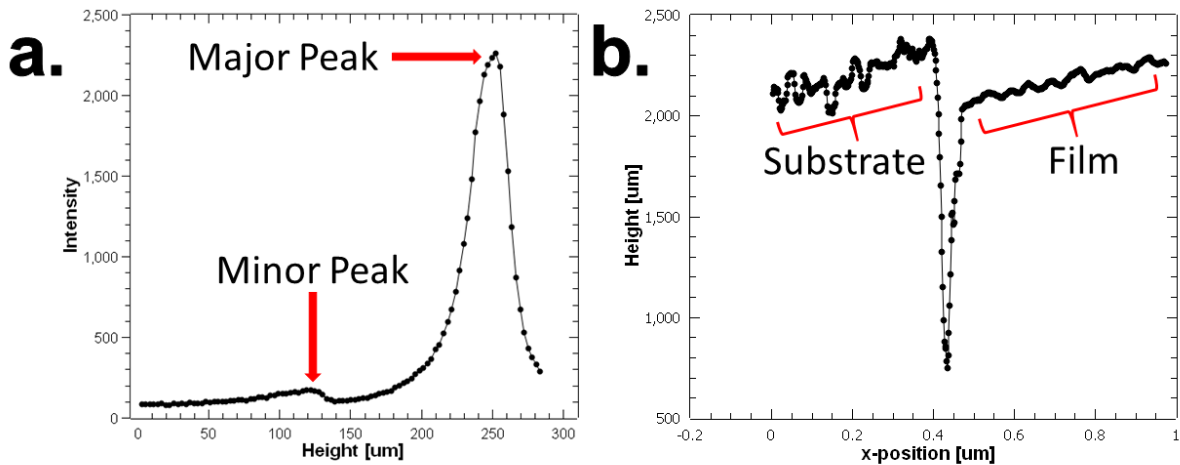
Figure 1.17. a.) Plot of intensity vs. height for a vertical scan through a thin film and its glass substrate. Higher intensity peaks represent flat and reflective surfaces. The major peak represents the uppermost film surface in air. The minor peak represents the interface between the film and glass. b.) A profile of the intensity maxima across the edge of a sample and substrate. The large spike between is the damaged edge of the film.

1.5.10.4. Atomic Force Microscopy

The thinnest samples studied were of the thickness of tens of nanometers. These samples, and any others that were too thin to find an accurate profile for using confocal microscopy were scanned to create a profile using atomic force microscopy (AFM). After samples were created, a small portion of the experimental sample was cut off and floated onto an atomically flat silicon wafer. After drying, a razor blade was used to score a cut into each sample. The sample was placed under the AFM (Veeco Dimension 3100), and the area of the cut was scanned. This gave a profile that included the top of the un-scored film and the surface of the silicon wafer. The difference between these two heights was the thickness of the film, and was averaged with other measurements from a sample to give the reported thickness.

2. MICROSCOPIC DETAILS OF A FLUID-THIN FILM TRIPLE LINE

Author Contribution[†]

2.1. Introduction

Capillary fluid interactions can be (and have been) summarized as fitting into one of two categories depending on the substrate the capillary fluid is acting on. Either a fluid is acting on a solid substrate and the position of the triple point is easily described by the Young-Dupré equation (Eqn. 1.29), or the fluid rests on a liquid substrate and the Newmann Construction (Eqns. 1.30-1.32) describes the surfaces around the triple point. On a solid substrate, only horizontal movement of the triple line is allowed, since the upward component of the capillary force is always balanced by the normal force of the solid substrate. Alternatively, if the the capillary drop is acting on a substrate liquid, the upward capillary force must be balanced by the movement of the substrate fluid. A compliant elastomeric or hydrogel substrate will also follow the Newmann construction. As the elastic modulus of the substrate approaches that of a solid, the upward movement of the triple line diminishes until the upward deformation disappears and the Neumann Triangle Equation becomes the Young-Dupré Equation.

Notably, these expressions do not definitively describe a situation where a thin solid film separates a capillary fluid from a liquid substrate. The upward force of the capillary drop will not be balanced by the normal force of the solid, instead the thin film can bend as it is drawn upwards. This upward bending from the film being drawn around the drop can be convoluted with a wrinkling pattern seen in many recent studies of a capillary drop on a floating thin film.[46, 103, 91, 90] The two-dimensional nature of a spherical cap capillary drop complicates the study of the equilibrium of the forces acting on the triple line. The upward and inward force of the triple line acting on the

---

[†]This chapter is largely based on a paper that was co-authored by Timothy Twohig, Sylvio May and Andrew B. Croll.[134] The original experimental idea and experimental design were contributed by Timothy Twohig and Andrew B. Croll. Timothy Twohig, Sylvio May and Andrew B. Croll worked together to write and revise the mathematical derivations found in this paper. The text of this paper was contributed by Timothy Twohig, Sylvio May, and Andrew B. Croll.
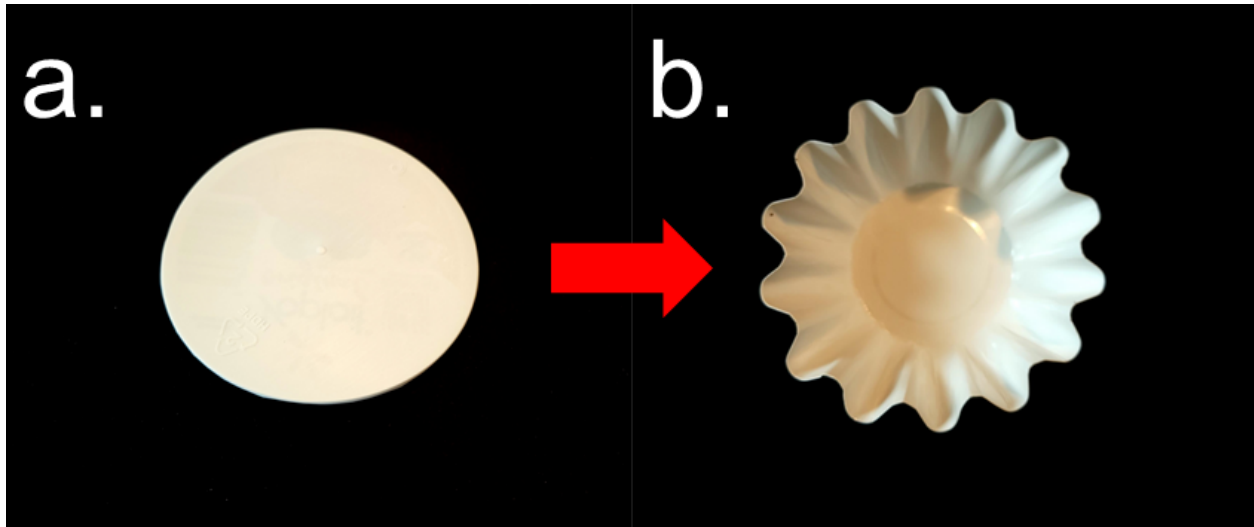
Figure 2.1. a.) A flat circular sheet with no inwards compression. b.) Wrinkled circular sheet from a compression of the outer parts of the sheet.

film (Fig. 2.1a) results in buckling and oscillations to accommodate the increased length of film that is now forced to exist in a smaller radius region (Fig. 2.1b).

The research into this phenomena has led to relations between the capillary force, the modulus and thickness of the sheet, the size of the drop, and the period and length of the wrinkles created. Much work has been devoted to studying wrinkles, but the actual details of the liquid and solid surfaces around the triple line have not received much attention. One reason for this is the difficulty that is inherent in imaging surfaces that consist of a floating solid in the air, floating solid submerged, and a liquid surface in air. The imaging techniques used in the drop on the floating film experiments, take still pictures from above these drops, so there is no vertical scale to determine the ultimate rise of the film. Atomic force microscopy can resolve any one of these surfaces separately, but there is difficulty finding all of the surfaces in a single, nondestructive experiment.

A greater understanding of the interactions between fluids and thin films has become increasingly important in recent years due to developments in smaller and smaller technologies requiring guided assembly of components,[122] sometimes using capillary forces as a nondestructive mode of assembly for even the thinnest and most fragile components.[93, 94, 9, 96, 42] Interest has also grown from the study of the interactions of capillary fluids on compliant substrates, such as hydrogels or elastomeric substrates.[39] These substrates are technically solids, but can be easily deformed by even small forces and tend to act locally more like a fluid substrate when acted upon by a capillary

fluid. An experiment that demonstrates this phenomena involves placing a drop of water on an elastic half-space. Experimentally, this means a very thick substrate of some sort of elastic material. The surface tension of the water drop pulls the substrate upward along the outside of the drop. A high modulus substrate will act more similar to a perfect solid and will not be deformed by the water. The drop will adapt to the shape determined by the Young-Dupré Equation for a fluid on a solid substrate. As the substrate modulus is lowered, the fluid will eventually have enough force to deform the substrate upwards creating a cusp around the drop. This cusp will start as a tiny deformation and grow as the modulus decreases until the equilibrium condition of the Neumann Construction is reached.[119] A particular experiment from Extrand *et al.* (1996) placed a water drop on a very compliant substrate and after a cusp had formed, flash froze the entire setup.[39] This allowed the removal of the water drop, which in turn, allowed the cusp shape to be imaged and profiled directly. This experiment provided an interesting solution to the problem of imaging the effect of a capillary drop, but relies on the assumption that the elastomer does not move or shrink after being frozen. The removal of the water drop also eliminates any possibility of finding the shape of the liquid component of either the Young-Dupré or Neumann Constructions equilibrium. This experiment is compelling, but at most only allows for research of half of the system of a drop resting on a compliant substrate-the compliant substrate part. A more complete experiment is needed to explore both of these components simultaneously and uncover relations that may have been missed.

Soft elastomeric materials and gels are easily deformed by capillary fluids due to their ability to stretch when a force is applied. However, thin sheets can also be easily deformed by these capillary forces through their ability to bend when a force is applied. As sheets get thinner, they become more and more easily bent. Most polymer thin films are easily bent and manipulated by capillary forces such as the surface tensions produced by water or glycerol drops. This means that a relatively small capillary force can cause more extreme bending deformations in a film. This phenomena has been studied by many researchers exploring a multitude of interactions-including a capillary drop placed on a thin film which produced bends of the scale of the sheet.[93, 94, 51] Other projects have produced interesting geometric patterns from capillary drops interacting with thin films.[46, 103, 91, 90] Research into the complete wrapping of capillary drops suggests possible uses of these minute forces for encapsulation or self assembly applications.[89, 57] The main difference between a drop resting on a soft, elastomeric substrate and a drop resting on a thin film is that of

high-modulus films to resist stretching when a force is applied in favor of bending. These same films will be drawn radially inwards by the triple line of a circular drop placed on the surface. This inward force acts to draw the film inwards and upwards along the surface of the drop, working to create a Gaussian Curvature in the sheet. If this curvature is further developed, high-energy deformations known as developable cones (d-cones) may appear. Since this is a high energy process, the system tends towards straight triple lines when possible. This complex "faceted" triple line can obscure the true interactions taking place at the triple line. The research covered in this chapter examines the fluid-air-film triple line of a system that has been forced to adopt a one-dimensional triple line. This configuration simplifies the interaction by eliminating in plane stretching, wrinkling, buckling, and stress localization that occur when a circular configuration is used.[90] In this simplified, one-dimensional configuration a microscopic analysis of a flat and straight triple line is possible, which allows the experimental study of a wide range of systems. From very thick films that tend to follow Young-Dupré relations to the thinnest systems which adopt relations more similar to the Neumann Construction. Interestingly though, we observe that these interactions all behave Young-like at the microscopic scale since locally the triple line tends to represent a fluid interacting with an unstretchable solid. Macroscopic views of these same situations will often suggest a different picture more similar to that of a Neumann Construction. It is shown in this work how the interplay of elastic bending, gravity of fluid, and external tension all contribute to the overall shape of a deformation and the contact angles produced by a capillary drop on a thin film.

The effects of fluid drops on thin film substrates have been studied on the macroscopic scale by many researchers, but bridging the gap between the macroscopic picture and microscopic details of this interaction has received much less attention. A drop resting on a thin film that was, in turn, floating on a water bath was first studied by Russell and coworkers.[46] The capillary forces of the drop draws the film inward and upward along the surface of the drop. This movement is resisted by the surface tension of the bath on the outermost edges of the sheet, but adjustments can be made to the fluids to ensure that the capillary drop is able to overcome this resisting force. One such adjustment is to add surfactant to the bath, drastically dropping its surface tension. The inward movement of the film towards the drop creates a hoop stress in the film; a hoop stress is created when a larger circumference two dimensional object is drawn in and forced to exist in a smaller circumference. If a film is rigid but thin this stress leads to buckling and the creation of wrinkles in

the film. A set of equations known as the Föppl-von Kármán equations can be used to model this system in the limit where film thickness approaches zero and bending energy is ignored.[103, 30] The work done by Russell and coworkers has explained the relation between the wrinkle pattern that is formed by the capillary drop and the material properties of the film.[46] However, the three-dimensional nature of this wrinkling pattern can severely hamper any observations of the film/fluid/air triple line. This becomes even more difficult when the wrinkles are pushed past the point of localization and collapse from many smooth wrinkles to a few sharp out of plane folded features.[90]

Similar studies have explored the relation where a drop is placed on a thin film that has its outer edges secured to a solid substrate, but is otherwise free to move, resulting in the observation of no microscopic buckling.[105, 106, 108, 87, 47] In this case the drop did deform the film underneath it into a parabolic shape; again obeying the Föppl-von Kármán equations in a limit where bending is ignored and stretching of the film is also neglected past the stretching contribution of the secured boundaries.[106] From a macroscopic point of view, these experiments successfully allow the researchers to directly measure the local strain variations in the film,[105, 87] and strain-dependent surface energies of polymer glasses.[108] This measureable success notwithstanding, these studies do not go far enough to explain what is happening at the scale of microscopic (and smaller) lengths in the film where stretching and bending effects may be important.

In this research project, an experiment is described that vastly simplified the circular geometry of the previously mentioned studies down to a one-dimensional configuration. This eliminated the buckling of the film or the need for the film to be secured at the boundaries, while allowing for the relatively simple, direct observation of the shape of a floating thin film when in contact with a capillary drop. Briefly, a glassy polymer thin film (polystyrene or polycarbonate) that is floating on a fluid bath had a second fluid placed on top of the film. This capillary drop was deformed into a relatively long and straight-edged drop by having a glass slide cap forced into contact with the capillary drop, as described in Fig. 2.2. Confocal scanning microscopy was used to locate the surface of the film and the capillary drop in three dimensions, allowing for the microscopic contact angles to be found. The thicknesses of the films were varied revealing that the capillary deformations created by the drop in the film are present even in film 10's of microns thick. Dropping the film thickness
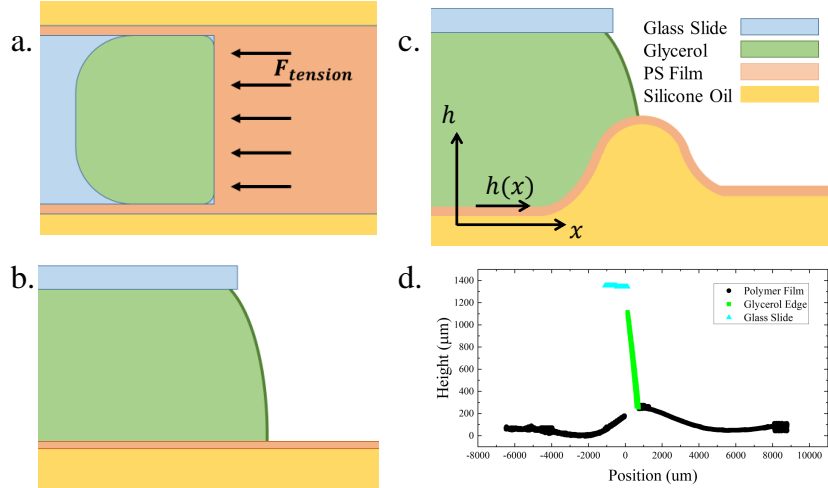
Figure 2.2. Schematic of the experimental setup. a.) Top view of the glycerol drop on polymer film floating on oil bath. Glycerol edge is straightened by the glass slide reducing the problem to one-dimension. b.) Side view of the initial setup of the experiment. c.) Side view of the final state of the experiment. d.) Profile data of a real film extracted from the three-dimensional confocal microscope scan of a 4.3 micron thick PC film. Blue represents the glass surface, green the glycerol surface and black is the film and oil surfaces (oil is the thicker line on the right). The gap in the black curve is due to reduced scattering intensity at this resolution. Note the oscillatory profile is strong evidence that film bending cannot be ignored.

below 1 micron revealed that the contact angles observed shifted towards those predicted by the Neumann Construction for a fluid/fluid/air interface.

The contact of a capillary fluid drop on a solid floating thin film was modeled using a composite of capillary and bending models. A more general way of thinking of the model would be to consider an Euler-Bernoulli beam attached to a Winkler foundation on its bottom side and subject to an upward point load. These models can further the discussion of the experimental findings and offer insight into related soft matter problems. The experimental findings were well represented by these simple models, suggesting that the experimental setup is consistent with a Young-Dupré force balance for a triple line of a fluid on a solid substrate. This is true because the films are locally flat at the point of contact with the fluid. Since this contact point is where the upward force on the film is applied, it is also the highest point of the bent film. The film rises due to the unbalanced vertical component of the fluid's surface tension, but the Young-Dupré equation does not fully describe the rest of the components. An incorporation of the contributions from the film bending, fluid weight, and film tension is also necessary to gain a more complete understanding of the entire one dimensional system. The models highlight several important lengthscales which

van be used to qualify dominant variables in this system. These variables are discussed in relation to several limiting cases which would be impossible to work into an actual experiment, such as tension-free films or zero density fluid substrates.

2.2. Experimental

2.2.1. Film Preparation

Solutions of polystyrene (PS) were created by dissolving bulk PS (Aldrich, Mw = 192 kg/mol) in toluene. To facilitate imaging, Nile Red fluorescent dye (MP Biomedicals, LLC) was added to the solution. The solutions were between 0.1% and 10% PS by weight, depending on the desired film thickness. Polycarbonate (PC) films were created in a similar manner by dissolving bulk PC (Scientific Polymer Products Inc., Mw = 60 kg/mol) in chloroform (Nile Red was also added to these solutions). PC solutions were made between 0.1% and 10% by weight. Thin films were created by spin coating or drop casting the PS or PC solutions onto freshly cleaved mica sheets (Ted Pella, Inc.). Spin coating was used to create polymer samples of thickness 10 nm-700 nm, and drop casting was used to create polymer films of thickness 0.700 μm - 10 μm. Samples were annealed at a temperature of $\sim$ 30 °C above their respective glass transition temperatures. We note, these materials both have high moduli (E = 3.5 GPa and 2.2 GPa for PS and PC respectively) and can be considered almost inextensible.[2]

2.2.2. Film Transfer

The polymer films were cut into rectangular pieces and floated onto a pure water surface (MilliQ, Millipore inc). A slide coated with a high viscosity silicone oil (5100 Cp) and chilled to approximately -20 °C, was gently pressed onto the floating film and removed from the bath taking the film with it. At this point, the film is floating on a silicone oil bath. The sample was allowed to float on the bath overnight in order to relax any stresses that were still present in the film from the floating and lifting process. Film thicknesses were measured by cutting pieces adjacent to the floated films and placing them on silicon wafers. Atomic force microscopy (AFM) was used to measure films of thickness 10 nm-1000 nm. Films thicker than this were imaged with a laser scanning confocal microscope. Reflectance maxima (that corresponded to the top and bottom surfaces of the film) were extracted and were used with the index of refraction for the relevant polymer to find the thickness of each film. Alternatively, the top surface of a film and the top surface of the substrate could be used near a sample edge. No differences were noted between the various techniques.
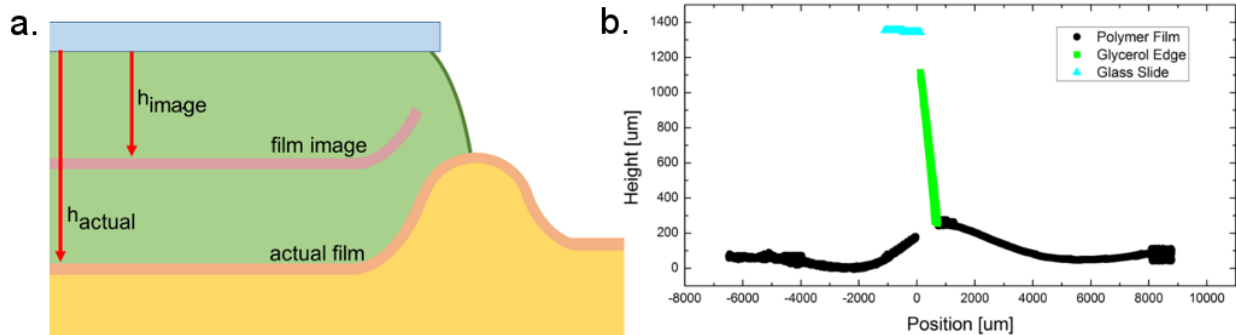
Figure 2.3. a.) Illustration of the measurements taken to adjust the apparent height position of the submerged film to its actual height. b.) Profile of an experimental setup with corrected height data for the submerged film.

A solution of glycerol (99.9% Fisher Chemical) and fluorescent dye (fluorescein sodium, FUL-GLO) was created. A few drops of glycerol solution were deposited on the top of a film floating on (now room temperature) silicon oil, about 1 cm away from the oil-film edge. To create a flat, elongated contact line, a glass slide with an edge parallel to both the film edge and the glycerol line, was placed in contact with the glycerol drops. The geometry is shown in the schematics of Fig. 2.2a,b. The setup was allowed to equilibrate over two hours, resulting in the state shown in Fig. 2.2c. The system was then scanned in three-dimensions using confocal microscopy (Olympus FLUOVIEW FV1000), from which the film and glycerol surfaces could be located (Fig. 2.2d).

Any of the surfaces imaged through a transparent liquid or solid appeared to be shifted upwards due to the index of refraction of that transparent material being different than air. This included the film surface submerged under the glycerol and glass slide. To find the film's actual position, the Eqn. 2.1 was used with the observed film height position (h_i), the depth of the glycerol drop (d), and the index of refraction of the glycerol drop (n) to find the film's actual height position (h):

$$h = d - (d - h_i)n \tag{2.1}$$

The variables are illustrated in Fig. 2.3a, showing which direction all measurements were taken. The slide was set as the zero position and positive lengths were below the slide. Fig. 2.3b gives a profile of the relevant surfaces involved in this experiment: the glass slide (blue), the film surface (black), and the glycerol edge (green).
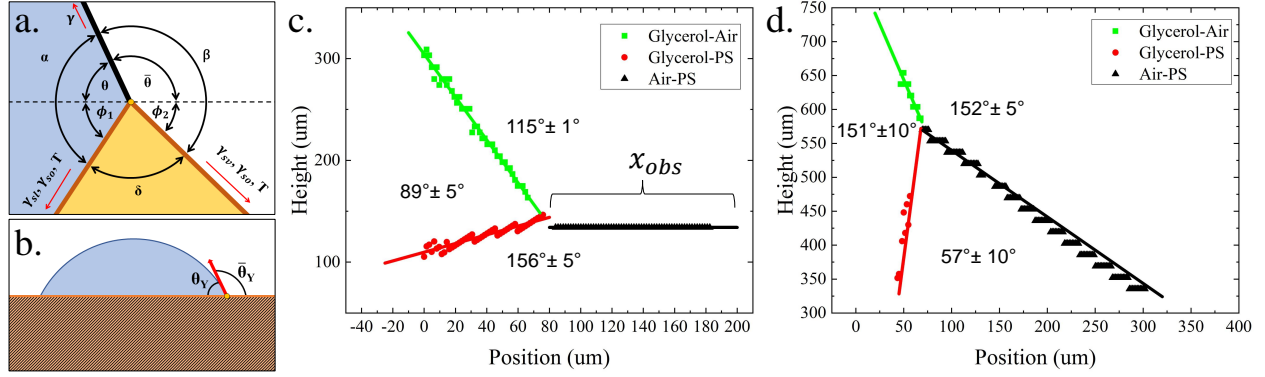
Figure 2.4. Surfaces around the triple line. a.) Schematic defining the various angles discussed in the text. b.) The Young-Dupré limit for reference. c.) Experimental measurement of the triple line in a thick (3.4 μm) PS film. Green represents the glycerol surface, black represents the film surface outside the fluid, and red represent the film surface below the glycerol. Solid lines are linear fits over the distance x_{obs} used to determine the angles at the triple line. For comparison, x_T for this film is 7.7×10^{-4} m. d.) Similar measurement with a much thinner film (185 nm). The relative position of the polymer film has changed, while the fluid surface remains in a similar position. In this case, x_T is 9.7×10^{-6} m. Each of the surfaces in c.) and d.) were found by fitting a line to the intensity maxima for that coordinate. The error associated with this fit was found using the "LINEST" function in excel. The error of the three lines was used to find the error of other measurements in the height of the triple point or the angles between surfaces.

The thickness of the glass is exaggerated in Fig. 2.3a, and was actually much smaller than the height of the glycerol drop, so it was neglected in the calculation. The surface represented by the blue line in Fig. 2.3b is the top of the glass slide, and since the index of refraction of glass is also quite close to the index of refraction for glycerol the error from this assumption was minimized.

2.2.3. Data Processing

Intensity data was processed using ImageJ software and an algorithm to extract the peak intensity for each vertical slice in the three-dimensional scans. Reflectance and fluorescence channels were separated, allowing discrimination between the glycerol, glass slide, and polymer film surfaces. The height coordinate of submerged portions of films was then corrected to account for the refractive index of glycerol. An example profile with the corrected film heights is given in Fig. 2.2d. This profile data was used to find the height difference between the oil bath (far right of the film data) and the peak of the deformation.

The relative angles of the glycerol-air interface, film in air, and film submerged in glycerol were extracted from the slopes of the data for these surfaces near the triple point. While data sets span several millimeters, data is often curved on these large scales and therefore fitting the entire

dataset with a linear function would be extremely error prone. To avoid the curvature, we focus on a small region starting at the triple line and extending outward along each interface. Specifically, data from the triple point to a distance of ∼40 pixels away along the glycerol surface (∼65 μm) is fit. While a distance from the triple point to ∼75 pixel along the polymer surface (∼120 μm) is used for fitting. We refer to this length as the observation length for convenience, and denote it with the symbol x_{obs}, which we show in figure 2.4. The number of data points was selected in order to minimize distance from the triple line, while incorporating enough data points to account for noise in the measurements. Obvious out-lying data points were removed by hand (caused by intensity fluctuations for example). Occasionally, the data within x_{obs} of the triple line was indeterminate when fitting an intensity peak. In this case, the data nearest to the triple line where an intensity peak could be reliably fit was used to determine the slope, with the error calculations being adjusted to reflect the shift away from the ideal measurement location. The slopes of the linear fits to the glycerol surface and the polymer surface data were used to calculate the relative angle between the glycerol and polymer surfaces.

2.3. Results and Discussion

A droplet of glycerol placed on top of a thin film will pull upwards and inwards on the film's surface, deforming the film into the curved shape shown in Fig. 2.2d. The tension created by the glycerol surface is balanced at the triple line by the interplay of the outward pull of tension in the film, the change in surface energy of the film as the glycerol spreads, and the weight of the fluid displaced below the film. These quantities are also intrinsically linked through bending in the plate as it deforms to accommodate the force balance. If the film is thick, bending becomes the dominant energy, the plate remains flat, and the lift generated at the triple line is balanced by the weight of the fluid beneath the entire plate. If the film is very thin, bending is less relevant, and the amount of fluid lifted is determined by the capillary length ($\sqrt{\gamma_f/\rho g}$, where γ_f is the film's surface energy, ρ is the oil density, and g the gravitational acceleration). We note that in this geometry gravity and bending cannot be ignored in the thin film limit. The main purpose of this paper is to clarify this complex interaction.

Fig. 2.4 shows the surfaces near the fluid/film contact line for a typical thick (3.4 μm) and thin (185 nm) PS film. As it is of macroscopic convenience to discuss contact angles at a triple point, three angles at the contact line are directly measured, α, β, and δ. We sub-divide α and β into a

Figure 2.5. θ as a function of film thickness. Both polystyrene and polycarbonate films show relatively constant behaviour. The average angles are 71±7 ° and 69±9 ° respectively.

portion above, θ, and below, ϕ, the horizontal for convenience (Fig. 2.4a). Because we are focusing on small distances from the contact line, angle measurement can often be poorly defined because of the non-zero curvature near the film maxima (note this exact point is made by Davidovitch *et al.*[30]). Care must be taken in comparing an apparent angle with any theoretical predictions. We extract angles from theory (discussed below) in the same way as we approach experimental data in order to maintain consistency.

In a thick film (Fig. 2.4c), the angle β approaches a value of 115°, which is very close to what we measure independently with a sessile glycerol droplet on solid PS film (a PS film of ~ 200 nm which has been spin-coated on an atomically flat silicon substrate, see the subsection on contact angles of drops on solid substrates). Contact with a thick film can be treated exactly as in the bulk; the contact angle is a result of a horizontal force balance which is independent of any tension in the film caused by external means. In short, the film shows the classical balance of the Young-Dupré law, $\gamma_{sl} + \gamma \cos(\theta_Y) = \gamma_{sv}$, where γ_{sl} and γ_{sv} are the surface energies between the fluid and solid or solid exposed to air respectively and γ is the glycerol surface tension.

57

As the film thins, the bending energy is reduced and the contact line deforms and lifts the film, resulting in the angles α and β growing (Fig. 2.4d). To clarify, α is not equal to θ_Y, and the air-film interface is not horizontal as is often the case with higher tension free-standing films.[87, 47, 105, 107] The glycerol surface, however, remains at a fairly constant angle with respect to the horizontal (see Fig. 2.5). The measured angle is consistent with θ_Y determined from traditional sessile drop experiments ($\theta = 71 \pm 7°$ for PS and $\theta = 69 \pm 9°$ for PC measured in our experiment). This suggests that the fluid shape is determined by the Young-Dupré balance on a scale much smaller than the local radius of curvature of the film; a lengthscale where the thin polymer film is still effectively flat and horizontal.

If the hypothesis that θ is always equal to θ_Y (or any constant) is correct, creating a force balance with observed angles and surface energies becomes problematic. Consider the result of a horizontal force balance, $\gamma \cos(\theta_Y) + (T + \gamma_{sl} + \gamma_{so}) \cos(\phi_1) = (T + \gamma_{sv} + \gamma_{so}) \cos(\phi_2)$, where γ_{so} refers to the surface tension of an oil/film interface, T to the tension acting on the ends of the plate, and the other variables remain as defined above. The relationship between the two angles ϕ_1 and ϕ_2 is further constrained by the vertical force balance, $\gamma \sin(\theta_Y) = (T + \gamma_{sl} + \gamma_{so}) \sin(\phi_1) + (T + \gamma_{sv} + \gamma_{so}) \sin(\phi_2)$, ultimately permitting a single solution (the Neumann solution). How then can the measured angles ϕ_1 and ϕ_2, which clearly vary with film thickness (see fig 2.4) be explained? Either we do not observe the true angles (ϕ_1 and ϕ_2), the measured constant value of θ is somehow incorrect (and θ is not θ_Y), or there are more than just surface forces acting at the triple point.

To proceed, we focus on the directly measured angle β, which is plotted as a function of film thickness in Fig. 2.6. The data shows a smooth monotonic increase in β as films thickness decreases for both PS and PC films. The good overlap of both materials is consistent with their similar surface energies and material properties, and is also a sign that films are undamaged during processing and over the course of the experiment. There are two independent physical limits for β. First, β must approach $\bar{\theta}_Y = \pi - \theta_Y$ at large thicknesses where the film does not bend. Second, in the absence of bending energy and external tension acting on the free end of the film, the film will come into self contact and $\beta = \pi/2 + \bar{\theta}_Y$. Measurements seem to indicate that this second limit is never reached experimentally. As discussed above, a simple force balance is insufficient to describe how β relates to surface forces, bending, and applied tension because a force balance does not include a moment balance around the triple line. The failure of simple force arguments is

clear in the experimental variation of β with film thickness; no external forces or surface energies are related to thickness changes - only the bending moment relates to thickness. A comprehensive approach which correctly accounts for bending moments, external tension and substrate density is required to correctly describe observed contact angles.

Assuming the horizontal force balance occurs to set the contact angle locally, we treat the glycerol surface as a vertical line force of magnitude $\gamma \sin \theta_Y$ and model the system as a Euler-Bernoulli beam on a Winkler foundation.[33] The foundation stiffness is determined by the density of the oil bath, ρ and an external tension is supplied to the plate by the surface tension of the oil, T, pulling on the free end of the film. The result is the fourth order differential equation:

$$EIh''''(x) = \gamma \delta(x) + Th''(x) - \rho g h(x), \tag{2.2}$$

where $h(x)$ represents the position of the film, E is the Young's modulus of the plate, and $I = t^3/12(1-\nu^2)$ is the second moment of inertia per unit width. Film thickness and Poisson's ratio are denoted by t and ν, respectively.

Scaling analysis of Eqn. 2.2 reveals two important lengthscales. If the tension term is much larger than the gravitational term, we find the problem to be scaled by a length of $x_T \sim \sqrt{Et^3/T}$ (as has been pointed out for free-standing films).[47, 105] In the opposite limit, we find a gravitational length of $x_G \sim (Et^3/\rho g)^{1/4}$ to dominate the problem.[17] Comparison of the two lengthscales defines a cross-over thickness, $t_c \sim (T^2/E\rho g)^{1/3}$, where the behaviour changes from gravity to tension dominated. Using the plane strain modulus of polystyrene $E = 3.9 \times 10^9$ Pa, the density and surface tension of the oil (1110 kg/m and 22 mN/m respectively) we predict a transition thickness of $t_c \sim 2.2\mu$m, which matches the thickness at which β deviates from the solid film limit observed experimentally.

If bending is ignored in Eqn. 2.2, a capillary length, $x_C \sim \sqrt{T/\rho g}$, emerges from a similar scaling analysis. Remarkably, the capillary length is equal to the gravitational and the tension lengths at t_c, highlighting the interdependence of externally applied tension, film bending, and gravity in the problem. Nevertheless, the contact angles are determined by the smallest observable lengthscale, which in this case is x_T when $t < t_c$. Bending cannot be ignored at experimentally relevant thicknesses (x_T is still greater than a micron for a 50 nm thick film). Even if the film were

59
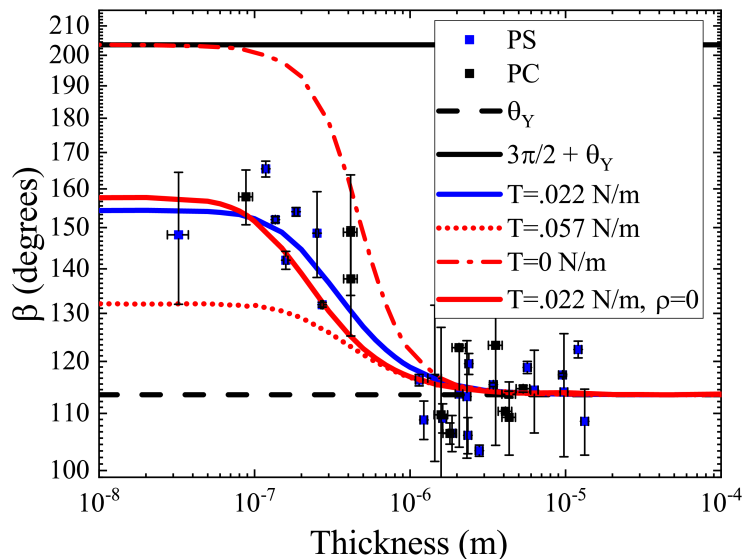
Figure 2.6. The external angle β as a function of film thickness. Data for PS films (blue squares) and PC (black circles) are shown along with the output of the numerical model (red curves). The self-contact limit (solid black line) and the solid film (Young) limit (dashed black line) are also shown. The error bars were calculated from the standard deviation of thickness measurements for the x-error. The y-error bars were calculated from the uncertainty of the errors associated with fitting trend lines to the air-glycerol and air-film surfaces using the "LINEST" function in Excel.

free of external tension, bending cannot be ignored because $x_C > x_G$ hence x_G is dominant at the contact line.

To gain further insight, we solve Eqn. 2.2 as a boundary value problem, and compare the numerical result with the experiment in several different ways. In Fig. 2.6 we overlay the previously discussed experimentally measured β values with the model predictions as a function of film thickness. Again, the angle was "measured" from numerically calculated shape profiles, which we show in figure 2.7. Here the model is compared to a typical thin and thick film (figure 2.7 a,b and c,d respectively). Finally, the last observable of note is the maximum height of the film which we show in figure 2.8 as a function of film thickness alongside experimental measurements. We numerically calculated four different curves, each motivated by different physical scenarios which we discuss in detail below. We note that the glycerol weight does shift the negative infinity plate boundary downwards, which can influence the apparent value of α, but has little baring on the overall peak height or the exterior angle β. Hence, we elect to use symmetric boundary conditions throughout (e.g.$h(\infty) = h(-\infty)$) in order to keep the analysis simple and focused on the contact point.

First, we calculate the zero gravity limit which eases comparison with existing free-standing film experiments ($\rho = 0$). The gravity free curve, assuming the external tension is still supplied by the oil phase surface tension, does fit the angular data. However, it is clearly not physically related to our experiment as can be seen in its profile (Fig. 2.7) or peak height (Fig. 2.8). The angular data smoothly changes from solid like (nearly constant) to a second limiting value as film thickness decreases. The transition at the lower thickness occurs because x_{obs} becomes greater than x_T, meaning the observation is not of high enough resolution to be influenced by x_T. It is now determined by a second lengthscale (in this case, the plate size L). The shape taken on by the film in the absence of a fluid substrate is nearly triangular; flat with an upward slope far from the contact line, curving only at a lengthscale comparable to x_T. The peak height is quite high (especially for thin films), and is strongly related to overall film length and the applied tension. The discrepancy between the measured and simulated peak heights is a clear sign that gravity plays a role in our experiment, whether films are thick or thin, and a zero gravity approximation is not applicable.

Next we consider the contact line in the absence of an external tension (often the limit in which surface energies are measured[47, 87, 105]). Here we find β is considerably overestimated in comparison with the data, especially in the thin film limit where the film has come into self contact. In this case, as thickness decreases and x_{obs} falls below x_T, the film shape is governed by the gravitational lengthscale, x_G. The result is an increased drive to narrow the peak width. At larger thicknesses the angle approaches $\bar{\theta}_Y$ as is expected. The height of the lifted region of film (Fig. 2.8) follows a single power law, again deviating from the data considerably in the thin film limit. The power law can easily be explained by using the scaling length derived above, x_G, in combination with Eqn. 2.2 to derive a natural height $h_G \sim \gamma(\rho g)^{-3/4}(EI)^{-1/4}$. The agreement with the scaling clarifies how gravity plays a critical role over the entire range of film thicknesses in the zero tension limit.

Finally, in solid blue we show a curve generated using externally measured values for γ, T and ρ. This curve fits both the measured β (Fig. 2.6) and also fits the height data quite well (Fig. 2.8), with no additional free parameters. While not inconsistent with a low thickness β plateau, the data does not show a clear transition to 'thin'. This is likely due to the low brightness levels and tiny peak widths increasing error in our experiments coupled with the fragile nature of extremely thin films (fewer experiments survive processing). The height data is much more reliable in the thin film limit,
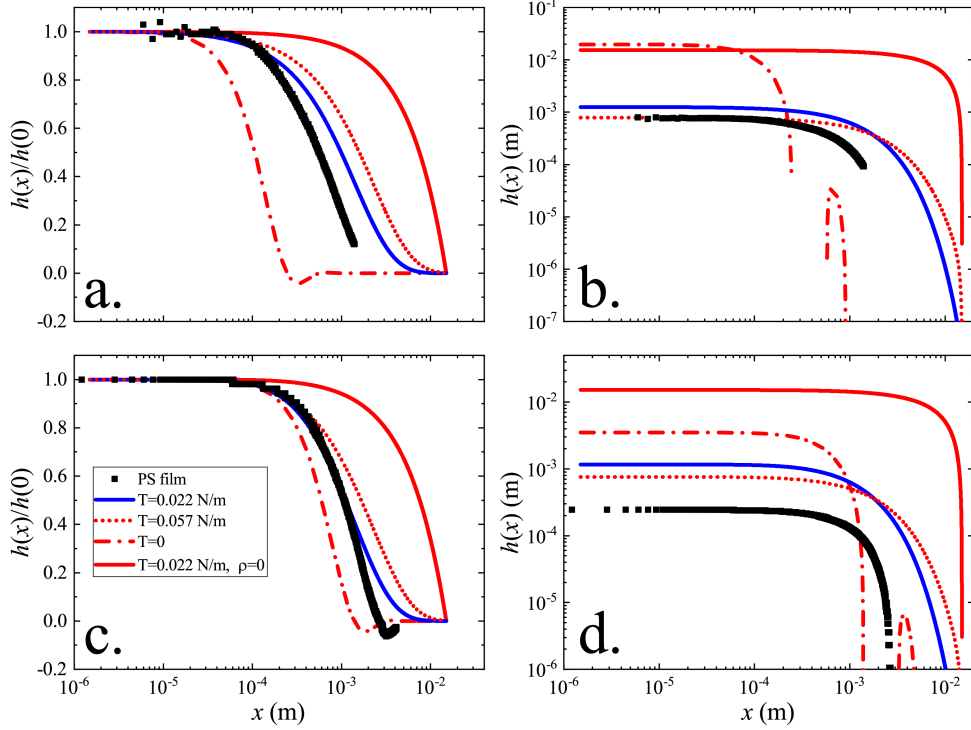
Figure 2.7. Height as a function of position for ~ 100 nm (a,b) or ~ 1 μm (c,d) films. Figures a. and c. show a linear-log plot in which height has been normalized by its maximum value, in order for all curves to be visible. Figures b. and d. show the same data but with the height unnormalized and a log-log axis, again to facilitate viewing of all curves. a. and b. show data from a 200 nm PS film (black squares), and c. and d. show data from a 1.5 μm film (black squares again). Data shows good agreement even though none are "fit" by the model.

but shows some deviation in the thick film limit (where β shows good agreement with the model). This is due to a combination of experimental effects, including plate lengths being comparable to the contact region width, and the weight of the fluid resting on the film altering the boundary conditions (we use symmetric hinge boundaries and large plates in the model). We additionally show model predictions for a film with a slightly larger tension to highlight the sensitivity of the experiment. In this case the low thickness β plateau occurs at a lower angle which is inconsistent with the data.

The beam model of Eqn. 2.2 can be supplemented by calculating similar height profiles from a free-energy based capillary model. This method has the advantage of producing simple, analytic results for various measured properties and removes some of the complexity of a full continuum theory. This capillary model is constructed to describe the free energy of a fluid resting on a thin
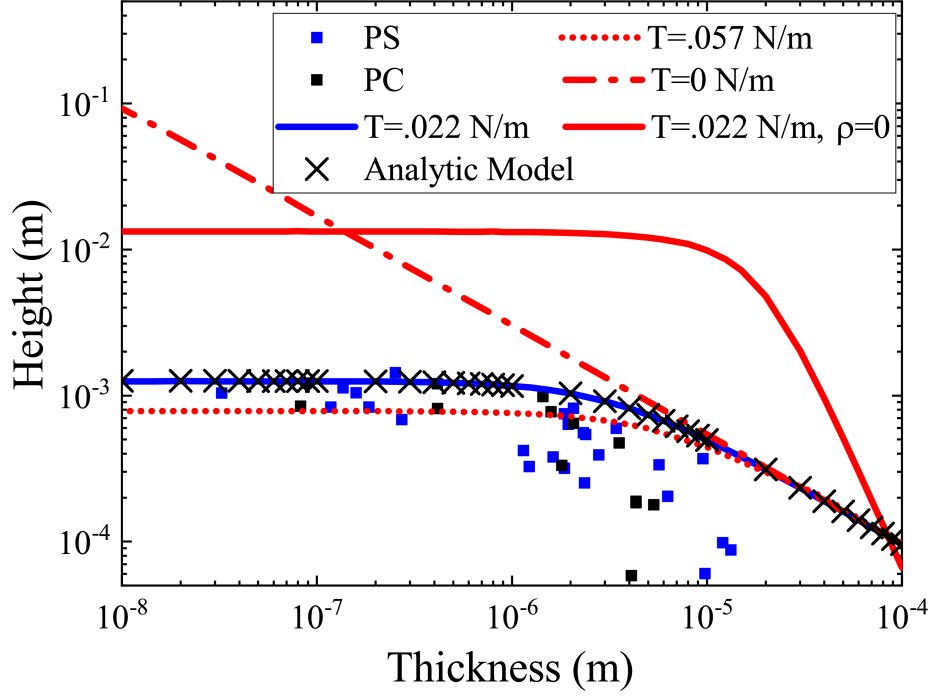
Figure 2.8. Maximum height of the triple line as a function of film thickness for PS (blue squares) and PC (black circles) films. Numerical model results are shown for zero gravity, zero tension, and two other possible external tensions. Analytic model results are shown as X's.

film in one dimension. Minimizing the difference in free-energy per unit width before and after the film is deformed allows analytic solutions to be developed in several useful situations. From this point of view, each surface contributes a term to the free energy which is proportional to its surface energy, and its surface area, A. For example, the fluid resting on top of the film has a free energy, $\int \gamma dA$ which can be reduced if the film is lifted and decreases the fluid/air interfacial area. The fluid bath beneath the film is lifted if the film is deformed above the horizontal plane and thus contributes a term proportional to the height of the deformation and the density, ρ, of the fluid bath ($\rho g \int dx \int h(x) dh$). The bending of the film as it is lifted also adds energy per unit width of film, $U_B = B/2 \int \kappa^2 dx$ where κ is the film's curvature, $B = EI = Et^3/12(1-\nu^2)$ is the bending modulus with film thickness t and Poisson ratio ν. Assuming, for simplicity, the problem is symmetric about the origin $x = 0$ and all deformations are small, the total change in free energy per unit width can be written:

$$\Delta F = -\gamma h_0 + \frac{\gamma_S}{2} \int_{-\infty}^{\infty} h'^2 dx + \frac{\rho g}{2} \int_{-\infty}^{\infty} h^2 dx + \frac{B}{2} \int_{-\infty}^{\infty} h''^2 dx, \qquad (2.3)$$

63

where h_0 is the film height at the origin (we assume a purely vertical fluid surface lifting the film), γ is the surface tension of the top fluid, and γ_S is the net surface energy change of the film and oil interface. Using the capillary length, $x_C = \sqrt{\gamma_S/\rho g}$ and the gravitational length $x_G = (EI/\rho g)^{1/4}$, Eqn. 2.3 can be simplified to:

$$\Delta F = -\gamma h_0 + \frac{\rho g}{2} \int\limits_{-\infty}^{\infty} \left[x_C^2 h'^2 + h^2 + x_G^4 h''^2 \right] dx. \tag{2.4}$$

Eqn. 2.4 is minimized when the differential equation,

$$h - x_C^2 h'' + x_G^4 h'''' = 0, \tag{2.5}$$

is satisfied. Subject to the symmetry requirement $h(x) = h(-x)$ and the boundary conditions $h(0) = h_0$, $h'(0) = 0$, $h(x \to \infty) = h'(x \to \infty) = 0$ the solution for $x \geq 0$ is given by

$$h(x) = \frac{h_0}{w_1 - w_2} \left(w_1 e^{-w_2 x} - w_2 e^{-w_1 x} \right), \tag{2.6}$$

where the inverse lengths w_1 and w_2 are related to the two rival lengthscales x_C anbd x_G through $w_1^2 w_2^2 = 1/x_G^4$ and $1/w_1^2 + 1/w_2^2 = x_C^2$. Inserting the solution back into ΔF and minimizing with respect to h_0 yields for the optimal height at the origin.

For the sake of clarity, we only focus on the maximum height of the deformation and contact angle (β) in this work. Assuming a zero derivative boundary at the deformation peak (consistent with our interpretation of the true contact point), we find the peak height as a function of thickness to be:

$$h_0 = x_C \frac{\gamma}{2\gamma_S} \frac{1}{\sqrt{1 + 2(x_G^2/x_C^2)}}. \tag{2.7}$$

where γ_s is the surface energy associated with moving the plate upwards and increasing the surface length. Because the plate's extension is tiny, we ignore any change in plate length and associate γ_s with T the surface tension of the oil bath. Eqn. 2.7 is plotted in Fig. 2.8 alongside earlier numerical results, and the agreement is near perfect. This shows that there is no difference between energy-based or force-based models, and again highlights the interdependence of gravity, tension, and bending in our experiment.
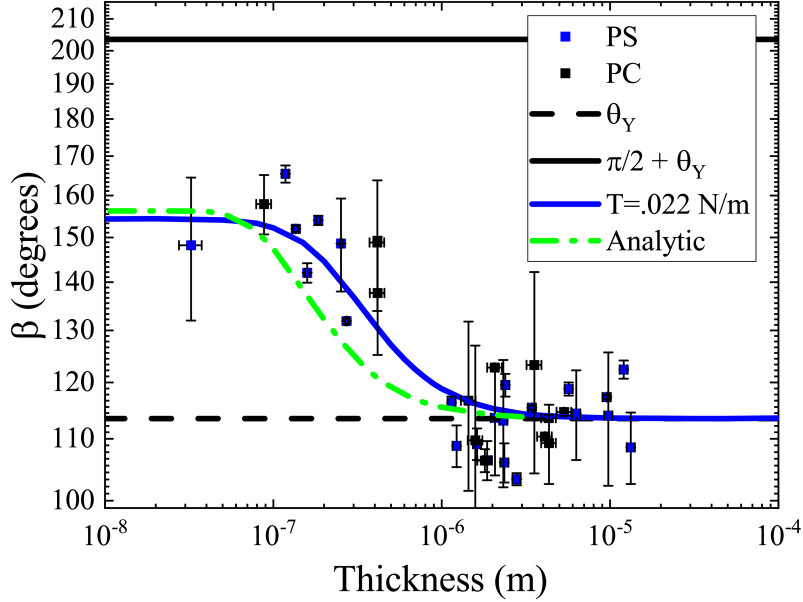
Figure 2.9. The external angle β as a function of film thickness reproduced to clarify demonstration of the analytic theory discussed in the text. Data for PS films (blue squares) and PC (black circles) are shown along with the output of the optimal numerical model (blue curve). Analytic theory calculated with a 5μm observation length is shown by the dash-dotted green curve.

A second useful expression, the slope of the curve, allows a determination of any apparent contact angle of interest. The slope of Eqn. 2.6 is simply its derivative, given by

$$h'(x) = \frac{h_0}{w_1 - w_2}w_1w_2\bigg(-e^{-w_2x} + e^{-w_1x}\bigg). \qquad (2.8)$$

For example, we use Eqn. 2.8 to calculate a contact angle for films of thickness ranging from 3 μm to 10 nm at a point $x = 5$ μm, which is shown in figure 2.9.

The contact angle in this model is simply θ_Y by construction (e.g. the zero derivative boundary condition at the deformation peak). However, as experimental angles are measured a distance away from the true contact line (x_{obs}), the true contact angle is not observed directly. Again, as with the numerical model, we can derive an apparent angle from the predicted curve shape. In this case, we can proceed analytically by using the derivative of the film shape (shown in the Eqn. 2.8) calculated at x_{obs}. Fig. 2.9 shows the resulting β plotted alongside the PC and PS data with the numerical "fit" to ease comparison. The analytic result is in good agreement with the numerical model and what is observed in the experiment. The two results do not prove that the

true contact angle is always θ_Y, but do show that the experiments are at least consistent with this hypothesis.

2.4. Conclusions and Future Work

We have examined the microscopic details of a fluid/thin-film contact line using confocal microscopy. We find that gravity, external tension, and bending are all important in the region of film thicknesses examined ($\sim 1 \times 10^{-8}$ to $\sim 1 \times 10^{-5}$ m). The experimentally measured angles, film shapes and peak heights show good agreement with with a Euler-Bernoulli beam or an equivalent, analytic, capillary model. Our results show that a tension only force balance, as in the Neumann construction, is not possible over most of the range of our experiments. Films with thicknesses above 100 nm have too much bending to consistently satisfy such a model, largely because the concept of a contact angle is ill defined. We suggest that, a Young-Dupré force balance always takes place on an extremely local scale (though a scale larger than molecular sizes). The contact may not be observable if the radius of curvature of the film falls below optically observable lengthscales. As film thicknesses increase, so does the radius of curvature, which leads to imprecise contact angles which are not useful in determining a force balance. Eventually, bending completely dominates, the film remains globally flat, and a Young-Dupré horizontal force balance is macroscopically observable.

Going forward, this work could be furthered by an in-depth study of different materials. The films used here were glassy, plastic polymers floating on a bath of silicone oil. This bath meant that the use of common silicone elastomers for films was likely to have altered results from adsorption into the film. Changing the bath to a different liquid would eliminate this danger. Water was not used in this experiment due to its volatility and tendency to evaporate on the timescales of study, but water is the ideal high-tension liquid to use in a capillary study. Water is also largely not absorbed by silicone elastomers. A different experimental design is needed to suppress evaporation while continuing the rest of the experimental procedures. The use of a different fluid for the bath could eliminate the observed contamination of liquids by the leeching of silicone oils. Pure liquids have known interactions and could give more reliable results using a similar experimnetal setup.

Computer modeling of this interaction could also prove useful in determining the molecular interactions at the triple point when there is a very sharp bend in the film. Such a bend would require an extremely thin film, which increases the difficulty of every facet of the experimental procedure. However computer models are uniquely suited to handle this difficulty of an impossibly

thin film. As technology continues to push towards smaller and smaller components, this knowledge will prove more utilitarian.

3. ADHESION DIRECTED CAPILLARY ORIGAMI

Author Contribution[‡]

3.1. Introduction

As problems in science and engineering have become more complicated, researchers have often found success by looking for solutions in seemingly unrelated areas. Consider, for example, the significant progress made toward solving many packing and deployment problems that has been inspired by the ancient art of origami.[135, 78, 61, 92, 131] Traditional origami involves folding thin (two-dimensional) paper sheets into three dimensional aesthetically desirable structures. The paper structures are stable due in large part to the irreversible folds and creases created during the assembly process. Constructing the origami structures requires the repetitive application of steps such as lifting, bending, creasing, and partial unfolding of portions of a sheet. Variants of these basic steps, have lead to advances in solar cell deployments[120, 20], impact mitigation systems[136], robotics[67, 98], batteries[114, 24], artery stents[58], and guided assembly.[86, 6, 50]

The success of origami inspired design at the macro-scale has caused the natural progression of the technique towards the micro and nanoscales.[22, 23, 19, 84, 96, 10] Downsizing is especially attractive to the medical field for the purposes of tailored drug delivery[22, 5, 40] and other microscopic medical devices.[58, 52] However, as the sheet materials are scaled down new difficulties arise due to the increased importance of surface interactions. In particular, adhesion due to the ubiquitous but weak van der Waals forces tends to complicate folding as contact becomes irreversible. Adhesion is ignored in macroscopic sheets because they are rigid enough that adhesive interactions lead to little deformation of the sheet and therefore little true contact between sheet surfaces. However, as a sheet's thickness, t, becomes small, sheets are more easily bent by adhesive interactions between substrates, actuators, and themselves. With respect to origami-inspired design, the consequences require that any force or object used to manipulate a micro-scale film must be strong enough to overcome adhesion, but at the same time must be gentle enough to avoid tearing or otherwise dam-

---

[‡]This chapter is largely based on a paper that was co-authored between Timothy Twohig and Andrew B. Croll.[133] The original experimental idea and experimental design were contributed by Timothy Twohig. Timothy Twohig and Andrew B. Croll worked together to write and revise the mathematical derivations and text of this paper.

aging the thin film. Furthermore, any manipulator used to create a particular pattern must not only firmly hold the film but also release the film on demand.

Capillary forces have offered an interesting solution to some of the issues of manipulating and joining materials at the micro and nano-scale.[93, 9, 97, 59] In the so called "capillary origami" process a thin film is cut to a desired shape and then laid on an adhesion free substrate. Placing a liquid droplet on the film drives folding as the surface tension of the drop draws the thin film upwards and around the volume of the drop.[93] Most commonly the fluid is water due to its relatively high surface tension, however, liquid metal can also be used to actuate thin plates.[45, 66, 22] Often, actuation points (hinges) are designed into the film to enable more localized bending and sharper origami-like geometric structure.[45, 66, 22, 95, 64, 63] When the drop evapourates, no residue is left behind and the film relaxes back to its initial state, unharmed. Capillary origami has thus far allowed the creation of many geometries, especially polyhedra [45, 93, 22, 66], but it still fails to achieve the full potential of origami designs. This is because complex, bistable origami structures require multi-step assembly processes which cannot be achieved with a single fluid drop.

Closely examining the steps for the creation of an origami model reveals that repetition of only two actions are needed to create a non-trivial sculpture: 1.) A force is applied such that it causes a film to lift from a substrate and to bend. 2.) The bend is held in place (creased) enabling additional steps to occur.[60] Using paper origami as an example, the first step involves the artist's fingers and the second step is accomplished by fingers driving the curvature to localize and create a plastic defect (a fold). Careful alignment of where folds are placed and repetition opens the door for a multitude of origami shapes. Unfortunately, capillary forces alone are usually insufficient to create plastic damage in a sheet.

In this work we explore how adhesive forces, which are typically removed in order to enable capillary origami, are in fact the key tool needed to overcome the limitations of single-step capillary driven origami assembly. We conduct simple experiments to show how and when capillary forces can become strong enough to peel a film from a substrate (see Fig. 3.1 and Fig. 3.2). We show how self-adhesion represents a new mechanism that can be used to "fix" sharp bending in a desired position. We note the importance of peel-mechanics in both of these processes, and show how the peel front (crack tip) can be guided with textured substrates to facilitate finer control of the process. We demonstrate that higher order structures are made possible by adhesive elastocapillary control

69
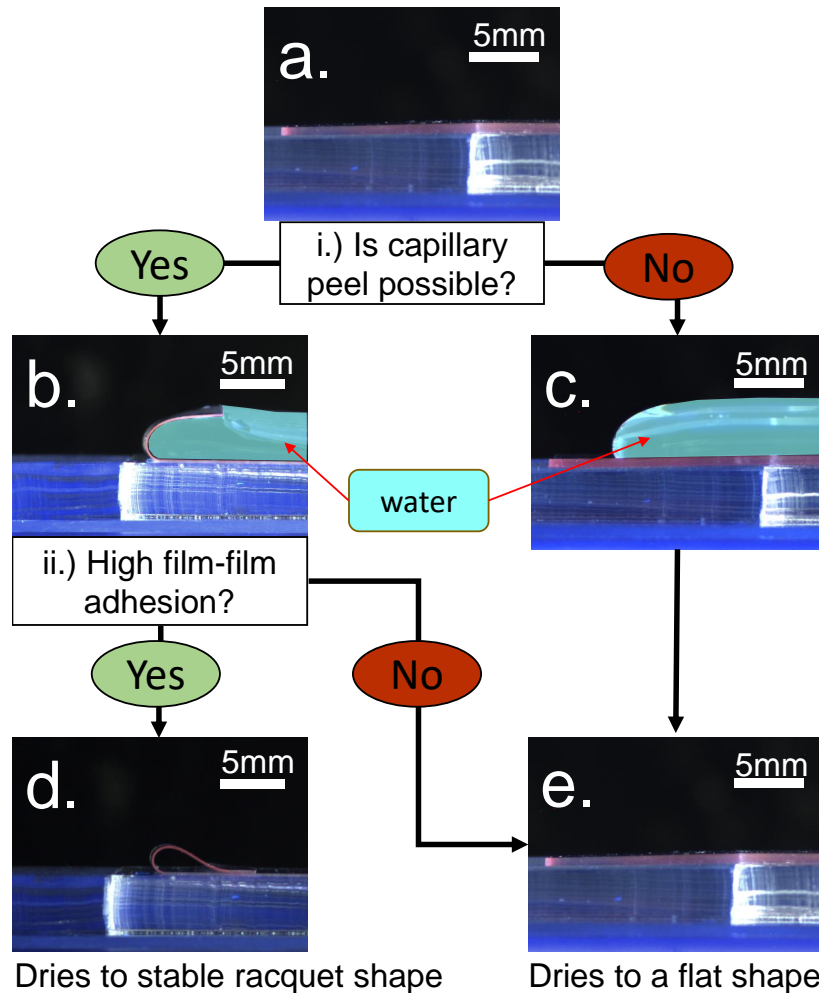
Figure 3.1. Possibilities for a thin-film capillary origami system. A film resting (a.) has a drop of water added to it. If the capillary forces are greater than the adhesion forces, peel is possible (b.). If peel is not possible, the film will remain in the flat state while the drop slowly evapourates (c.) and will remain flat when the drop completely dries (e.). Films that did peel form a bent shape around the droplet which persists as the drop dries, but slowly takes on a higher radius of curvature. If the film is long enough it will eventually come into self-contact. If self-adhesion is strong enough the film will retain a racquet shape indefinitely (d.), otherwise it will open in order to reduce bending energy and relax to a dry, flat final state (e.).

by combining peel front guiding between a film and substrate and staged delivery of water drops. Finally, we use the technique to assemble a prototype "complex" origami: a "paper" airplane.

3.2. Experimental

3.2.1. Thin-Film Preparation

Thin films were created from Sylgard 184 polydimethylsiloxane (PDMS) at a weight ratio of 10:1 (prepolymer to crosslinker) according to the following protocol. First, prepolymer and
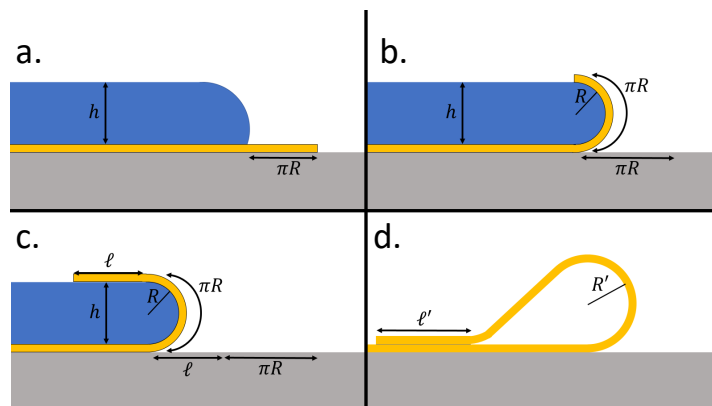
Figure 3.2. Illustration of capillary peel for a water-PDMS film system. a.) Water is placed on a flat film and the upward capillary forces of the water pull on the film. As the water approaches the edge of the film, the upward forces are larger than the forces keeping the film in place and the film will detach from the substrate. For convenience in the scaling argument, we imagine the drop at rest at a position some small distance from the film edge such that the "free length" of film is just enough to bend around the drop as in b.). Note that the water does move closer to the film edge in reality. b.) The detached film will be pulled along and up the surface of the water drop, acting to cover the greatest amount of liquid as possible. c.) Once a full 180° bend is created, there is a runaway rolling capillary peel front causing more of the water surface to be covered by film. This will continue until the peeling is stopped by some other interaction or limit. d.) If enough of the film has capillary peeled to allow for large film-film adhesion to be created after the film dries, the remaining shape is known as the "racquet" shape.

crosslinker is measured at a 10 to 1 weight ratio and mixed thoroughly. The mixture is then degassed in a vacuum oven. Next, the uncured PDMS was coated onto polyacrylic acid (PAA) coated glass slides and placed onto a spincoater (Laurell Technologies Corporation Model WS-400BZ-6NPP/LITE) and quickly rotated to create a thin, uniform film on the slide. PDMS films created by spin coating were on the order of tens of microns in thickness. Thicker samples (over a hundred microns in thickness) were created by drop-casting uncured PDMS onto a PAA coated glass slide.

The film samples were then placed in a vacuum oven at a vacuum pressure of 25 inHg for approximately 20 minutes to remove any air bubbles incurred during the casting process. Samples were then annealed at 85°C for 90 minutes. Samples were allowed to cool and then scored into strips 1 cm by 3 cm, with longer samples occasionally being created to test the effects of sample length. Samples were submerged in MilliQ (Millipore Inc) filtered water to dissolve the PAA release layer and allow the film to float to the top of the container. Floating films were gently placed onto kimwipes to dry overnight in a closed container.
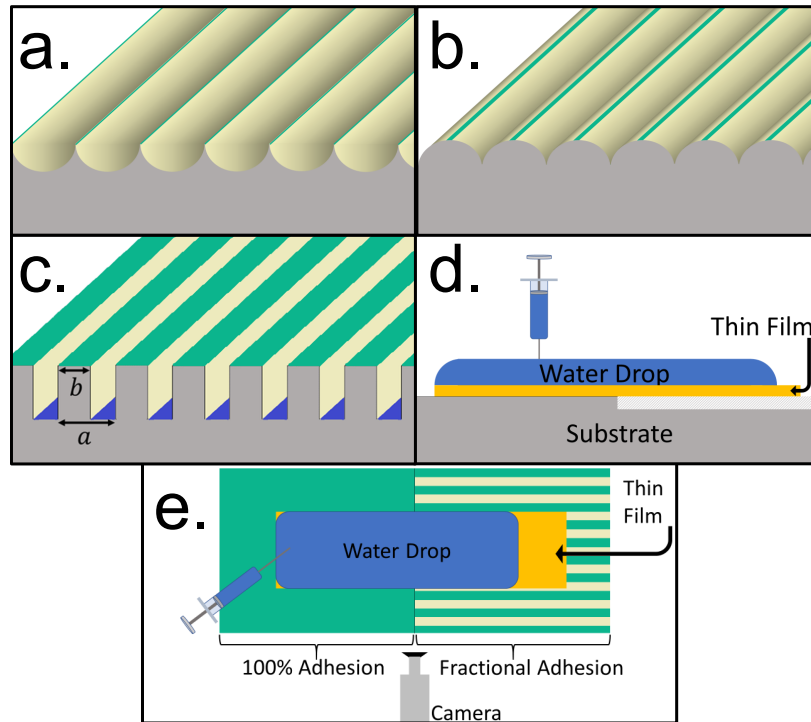
Figure 3.3. Experimental setup of the film, substrate, water drop and application, and camera setup. a.) Cusp-shaped substrates used for the lowest adhesion to the film. b.) Rounded substrates giving adhesion values of 5-10% to the film. c.) Rectangular substrates for adhesion values of 20-90% to the film. Raised areas that adhere to the film are colored in green to show relative adhesion. d.) Side profile of the experimental setup. Water drop placed on the film which is adhered to the substrate. Substrate may consist of two different adhesion values to force peeling to only occur at one end of the film. e.) Top view of experimental setup, showing two film-substrate adhesion areas and how the direction of peeling is parallel to the direction of the substrate pattern.

Thickness values for each sample were determined using three-dimensional scanning confocal microscopy (Olympus FLUOVIEW FV1000). Thickness measurements were conducted after capillary experiments were completed. Each film sample was placed on a glass slide and the height of the film from the glass surface was scanned at three locations around the perimeter. The average was reported as the thickness.

3.2.2. Substrate Preparation

Moulds for substrates were created by hot-pressing a glass pattern into a polystyrene (PS) plate. Hot pressed PS moulds were ready to use after cooling, cleaning, and drying.

Additionally, 3D printed moulds were created using Formlabs clear photopolymer resin in a Formlabs form2 3D printer. Substrates were designed to have a repeating pattern with cross-sectional slices of cusp, circular, or rectangular shapes as seen in Fig. 3.3a, b, & c, respectively.

Each shape allowed for different adhesion values to the films with the cusp shaped substrates giving values less than 3 % adhesion, rounded substrates giving around 5-15 % adhesion, and rectangular substrates for approximately 20 %-95 % adhesion compared to a flat piece of PDMS. As discussed below, the altered adhesion is due only to altered contact area between film and substrate. Raised features were 1-2 mm in height with a repeating period of 1-2 mm. All 3D printed moulds were prepared for patterning of PDMS by placing the mould in a bath of isopropyl alcohol and agitating two minutes, then resting in the bath for ten minutes. The mould was then allowed to dry in the air for at least 24 hours. Moulds were then soaked in filtered MilliQ water for 2hr, rinsed, and placed into an oven at 85 ° C for 24 hours. The moulds were allowed to cool, then washed with detergent and water, rinsed with MilliQ water, and allowed to dry. Cusp-shaped moulds were then ready to be used to directly create PDMS substrates, since the roughness of the printed surfaces lowered adhesion as was desired. Rectangular moulds were printed too rough to create adhesion at the values desired, so these moulds were sanded to remove large roughness features, and then coated with a solution of PS in toluene and allowed to dry to create a smooth surface. These moulds were then used to create a 10:1 PDMS negative.

The PDMS was prepared with the same procedure outlined above for the thin films, but after the 10:1 mixture was poured into the mould, the degassing process was cycled twice though 5 minute vacuum depressurizations and once through a 20 minute depressurization. All depressurizations were brought to 25 inHg and held for the set amount of time to ensure PDMS would reach all parts of the mould, then put in an oven set to 85 °C for 90 minutes. After cooling, substrates and negatives were gently peeled out of the moulds and placed pattern side up on glass slides. Negatives were placed in a UVO Cleaner (Jelight Company Inc. Model No. 42A) and oxidized for 35 minutes. After cooling, these negatives were used as moulds to create 10:1 PDMS substrates.

3.2.3. Capillary Peel Experiment

Dry sample films were placed onto substrates so that the long axis of the film was parallel to the ridges patterned on the substrate (Fig. 3.3d & e). Films were arranged so that a length of many times the elastocapillary length ($L_{ec} = \sqrt{\frac{B}{\gamma_{lg}}}$) was adhered to the patterned portion of the substrate in order to ensure that if capillary peel and bending were possible, a film is able to achieve a full 180° bend. The opposite end of the film was adhered to an unpatterned portion of substrate (Fig. 3.3d & e). This was done to ensure that capillary peel would occur at only the end of the
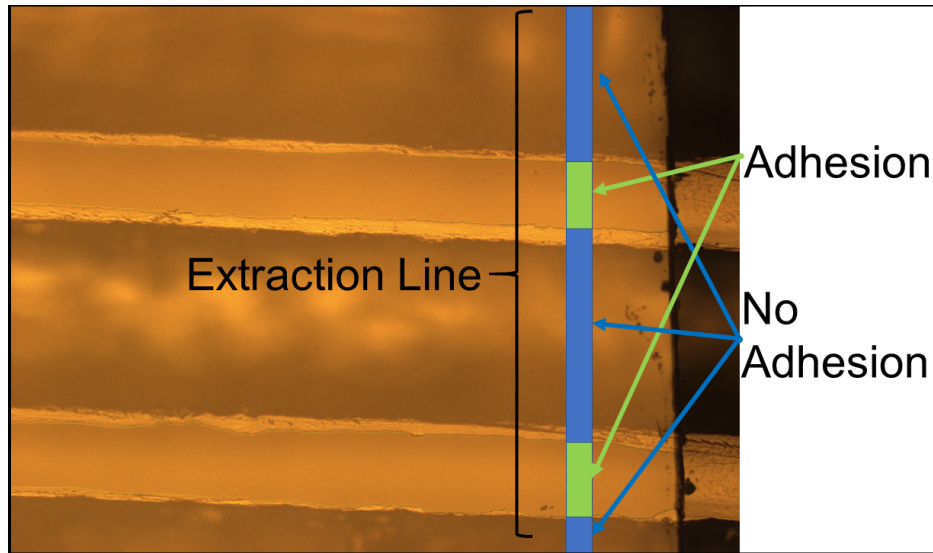
Figure 3.4. Top-down view of the peeling edge of a film. A vertical extraction line is drawn parallel to the peel edge with the adhered areas (green) and the non-adhered areas (blue) highlighted. The width of the extraction line is not to scale.

film with the lower substrate adhesion which prevents the scenario in which symmetric film peeling occurs and film ends interfere with one another. Ten to thirty minutes after placing the film on the substrate, the film-substrate adhesion was imaged near the intended fracture edge by optical microscopy, producing an image similar to Fig. 3.4. Images were taken from above, near the peeling edge, with an Olympus BX51 upright microscope at 5x magnification. Pictures were later analyzed in order to determine the true fraction of film-substrate contact area using ImageJ image analysis software. This analysis consisted of drawing a line parallel to the film edge and determining what percentage of that line was adhered to the substrate. Fig. 3.4 shows an expanded (for visibility) extraction line with adhered areas shaded in green, and non-adhered areas shaded in blue. This process was repeated along the entire peeling edge of the film and results were averaged to produce a k-value.

These values were reported as k, the fraction of contact area to total film area. Note that no attempt was made to estimate any strain energy stored in the film as it contacts the substrate. Strain was assumed to be negligible compared to the other energies present in the problem. The lowest adhesion samples were created by applying a nonstick coating to the underside of the film. When there was no film-substrate adhesion visible using microscopy, an adhesion value of $k = 0.0001$

was assigned, representing a lower limit of what is observable with this method (zero contact is physically impossible).

Next, the samples and substrates were placed on a stage and a side-on picture of the profile was recorded by a camera (Fig. 3.3d & e) every few seconds. MilliQ filtered water was placed onto the center of the sample and allowed to spread to the edges. If the water caused the film to peel and fully bend onto itself, water was added until all of the remaining flat film was covered, then the water was removed by evaporation or syringe. Films that did not fully peel and bend had water added until all of the flat surfaces were covered, creating a large "pancake" drop resting on the film. Water was then slowly removed, while the peel edge was observed carefully for signs of capillary peeling and bending. Samples were removed from substrates and allowed to dry. Clean substrates were reused until changes in the fraction of adhesion were observed.

3.2.4. Racquet Stability Experiment

The "racquet shape", shown in Fig. 3.2d, is the geometry which occurs when a thin film is adhered to itself and placed on a substrate. It is often modeled as an elastica, and has been explored theoretically by several researchers.[93, 21, 81, 138, 44] Experiments to determine the stability of a "racquet" structure created by capillary peeling a thin film from a substrate and then allowing the water to dry were conducted in a manner similar to the capillary peel experiment. A thin film was placed on a substrate split into two adhesion zones. The "adhesion zone" was nearly 100 % adhered to the film and the other "non-adhesive zone" was a very low adhesion value substrate (1 %), identical to the setup in Fig. 3.3d & e. A top down picture of the setup was taken to record the length of the film extending into the non-adhesive zone from the edge of the adhesion zone. This was recorded as the free length of the experiment. Following the steps illustrated in Fig. 3.2, water was added to the top of the film and then removed to lift and roll the film's edge in the non-adhesive zone onto the flat film in the adhesive zone.

In the case where a film did not capillary peel, the free edge was lifted and placed upon the top of the water puddle at a 180° bend, further peeling to the adhesive edge was facilitated by the capillary puddle. These samples were noted as "forced peel" samples. The water was then allowed to dry, leaving either a stable racquet shape or a film that relaxed back to its flat state without the capillary drop present, represented in the final states in Fig. 3.1. These final states were recorded.

The free lengths were adjusted and the experiment was repeated several times with films of the same thickness.

3.2.5. Double-Fold Experiment

An experiment to create a multi-step, double fold structure was also conducted, following a modified repetition of the procedure of the capillary peel experiment described above. The major modifications were to arrange a square film on a patterned substrate so that only one-quarter of the film was on an unpatterned substrate and fully adhered (lower-left quadrant in Fig. 3.13a). Second, two very low adhesion patterns were placed so that their axis was 90° to a final low adhesion (bottom right in Fig. 3.13a) quadrant. This substrate design (top-down schematic in Fig. 3.12) ensured that water added to the center of the square film would create a fold running horizontally along the middle of the film, where the peel front would stop upon encountering high adhesion along its length as it encounters the two higher adhesion quadrants. This first water drop was then allowed to dry. A second water drop was deposited from the center of the folded rectangular film and caused a secondary peel of the film from the remaining lower adhesion quadrant. Ultimately, this left only the lower-left quadrant anchored to the substrate and the peeled film folded into a small square shape on top of that section. The sequence of events is shown in Fig. 3.13 (time-lapse video available in in the supplementary file for Twohig *et al.*[133]).

3.2.6. Adhesion Measurements

Adhesion measurements for the PDMS film and PDMS substrate interfaces were measured with the same procedure and setup as is outlined for macroscopic films by Elder *et al.*[36] A top and bottom plate were coated with PDMS and a drop coated film was bent between the two plates in a "tape loop" geometry Fig. 3.5.

The film was prepared with the same drop-casting procedure as described above for creating thin PDMS films. The PDMS-coated plates were prepared in the same manner as the drop coated films, except that the PAA release layer was not used, meaning that the PDMS has likely bonded to the glass slide during curing. The top plate's position was cycled, first compressing the tape loop past the elastocapillary length of the system, L_{ec}, then relaxing back to the starting point. The cycle was then repeated several more times. The force from the tape loop on the bottom plate, the separation distance of the two parallel plates, the speed of plate movement, and the width of the film loop were all recorded. The measured force was plotted against the plate displacement, creating
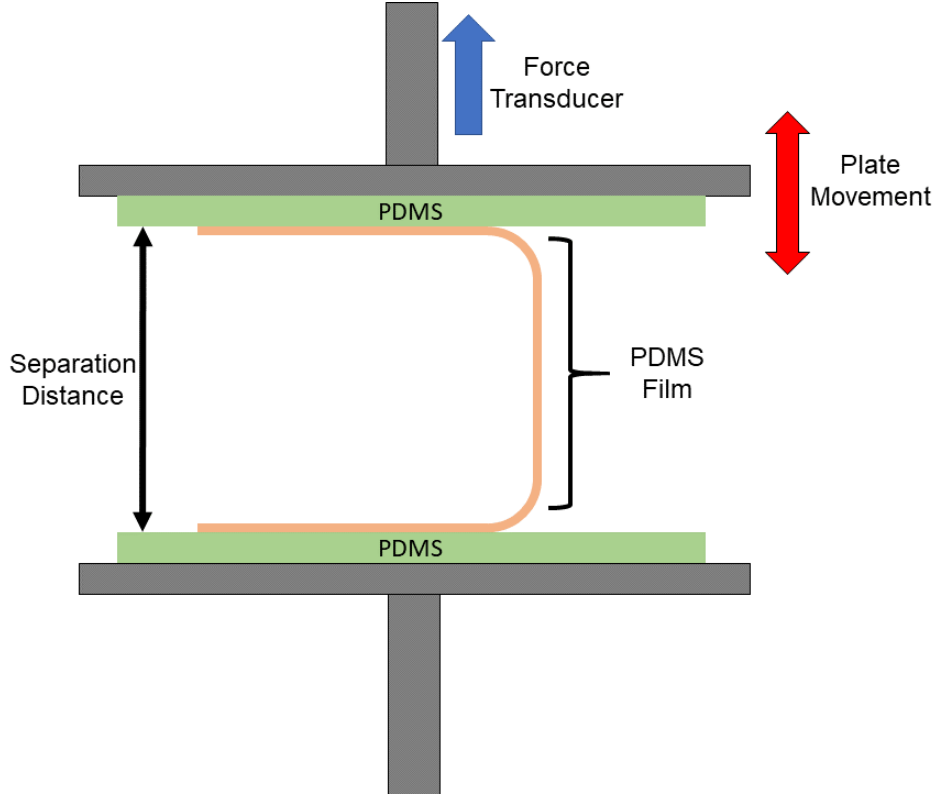
Figure 3.5. Illustration of the experimental setup for measuring the adhesion values of a PDMS-PDMS interface.

a the curve seen in Fig. 3.6. The force difference between the flat portions of the compression and relaxation curves (Fig. 3.6 was measured for these experiments.

This measurement was divided by the width of the tape loop. This gave a G_c-value of 0.124 N/m. Using this value with the following equation and known values for the surface energy of a PDMS-air interface, the interfacial energy of a PDMS-PDMS interface can be found:

$$G_c = \lambda_{PDMS-air} + \lambda_{PDMS-air} - \lambda_{PDMS-PDMS}, \tag{3.1}$$

this was the value for the slowest peel that was conducted during this experiment, at a plate velocity of 9×10^{-5} m/s. This experiment was repeated several times at this velocity, as well as at other, similar, velocities. These results show a trend of G_c-values rising with test velocity. These results are presented in Fig. 3.7.
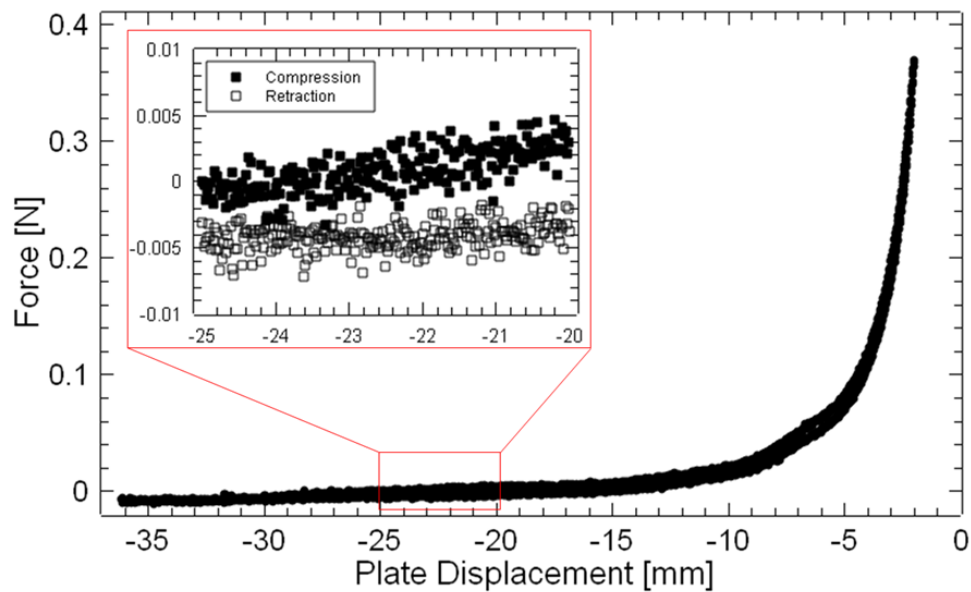
Figure 3.6. A typical force-displacement curve for a PDMS loop in contact with two PDMS surfaces. Inset shows the difference between the closing and opening part of the data in the "plateau" part of the cycle.
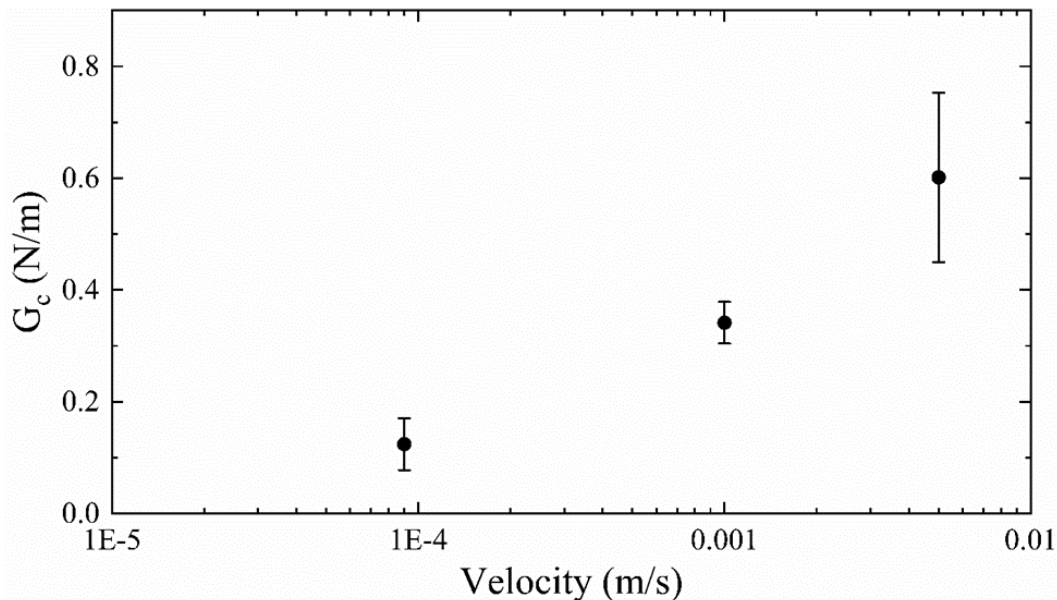
Figure 3.7. Gc values for PDMS-PDMS contact at various velocities. In this work the value at the lowest velocity is used as it is near the "zero velocity" limit of the true work of adhesion. The trend suggests that very slow peels would have a smaller adhesion value, but experiments at these speeds proved difficult. Likewise, the capillary peel experiments did not show peel over very long time-frames, with capillary peel observed within a few minutes on all of the peeled films.

3.3. Results and Discussion

3.3.1. Capillary Peel and Substrate-Adhesion Fraction

When a drop of fluid is placed on a thin film, it will spread out to reach the advancing contact angle permitted by the system's Young-Laplace balance (θ_e). If that contact point is far from the edge of the film it is unlikely for the drop to cause the film to peel and lift from a substrate due to the overall weight of the film and the increased in-sheet stretching cost required to form a circular ridge around the droplet. Even if the ridge is only transient, the Gaussian curvature will change from the flat state and a stretching cost must be exceeded for any peeling to occur. On the other hand, if the droplet reaches the edge of a film, it is likely to be pinned there by defects. This means that the contact angle is not likely to remain in equilibrium and the drop is likely to spread out along the edge flattening the formerly circular contact line and allowing bending to occur.[3] The weight of the film to be lifted is minimized and, more importantly, any changes to the Gaussian curvature at the front are avoided. This is the most likely case for capillary peeling to occur and what we focus our experiments on.

For a film to peel from a substrate two things must happen. First, the capillary force of the drop must exceed the work of adhesion between the film and the substrate on which it rests. In fact, due to losses which occur during the propagation of the interfacial crack (the peel front) the true work of adhesion can only be considered a lower limit for the process.[80, 112] Secondly, the bending cost of the film must be smaller than the difference between the work of adhesion and the capillary force. If the former is not true, there is no drive for the system to lift from the substrate. If the latter is not true observation would not be able to determine that the film edge is not adhered to the substrate (as it would not be lifted and the film as a whole cannot hover).

Capillary peel experiments were performed in order to study the basic ability of a fluid drop to peel a film from an adhesive substrate. In these experiments, the film thickness was varied in order to alter bending energies and the fraction of the film adhered to the patterned substrate was varied in order to alter the system's work of adhesion while keeping interfacial chemistry constant. In this manner, a state diagram can be constructed as shown in Fig. 3.8. Here blue solid circles are used to show experiments where capillary peel was observed (where the fluid could bend the film 180°) and light blue open squares represent the combinations where no peeling from the substrate
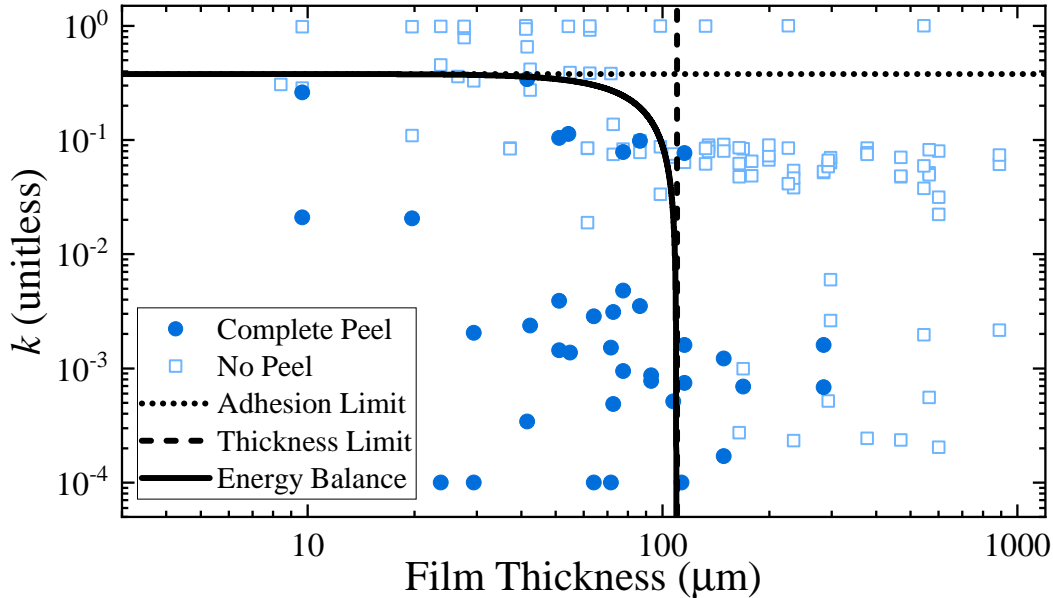
Figure 3.8. A plot comparing the fraction of the thin-film adhered to the substrate (k) against the thickness of the film. The color of each data point represents if the film was observed to peel from the substrate when a water drop was placed on top of the film. Blue circles represent films of a given thickness that capillary folded (bent 180°) and peeled from a given substrate. Light blue open squares represent combinations where no capillary peeling was observed. The horizontal dotted line illustrates the cutoff line above which surface energies do not allow peeling. The vertical dashed line represents the maximum thickness film that could be bent around the water puddle. The solid line shows the full balance of surface and bending energies. Films that exist below the solid line can be expected to peel.

was observed. As might be expected, the experiments that showed complete film folding tended to be the thinnest films with the least adhesion to the substrate.

Fig. 3.8 suggests an apparent upper limit for the fraction adhered to the substrate with the highest observed capillary peel occurring at $k = 0.34$. Capillary peel reliably occurs when fraction adhered is below $k = 0.10$. As the thickness of a film increases, the limiting adhesion values for capillary peeling decrease. This trend continues until film thickness of approximately 250 μm are reached (the thickest capillary peel is observed in a film of thickness 285 μm). Above this film thickness value, the capillary drop cannot peel and fold the PDMS film.

A simple scaling argument can be constructed by considering the free energy before and after wrapping. The basic geometry is shown in Fig. 3.2a, b and c. Note that the figure shows the drop a small distance from the end of the film. In reality the drop will usually reach near to the film edge before folding occurs. The length in the schematic is a convenience, because it enables the

drop to be considered stationary. The drop is large but not infinite, so if it reaches the film edge and then is wrapped by the film, its center of mass would have to move during wrapping. Before a film is lifted from a substrate, in the limit of a large droplet, the systems energy is given by

$$\frac{U_1}{b} = \pi R(\gamma_{la} + \gamma_{fa} + \gamma_{fs}) + \frac{1}{2}\rho g h^2 L, \tag{3.2}$$

where the γ values represent the surface energy of an interface and the subscripts of f,s,a, and l correspond to the film, substrate, air, and liquid surfaces, respectively. ρ is the fluid density, L is the horizontal extent of the droplet, and b is the length of the contact line (out of page dimension of the film shown in Fig. 3.2). Though not necessary, we assume the radius of curvature, R, scales as $h/2$ for simplicity. We further assume that h is unchanged after wrapping, which is true if the drop volume is large and the film thickness is relatively small.

Just after wrapping, with the same assumptions as above, the free energy is altered to

$$\frac{U_2}{b} = \pi R(\gamma_{lf} + \gamma_{fa} + \gamma_{sa}) + \frac{1}{2}\rho g h^2 L + \pi B/2R, \tag{3.3}$$

with the bending modulus given by $B = Et^3/12(1 - \nu^2)$ where E is Young's modulus and ν is the Poisson ratio. Hence the change in energy due to wrapping is,

$$\frac{\Delta U}{b} = \pi R(\gamma_{lf} + \gamma_{sa} - \gamma_{la} - \gamma_{fs}) + \frac{\pi B}{2R}. \tag{3.4}$$

The energy difference can be used to determine the function $k(t)$ that delineates the boundary between successful capillary folding and unsuccessful folding.

Before determining the full function, it is instructive to explore two limiting cases. First, if a film is infinitely thin the bending cost can be ignored, and the final term in Eqn. 3.4 can be dropped. ΔU must be less than zero in order for wrapping to occur spontaneously, and a critical γ_{fs} can be determined. In our experiment we note that $\gamma_{sa} = \gamma_{fa}$ and can rewrite the film substrate energy as $\gamma_{fs} = k\gamma_{ff} + 2(1 - k)\gamma_{fa}$ as the substrate material and film material are identical by design. Setting $\Delta U = 0$ allows a limiting k to be determined:

$$k_{t\to 0} = \frac{\Delta\gamma'}{\Delta\gamma} \tag{3.5}$$

81

where $\Delta\gamma$ is the work of adhesion between the substrate and film ($\Delta\gamma = 2\gamma_{fa} - \gamma_{ff}$) and $\Delta\gamma'$ is the equivalent term for the water/film interface ($\Delta\gamma' = \gamma_{la} + \gamma_{fa} - \gamma_{lf}$). In our experiments, surface energy values give a $k_{t\to 0}$ value of 0.38.[34, 118, 134]

The maximum adhesion percentage predicted by Eqn. 3.5 is indicated by the dotted horizontal line in Fig. 3.8 and shows good agreement with the apparent transition between peeling and non-peeling states in low thickness films. As the film thickness increases, agreement is reasonable until a thickness of approximately one hundred micrometers. Here the limit between these two peeling states begins to fall from the zero-thickness prediction.

A second limit can be determined by considering a zero adhesion limit which would correspond to the work of adhesion falling to zero ($\Delta\gamma \to 0$) or equivalently in our experiment $k \to 0$. In either case, Eqn. 3.4 reduces to

$$\frac{\Delta U}{b} = -\pi R \Delta\gamma' + \frac{\pi B}{2R}. \tag{3.6}$$

and the limiting thickness can be written as

$$t_{\Delta\gamma\to 0} = \left[\frac{24R^2\Delta\gamma'(1-\nu^2)}{E}\right]^{\frac{1}{3}}. \tag{3.7}$$

In simpler terms, the critical thickness is related to a balance between the elastocapillary length ($L_{ec} = \sqrt{B/\Delta\gamma'}$) and the capillary length ($\kappa^{-1} = \sqrt{\gamma_{la}/\rho g}$).[9, 31] The driving force must be able to bend the film around the droplet, the height of which is determined by the capillary length. This is an important design consideration if driving fluids are exchanged, density as well as surface tension are important.

Explicitly, the drop height is expected to be

$$h = 2\sqrt{\frac{\gamma_{la}}{\rho g}} \sin\left(\frac{\theta_e}{2}\right), \tag{3.8}$$

where θ_e is the equilibrium contact angle of the fluid on the (flat) film.[31] With the surface energies relevant to our experiment, we calculate a height of 3200 μm and and a thickness limit of $t_{\Delta\gamma\to 0} = 110$ μm.[34, 118, 134]

The thickness limit is shown as a dashed vertical line in Fig. 3.8, which agrees reasonably with the majority of the data, though films over 2 times as thick were observed to fold. We believe the discrepancy lies in dynamics between the film and droplet that were not controlled precisely enough in our experiments and not considered in the scaling model. For example, if an interfacial crack begins in a film corner (where b is effectively smaller) or on a defect in the pattern, it may be able to propagate more easily. There may be additional details due to the approximations of considering the system 2D. In reality, the fluid has curvature in other directions which are ignored in this model. Furthermore, there is no consideration of exactly how the crack between film and substrate is nucleated in our model.

Finally, we solve Eqn. 3.4 directly and plot the full boundary as a solid line in Fig. 3.8, which is determined to be

$$k(t) = -\frac{\Delta\gamma'}{\Delta\gamma} + \frac{E\rho g}{24(1-\nu^2)\Delta\gamma\gamma_{la}\sin^2(\theta_e/2)}t^3. \tag{3.9}$$

Eqn. 3.9 smoothly connects the two limits discussed above, and forms a good guideline for understanding substrate adhesion in the design of capillary origami systems.

3.3.2. Guiding a Capillary Peel Front

One aspect of capillary peel which has been overlooked up to this point, is the ease at which the direction of a peel front can be controlled with patterned interfaces. Once capillary forces have initiated a peel, a film will typically peel until the driving droplet is covered. However, if the work of adhesion is altered locally this need not be the case. This is an important feature because a substrate can then be used to determine the final position of a pivot point or fold. In our experiment, this can easily be accomplished through a change in pitch, or pattern orientation.

Consider a substrate which is designed with two different regions of pattern. In the first region the long parallel channels of the substrate are orthogonal to the (assumed) peel direction of the film (Fig. 3.9a), but in the second the pattern is rotated by 90°(Fig. 3.9b). The substrate will allow a crack to propagate in region one but will cause the crack to stop in region two. This is because the quasi-one dimensional contact line will interact with the surface and "feel" the average k along its length. When the peel front is orthogonal to the pattern (Fig. 3.9a) it experiences a low k because the contact line touches the substrate at several points - the contact line does not touch
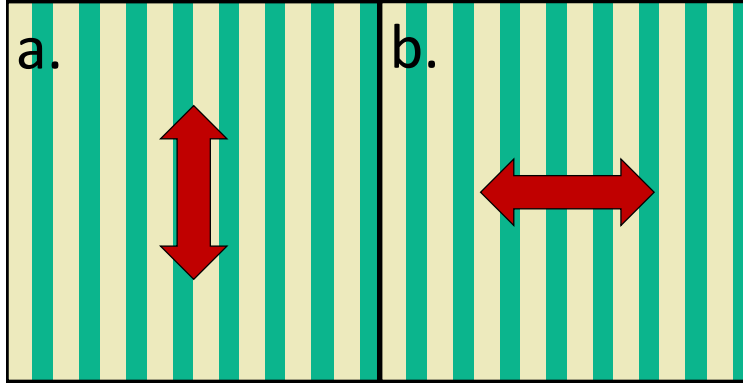
Figure 3.9. Schematic of patterned substrates. In a.) a film will continuously peel in the direction of the arrow because the peel front experiences a constant value of adhesion (in this figure approximately 50%). While a peel initiated in the direction of the arrow in b.) will alternate between periods where there is no adhesion and 100% adhesion, depending on if the front is crossing a raised or lowered section of the substrate.

a continuous region of substrate (regions touching substrate and regions over a gap are averaged together). When the peel front reaches the second region of substrate where the pattern is now parallel to the front (Fig. 3.9b), it will experience $k = 0$ if it is over a gap, but will experience $k = 1$ when it reaches the portion of pattern which touches the film. Here the line will not average the contact and noncontact regions, but experiences each separately.

Manipulating the films and peel fronts using thin strips allows peel to be guided in useful directions. Further examples of how thin strips of adhesive substrate can act to stop or to guide peeling are presented schematically in Fig. 3.10 and experimentally in Fig. 3.13 discussed below. Fig. 3.10 demonstrates several orientations in which a crack can be arrested, but also shows how a front can be directed to fold in different directions.

Finally, we point out how patterned substrate blocks can be used much like typesetting. Different patterned blocks (characters) can be arranged side by side to create the desired overall substrate. For example, pattern free blocks can be arranged to stop bends, patterned regions where peeling in a certain direction is desired and so on. Once such a "character set" is developed, endless arrangements, and thus endless fold patterns are possible.

3.3.3. "Fixing" Structure with Adhesion

Creation of complex, multi-step structures requires both pivot points as well as a means to hold structures in place. While directional adhesion can create pivots, self-adhesion is needed to fix structures after the driving capillary fluid evapourates. The capillary peel experiments described
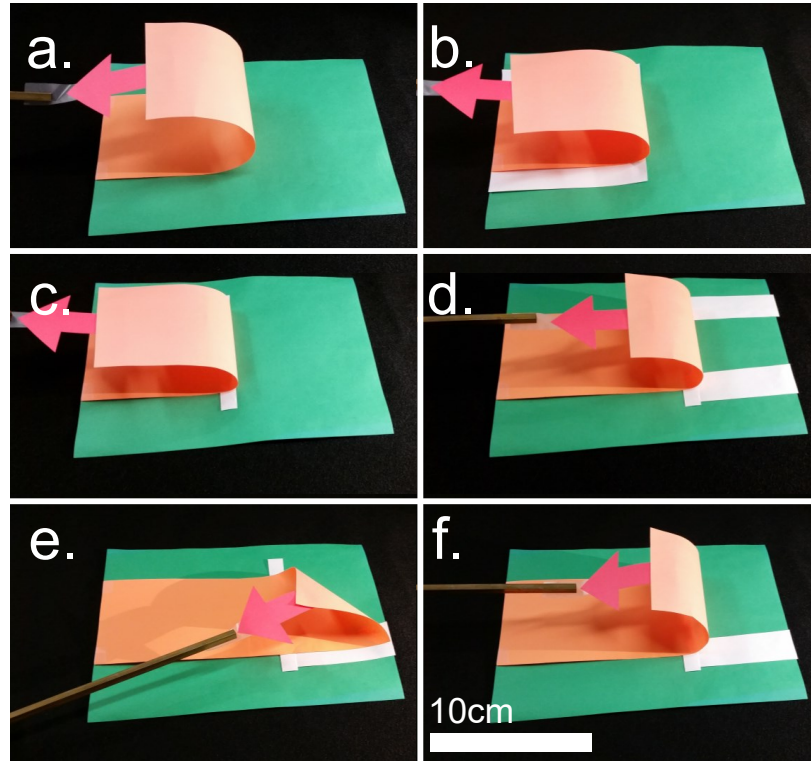
Figure 3.10. Demonstrations of how thin strips of adhesive substrate can be used to manipulate the direction of, and amount of capillary peel. Green represents low-adhesion substrate where capillary peel of the film (orange) is possible. White substrate represents areas with high film-substrate adhesion, where capillary forces are lower than adhesive forces when compared directly. Red arrows point in the direction of the capillary force created by the liquid drop. All films are assumed secured on the left side of the setup to ensure peeling occurs on the right. a.) A film that is completely on a low-adhesion substrate will peel until the capillary drop is covered, or there is no film left to peel. b.) A film placed with half of its length on the adhesive substrate will begin by capillary peeling the low-adhesion "free end", and continue peeling until the peel front reaches the area of high adhesion. c.) A thin adhesive strip placed perpendicular to the direction of peel will act similar to a large area of adhesive. Peel will stop as the peel front reaches the adhesive strip and encounters high adhesion along the entire peel front. d.) Two thin adhesive strips running parallel to the peel direction can act as a guide to the direction of peel. e.) Two thin adhesive strips at a right angle from the peel front will allow a triangular peel from the "free" corner. If these strips are large and adhesive, peel will stop in this folded shape. f.) A thin adhesive strip parallel to the usual direction of peel will allow the previous state (e) to progress into the same folded state as the other capillary peel examples.

above, showed that once a film peels from its substrate it will often form a 180° bend around the capillary drop and continue to peel from the substrate until the fluid is almost entirely covered with film. When the fluid volume is reduced, it is likely that the film will come into contact with itself, rather than simply opening to the flat state.[12] The result of the film folding onto itself in

the presence of adhesion between the film and itself, Fig. 3.2d., is the creation of a "racquet" shape structure. The structure is stable if the film-film adhesion outweighs the elastic energy stored in the bend. The racquet shape has been studied by various methods with respect to carbon nanotubes and graphene sheets in the absence of water [102, 81, 82, 27, 26, 138, 44, 21, 1] and in capillary origami systems.[93, 12, 70]

The conditions for a stable racquet shape come down to a balance between adhesion and bending and so must be related to the elastocapillary length L_{ec}. Practically speaking, it is useful to focus on the length of a film which can easily be controlled. A film shorter than some critical length, L_{crit}, will have to create a high curvature bend in order to come into self contact and adhesion will not be strong enough to hold the structure closed. On the other hand, a sheet longer than L_{crit} will not need to have as high a curvature and adhesion will hold it closed. Detailed models describing the film as an Elastica with a two-dimensional cross-section yield more quantative predictions.[44, 138, 70] In particular, the critical length to be given as

$$L_{crit} = \alpha \sqrt{\frac{B}{\gamma}} \tag{3.10}$$

where α is a numerical factor determined by the exact model used.

In order to validate Eqn. 3.10, we have conducted a set of experiments with PDMS films (see section 3.2.4 for details). In short, films are placed on a two phase substrate, such that a certain length lies on a low adhesion directional substrate and the rest of a film lies on a full adhesion substrate. In this way, the free length is easily measured before water is applied to fold the film, and its shape is easily observed after the water is removed.

Fig. 3.11 shows the summary of these experiments. The solid vertical line indicates the critical thickness for capilliary bending determined earlier. In this case, experiments can be conducted at greater thicknesses by circumventing the capillary drop and simply folding the films by hand and placing the free film on top of a capillary drop which is then allowed to dry (solid squares and open squares). It is possible that the film weight affects some of this data. Films folded by capillary action alone are shown as solid and open circles. In both cases we see the transition between stable racquet shapes (solid symbols) and open flat shapes (open symbols) falls along a straight line (in this log/log plot). Fitting Eqn. 3.10 yields an α value of 3.8, which is consistant with the
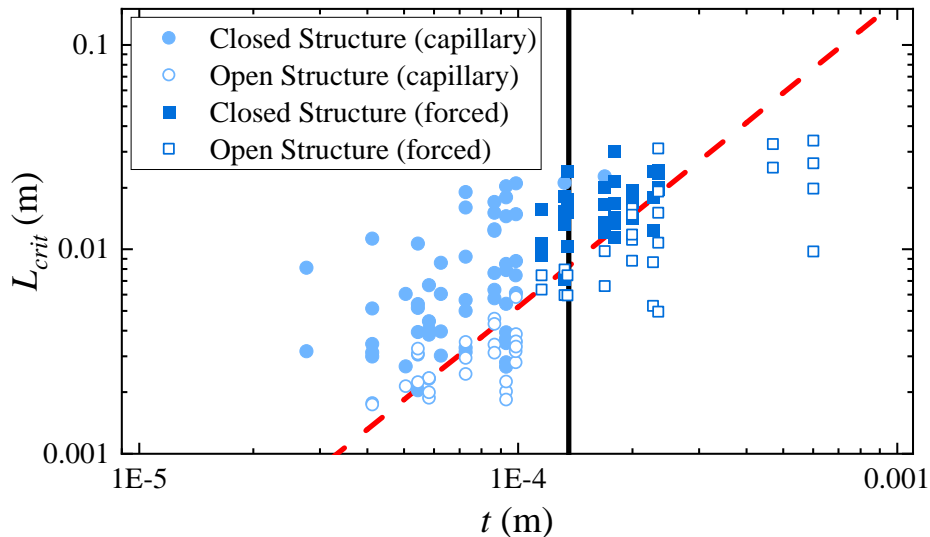
Figure 3.11. Experimental results for the racquet stability experiments comparing the length of peeled film (L_{crit}) to the film thickness (t) for open and closed racquet shapes. Solid symbols represent experiments where the closed (racquet-shaped) structure was stable. Open symbols represent experiments where the film released from its folded state and relaxed to its open structure. Experiments where only capillary forces were used to facilitate folding are represented by circles. Squares represent experiments where the film was manually lifted, bent, and placed upon the capillary liquid. The vertical black line largely separating these two situations is at a limiting thickness of 110 μm from Eqn. 3.7. The dashed line represents our fit of Eqn. 3.10 with $\alpha = 3.8$.

original measurements of Py and Bico ($\alpha = 4.9$) and modelling of Liu et al. ($\alpha = 3.03$).[93, 70] It is important to note that a higher value of α is predicted by considering the overall system energy ($\alpha = 12.11$ by Liu et al. and $\alpha = 4\pi$ by Zhou et al.), but is not observed here.[138, 70]

3.3.4. Double folding

A critical feature of any complete system of origami assembly is the requirement that it be possible for the sheet to be folded multiple consecutive times. The combination of directional patterned adhesion and self-adhesion which can fix bends in place allows adhesive capillary origami to meet this basic need. We demonstrate the formation and fixation of a double fold, the most basic example of a consecutive fold, starting from a flat, square film (Fig. 3.12a) sitting on a patterned substrate (Fig. 3.12b). the film is a thin sheet of polyvinylsiloxane, used for increased visibility. However, polydimethylsiloxane would behave in a similar manner as demonstrated earlier in this chapter and in the following section on airplane folding. The substrate was made up of four patterned blocks arranged such that the top two quadrants have a vertical line pattern, the lower right quadrant has a horizontal line pattern and the lower left quadrant is unpatterned and flat on
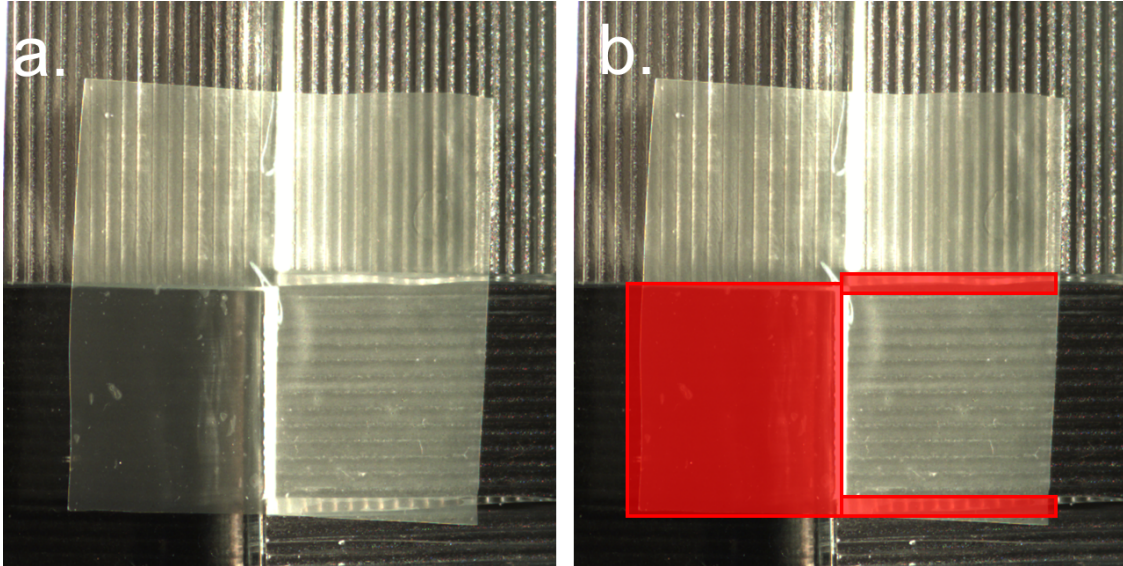
Figure 3.12. a.) Thin film resting on a patterned substrate. The top two quadrants have vertical patterns and the bottom right quadrant has horizontal patterning. b.) Areas highlighted in red have very high film-substrate adhesion values.

top. In addition, the lower right quadrant is bordered top and bottom with two wide adhesive strips. The areas highlighted in red in Fig. 3.12b have a very high adhesion value between the film and substrate. These adhesive areas are unlikely to achieve capillary peeling, and force peeling to occur in the top quadrants of the film. The thin strips also act to stop any diagonal peeling, ensuring that a top-down fold is the first event to occur from capillary peeling. Peeling can still occur in these areas if the peel front is of the correct orientation (right to left peeling), but a fold is likely to start at the path of least resistance. In this case-a top down fold.

As water is added to the center of the film in Fig. 3.13a, the top half of the film easily peels from the substrate forming the first fold (Fig. 3.13b). Occasionally, folds were observed to occur so rapidly that the momentum of the water and film moving to the half bent state pushed the peel front past the thin horizontal adhesive strip at the top of the lower right quadrant. The system did not fall into an undesirable deformation because the half folded state is the lowest energy state. So long as the lower right quadrant holds as the fold is initiated the desired symmetry is achieved. The momentum effect has the added benefit of making peeling of later stages easier but is also, to some degree, less predictable. We focus on low momentum experiments for simplicity.

After the first fold has been formed, we withdraw the large water drop with a syringe. The water could be left to evapourate without altering the outcome, but the syringe is used to speed
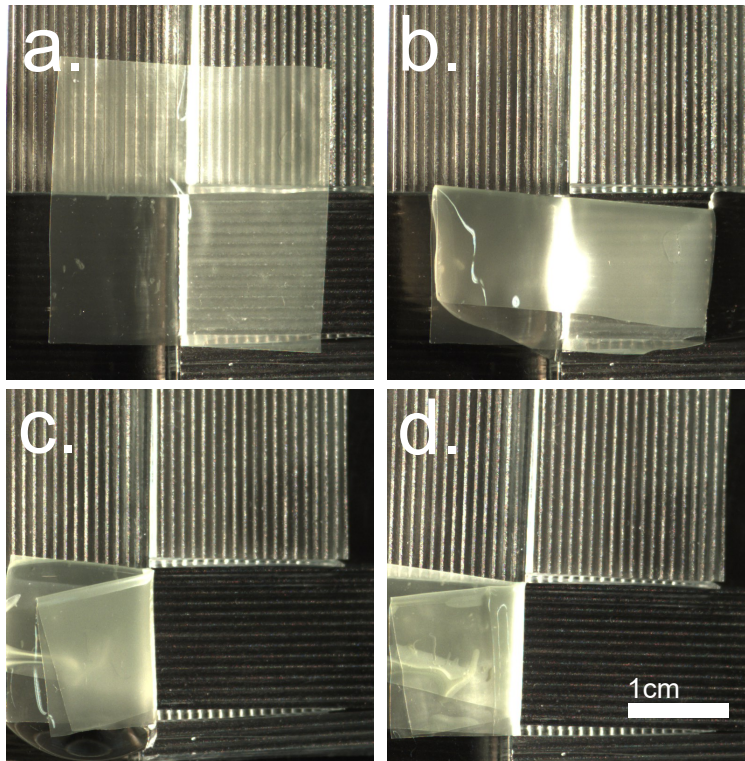
Figure 3.13. Sequence of capillary folding a flat sheet into a double-fold configuration. a.) Thin film laying on a patterned substrate. The bottom-left quadrant and two thin, horizontal strips in the bottom-right quadrant are fully adhered to the substrate. Other areas are on substrates with very low film adhesion. b.) Water was added to the center of the film and facilitated a peel and folded the sheet in half. As the film dried, the fold was made permanent. c.) Water was added to the center of the top of the single-folded sheet to facilitate the second fold. Capillary peel was strong enough to not only peel the double thick film, but to also peel the film from the thin strip of full adhesion. d.) After all of the water disappears, the double-fold is stable.

the experiment. Once self-contact occurs, the film remains in this half-folded state indefinitely as its length is many times larger than L_{crit}. Critically, the self-adhesion allows water to be added to the film to initiate the second fold. The second water drop cannot initiate a peel front anywhere on the full adhesion quadrant, so peeling from the right end of the film is the only option. The film then folds in half again, this time the right side folding on top of the left (Fig. 3.13c). Again, water is withdrawn to fix the double fold through self-adhesion, resulting in a folded area one quarter that of the initial sheet. After the remaining water has evaporated, the remaining double-folded structure continues to be stable (Fig. 3.13d). A time-lapse video of this process is available in the supplementary file for Twohig *et al.*[133]

We can again estimate the energies involved in bending the film the second time (steps b. to c. in Fig. 3.13). Clearly the fluid has not changed, but now the film is harder to bend because it is effectively twice as thick as it was during the first folding step[35, 32] From this point of view we need change the thickness in Eqn. 3.4, which ultimately moves our limiting thickness down to smaller levels. Explicitly, we find the limit to now be given by:

$$t_{\Delta\gamma\to 0} = \left[\frac{3R^2\Delta\gamma'(1-\nu^2)}{E}\right]^{\frac{1}{3}}. \tag{3.11}$$

From an alternative point of view, the elastocapillary length grows by a factor of $2^{3/2}$ for each additional "level" of folding. We note that the true cost will be slightly underestimated here because we ignore the cost of the d-cone formed at the intersection of the initial and secondary fold axis (the top right corner in Fig. 3.13).

This process is quite repeatable for a square sheet that is placed so the area of the sheet in each quadrant is equal. A capillary drop placed in the center of the flat sheet and added to until the first fold occurs in this configuration will reliably fold the top half onto the bottom half. An initial peel initiated at one of the top corners of the sheet will advance until it encounters one of the high-adhesion areas, which then acts as a pivot point securing an edge of the peel front and progressing until the entirety of the top quadrants have peeled. After the fold initiates, adding water until the entirety of the unpeeled sheet is covered allows the fold to progress to the furthest extent of covering the bottom sheet. Ensuring that the bottom-rightmost corner of the film is adhered to a thin adhesive strip stops peels from initiating in that corner. Occasional miss-folds would occur when the top right corner initiated peeling in a very quick manner. Effectively peeling through the adhesive strip separating the two right quadrants and leading to a diagonal fold where the top right half of the film would fold onto the bottom left half of the film. This could be avoided by adding the water drop more towards the left side of the film, or slowing down the addition of water to ensure there weren't large and fast folds. The second fold typically initiates at a corner on the right side of the film and peels from the thin strips individually. Again, water is added to cover the bottom left quadrant to allow the fold to cover the entire quadrant.

Occasionally, folds were observed to occur so rapidly that the momentum of the water and film moving to the bent state (for example, between the states of Fig. 3.13 a&b) that the peel front

moves past the thin adhesive strip. The system did not go to an undesirable state because it was already in its lowest energy state, with as much of the water's surface covered as possible. The thin adhesive strip had served its purpose of not allowing peeling to begin in certain directions. This momentum effect can make peeling of later states easier or less predictable. However, determining the conditions required for a capillary peel to progress past adhesion values deemed off limits by 3.5 due to momentum are beyond the scope of this study and should be explored in further research.

3.3.5. Construction of Complex Structures

The steps needed to create complex structures using thin-film capillary origami have now been described in this chapter, however, a clear demonstration of a functional, complex design is still lacking. The paper airplane is a less academically motivated structure, but is familiar to many who have been bored and had a piece of paper nearby. The airplane also represents an origami designed to have additional functionality, in this case gliding ability. The folding procedure required to make this structure is well-known and gives a good bridge between the discussion of basic physical guidelines and practical application of processes in a complex design.

A thin, PDMS film is placed onto a patterned substrate. This substrate has areas of high adhesion and areas of low adhesion. The areas of high adhesion were coated with polyacrylic acid that can be dissolved with water. The initial step requires peeling from the substrate and folding two corners of a sheet in to meet along the sheet's center line (Fig. 3.14a). This is achieved by placing water drops in the two bottom corners of the sheet. As these drops grow, they reach the corner of the sheet and peel the edges inward. The water is allowed to dry from the sheet, adhering the film to itself (Fig. 3.14b) Next, the sheet is folded along the center line by placing a drop on the right side of the sheet and adding water to it until the right side of the sheet folds onto the left side. The film is allowed to dry, solidifying the backbone of the airplane (Fig. 3.14c). The final step is to peel the wings apart and give the airplane its glider shape. This step required a modified implementation of the principles discussed earlier. In this case the sheet itself must also be patterned to facilitate a low self-adhesion between the wings. Specifically, here the wing tops were treated with a hard PS particle layer which reduced adhesion much like dirtying a piece of tape. This area is highlighted in green in Fig. 3.14 a. The final structure is shown in a floating state (to release it from its substrate) outlined in red in Fig. 3.14 d. A video with the intermediate steps is available in the supplementary file for Twohig *et al.*[133]
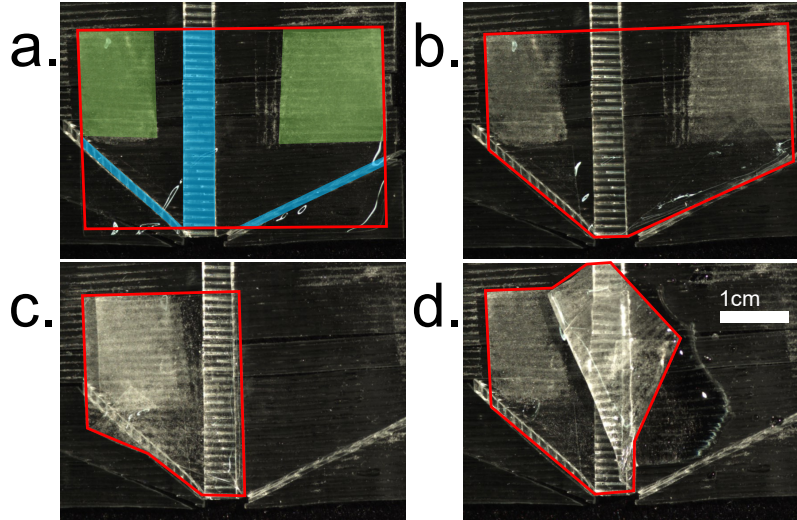
Figure 3.14. The major steps in the process of capillary folding of an airplane shape. In each step the outline of the shape is drawn in red to distinguish the clear PDMS sheet from the patterned PDMS substrate. a.) Thin film placed upon patterned substrate. Areas highlighted in blue have high film-substrate adhesion and have been coated with a water-soluble release layer. All other areas have low film-substrate adhesion. Areas highlighted in green have a nonstick coating applied to the top of the film, acting as a low adhesion area when the film contacts itself. b.) The corners of the film have been folded in, forming the nose of the airplane. c.) The right wing has been folded over the left wing, forming the backbone of the airplane. d.) The right wing has been partially unfolded from the left wing, completing the multi-step folding process to create a stable airplane shape. Further application of water under the airplane releases it from the substrate.

The airplane represents construction of a multi-step, complex, and stable structure using only capillary origami techniques demonstrating a realistic further development of guided self assembly with thin-films. The basic actions of origami - lifting, folding, creasing, and unfolding - have all been recreated with the tools of capillarity and adhesion. These new tools have expanded the library of what is possible, and point the way for the possibility of even greater innovation in the future through the many modifications to adhesion and capillarity currently available (switchable adhesion, use of different liquids, patterned changes in wetting, time dependent capillarity, and so on).

3.4. Conclusions and Future Work

This work has provided a simple summary of the role of adhesion in capillary peeling of thin films. The lift created by the surface tension of a drop must exceed the cost of adhesion between a film and a substrate in order for origami to be possible. Furthermore, if the substrate adhesion is anisotropic, folding can be guided in a symmetry breaking manner. Further, mechanisms can

be created through self-adhesion which allow a film to be folded in a sequential manner. Without adhesion complex origami could not be assembled by fluid droplets.

We have demonstrated the balance between capillary lift caused by a fluid's surface tension and the adhesion between a sheet and its substrate. A PDMS sheet must have a substrate adhesion lower than 0.38 in order for water to lift it from its substrate. Additionally, the film must be thinner than 110 μm or it cannot bend around a water droplet. Similarly, a film must have a length greater than L_{crit} in order to come into self-contact and maintain a fold after the water has completely dried. Combining these rules, we demonstrate a sequentially doubly folded sheet, a critical step towards complex guided self-assembly in this system. Finally, we have demonstrated a more detailed structure by assembling a paper airplane from a sheet with only water drops, guided adhesion and self-adhesion.

This work not only highlights what is currently possible for adhesion-controlled capillary origami, but opens the door for many possible variations in the basic technology. Adhesion, for example, is a well-studied concept and many innovations have been created over the years which could be combined with a thin sheet. For example, adhesive layers which are responsive to the environment could easily be patterned on sheets in order to create reversible or multi-state structures. Surfactant patches could be added in order to rapidly drop surface tension once a drop reaches the patch. Fluid mixtures could be utilized to create dynamic surface tensions, or to create or alter adhesion during folding. Finally, electronic response such as in electro-wetting could be used to drive origami between different states of assembly, and allow for more complex soft robotics applications.[68, 113]

Some notable questions that arose during this study center around the possibility of peeling a film from a substrate that is calculated as too adhesive to allow for capillary peeling. Some of these results are observed in Fig. 3.8 as points where capillary peeling was observed above the energy balance line. Some alternative mechanisms of peeling have been envisioned, such as peeling from a corner. Corner peeling could momentarily lesson the bending cost of peeling a film while still gaining a large contribution from the capillary surface energies. Corner peeling was sometimes observed experimentally, so this work would involve creating an experiment that favors corner-initiated peeling. A three-dimensional model of this capillary peeling could also work towards understanding the energy balance of this situation and possibly adjust the cutoff line for capillary

peeling presented in this work. The other observation-based question that arose during study was the momentum of a moving peel front and its possible ability to peel a film from a highly adhesive substrate. This was noticed in the double-fold experiment, but did not hinder the results since the folded sheet was already near its lowest energy state. However, study of how the momentum of a rapidly peeling system could be used to overcome small deviations in adhesion fraction could help to make the capillary peeling system more robust for application to creation of larger and more complex structures. This ability to push a peel front through small areas of difficult peeling could also be harnessed to further steer and guide the peel fronts, as noted by the inclusion of small adhesive strips elsewhere in this work.

The experimental findings of this research also beg the question of what other shapes can be made by utilizing the adhesion of thin films. The racquet shape was presented as a stand-in for the hinge in complex origami structures, but represents only one of a huge variety of possible pieces that could be used to create new shapes from thin films. This work is directly followed by the research into Kuttsukugami covered in the following chapter of this work.

4. KUTTSUKUGAMI: STICKY ORIGAMI

4.1. Introduction

Origami is an ancient art that uses paper folding to create three-dimensional structures. The purest form of the art has very simple rules. A square sheet of paper can be folded any number of times to create the sculpture. No cutting, measuring, marking, tape, or glue can be used in the construction of these shapes. The basic steps required to assemble an origami structure can be distilled down to a series of precisely placed paper bends that are pressed into permanent folds. Then the bend may need to be unfolded. This process is repeated any number of times and in a multitude of different configurations to create an uncountable number of different designs from paper. All of these designs can be reduced to a few base components: plates of flat paper, creases where the paper has been permanently deformed, and vertexes where creases meet.[61]

The possibility of the creation of any number of different three-dimensional shapes from a flat sheet eventually caught the attention of the engineering and scientific community. The incorporation of origami techniques and designs into real life structures and instruments has led to an explosion of interest and research into folding processes and structure design. This led to a multitude of new developments including foldable artery stents,[58] solar panel deployment systems,[120, 20] foldable microscopic encapsulants,[22, 5, 40] micro-robots,[67, 98] guided assembly,[86, 6, 50] impact mitigation systems,[136] batteries,[114, 24] and solutions for packing and shipping.[135, 78] However, a major drawback encountered when designing any of these applications was the need for weak points to be built into the sheets of plates that each system was made of. These weak points could be mechanical hinges for larger systems like satellite solar panel arrays. Macroscopic hinges rely on the movement of a knuckle around a pin and friction between these two pieces can lead to increased wear and failure. Lubrication can mitigate this, but often it is not possible or efficient to keep these surfaces lubricated (for example satellites). Microscopic systems like those developed for drug encapsulation were made of thin films that had had channels scribed or etched into the film at the designated weak points. When a load was applied to these materials, bends would reliably occur at these weak points. Both of these situations require a weakening of the overall structure to allow

for the creation of the repeatable and sharp bends that are required to created origami-like foldable structures.

Extremely sharp bends required for origami folding can also lead to an accelerated fatigue of any components on the sheet's surface. For example, electronics and wires that are connecting across the fold must also fold when the rest of the structure is actuated. This causes wear, fatigue, and eventually fracture and failure in any somewhat solid material that is not completely elastic when bent to sharp angles. This limitation means that electronics that are integrated into an origami structure are either limited to very few cycles of folding and unfolding, or are doomed to fail and need to be replaced long before the rest of the structure fails. This drawback may be acceptable for applications like solar panel deployments, where the plates making up the structure are unfolded once and rarely ever folded up again. However, a wide variety of uses could be greatly enhanced by the creation of origami structures that can be deployed and re-packed many times. Some simple examples include: wearable electronics that can fold with the skin they are attached to or with joints, microrobots that are expected to move and perform tasks through repeated folding and actuation motions, and reconfigureable electronics that are expected to fold into a useful shape and then be taken apart to a flat shape for transportation or safe keeping.

Applications that require high bendability and the ability to reconfigure often use elastomeric or rubber sheets to achieve repeated bending without failure. However, the steps and methods of traditional origami do not apply to sheets that cannot be permanently deformed. The creases are the fundamental component of any origami system, but cannot exist in a sheet that can always relax to its flat state. An elastic analog of the origami crease, which would solve many problems outlined above, requires a "handle" to fix these crease substitutes in a desired location. In this work, elasticity and adhesion are combined to serve as the solution to this need. A racquet shape is formed when a thin film or sheet is bent onto and adhered to itself, forming a shape that is stable but can be undone with enough peeling force applied.[102, 138, 44] This shape naturally forms a bending radius that is determined by the thickness, modulus, and adhesion value of the film. This radius can easily be tailored in order to stop any bends from becoming too sharp and damaging electrical components. Elastic bends can be cycled many orders of magnitude more times than a traditional bend, and racquet bends can often be directly substituted into origami designs in place of

96
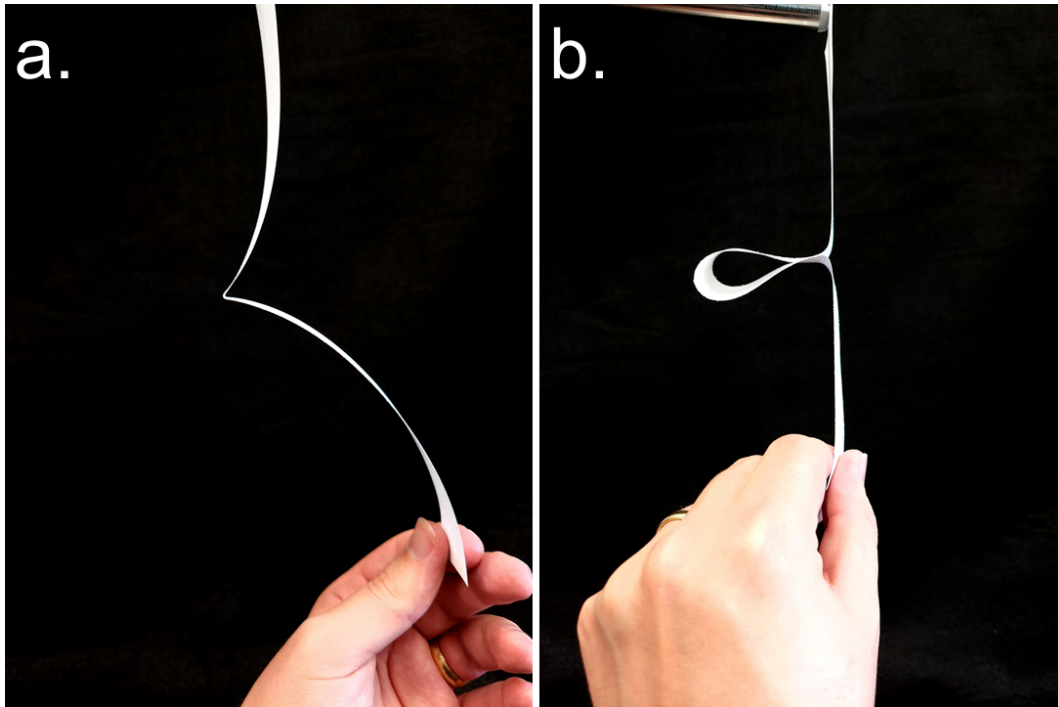
Figure 4.1. a.) A traditional fold as seen in origami. The paper is permanently deformed. b.) A raquet fold formed using adhesive forces between the paper and itself.

traditional creases. Fig. 4.1 shows a direct comparison of a paper fan design made from traditional plastic creases (Fig. 4.1a) and elastic-adhesive bends (Fig. 4.1b).

Simple origami shapes can easily be created when elastic sheets are substituted for paper sheets (as seen in Figs. 4.2 and 4.3), with the important distinction that the creases seen in Figs. 4.2a and 4.3a and absent in Figs. 4.2b and 4.3b. Additionally, instead of the vertexes seen in Figs. 4.2a and 4.3a where straight creases meet, developable cones (d-cones) can be seen in Figs. 4.2b and 4.3b forming where bends of different orientations meet.[18] It should also be noted that while elastic sheets lend themselves readily to this racquet-based folding, they are not the only materials that can be used. Paper can also work for racquet based folding, as long as its critical curvature for plastic deformation is not crossed and the paper remains in its elastic state.

Origami may have inspired much of the research presented in this chapter, but the move to use adhesion to create useful structures from highly deformable films and sheets is also related to the creations of chefs and bakers working with raw pasta, pastries, dough, and other easily-deformable and thin edible materials. These different foods are created and rolled out or extruded into thin sheets then made into unique designs tailored to specific purposes.[111, 4] The sheets are highly
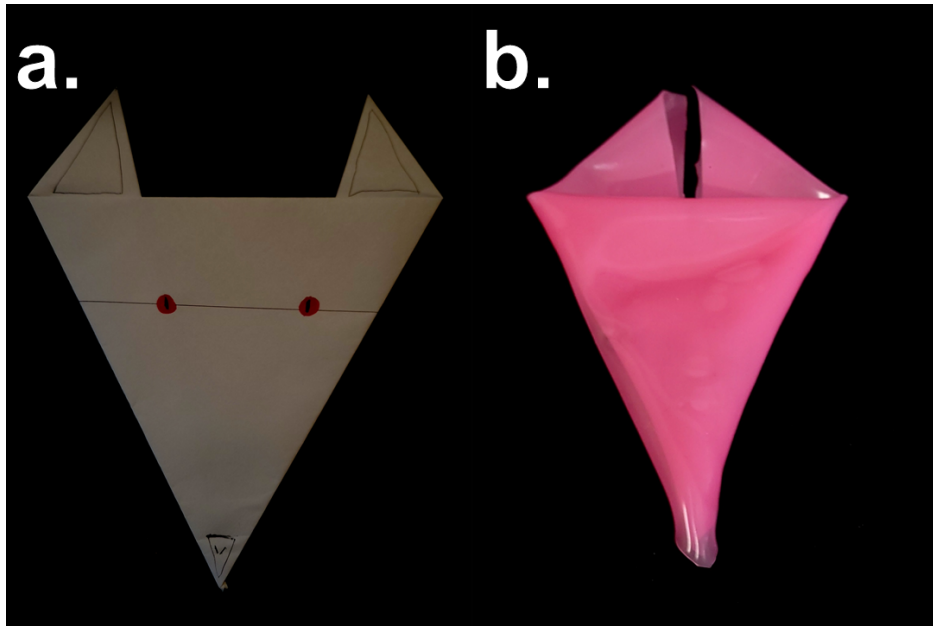
Figure 4.2. a.)An origami fox folded with traditional creases deforming the paper, locking the shapes in place. b.)A fox design created using the same folding pattern as the origami fox, but with an elastic sheet. All creased fold locations are replaced with racquet folds. D-cones appear at the corners of this shape.
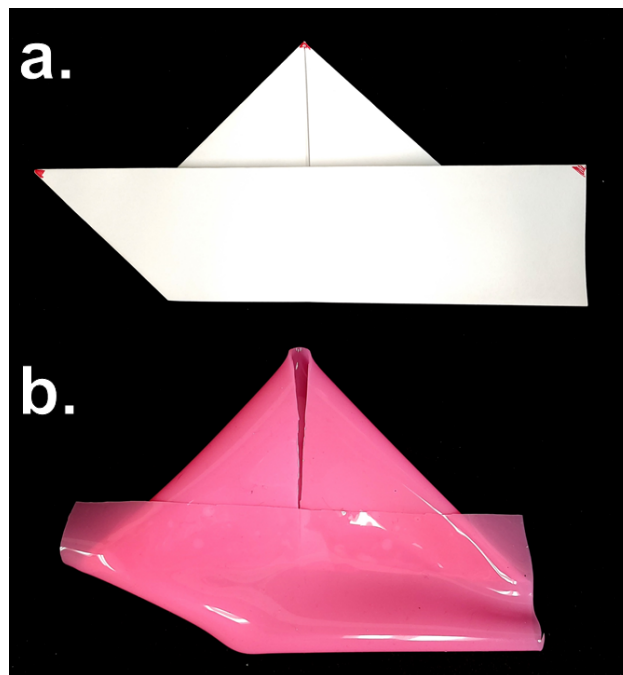
Figure 4.3. a.)An origami boat folded with traditional creases deforming the paper, locking the shapes in place. b.)A boat design created using the same folding pattern as the origami boat, but with an elastic sheet. All creased fold locations are replaced with racquet folds. D-cones appear at the top of the boat's sail, and at the ends of the diagonal on the bow of the boat.

Figure 4.4. a.) Egg wash is applied to the thin film of the egg roll to adhere it to itself before the roll is fried (Used with permission[48]). b.) Egg roll, held together by a thin sheet adhered to itself with an egg wash (Used with permission[48]). c.) Pumpkin roll, pastry scrolled up with cream acting as adhesive between layers (Used with permission[49]). d.) Galette, made from bready pastry holding zucchini filling. Top sheets of dough help maintain structural stability of the basket container (Courtesy of Elizabeth Twohig). e.) Waffle cone, made from a sheet of waffle, held together with chocolate before the sheet is fully hardened (Courtesy of Elizabeth Twohig). f.) Sushi roll, made from seaweed sheet wrapped around food cargo and adhered to itself with water (Courtesy of Elizabeth Twohig).

bendable in their raw state and cannot provide much structural support until they are cooked. If a chef wants to create a food delivery system from one of these materials, they need to work with the elasticity of the materials and an edible adhesive to create a stable structure (at least until the structure is cooked or eaten).[121] This can be seen in an enormous variety of foods including ravioli, canoli, tortelini, egg rolls (Fig. 4.4 a and b), fortune cookies, waffle cones, rolled pastries (Fig. 4.4 c), galettes (Fig. 4.4 d), spring rolls (Fig. 4.4 e), sushi rolls (Fig. 4.4 f), calzones, and many other food delivery systems not named here. The purpose for many of these foods are the same as the driving purpose for many of the fields exploring the possibilities of origami designs: packing cargo (food) into a stable container, and have it remain protected until some external stimuli releases the cargo. During this process, the container may be subjected to a variety of external conditions, but it should remain closed.

Other examples of thin sheets combined with adhesion to form useful shapes can be seen in packaging systems that utilize paper or cardboard folded in some way to encapsulate a cargo such as tea bags, milk cartons, and envelopes. These shapes consist of sharp, origami-like creases
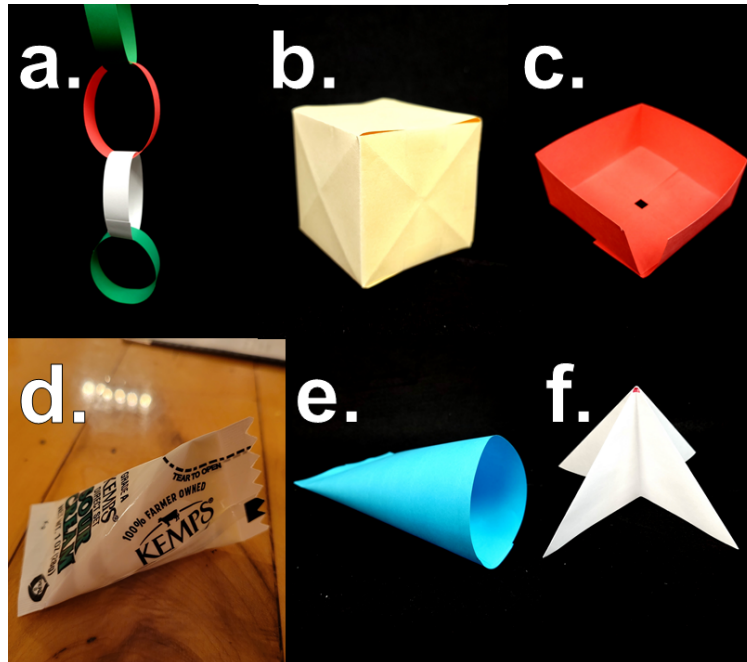
Figure 4.5. Structures made from thin films and adhesion. a.) Chain of loops made from strips adhered to themselves. b.) Box folded from a "t" shaped piece of paper folded and adhered to itself. c.) Square container created from a flat rectangular sheet and a series of folds. d.) Squeezable container created from a sheet that is first formed into a tube, then has both ends adhered together to encapsulate a cargo. e.)Open container version of the precious shape with only one side adhered closed. f.) Stable three-dimensional shape formed from folding a square sheet and adhering interior folds together.

and adhesion to attach paper sheets together. Many of these systems are very similar to the food systems mentioned earlier. In the case of cardboard boxes and cartons, the sheets are more rigid and can be used to create strong encapsulation systems. The use of creases and flat plates allows for the creation of many classical packaging systems, but the incorporation of bent plates or racquet folds into these applications has not been explored.

The combination of bending, folding, and adhesion to thin sheet systems offers the possibilities of entirely new assembled shapes and methods for assembly of traditional shapes. Many shapes that are very easy to assemble with adhesion can prove nearly impossible to build from a flat sheet otherwise. These shapes can be quite useful and include tubes, loops (Fig. 4.5a), Möbius strips, rigid boxes (Fig. 4.5b, containers (Fig. 4.5c), squeezable containers (Fig. 4.5d and e), pre-stressed bends, racquet folds, heart shapes, stars, clovers, self-supporting towers and pyramids (Fig. 4.5f), and many more.

Similar to how the incorporation of cuts into thin sheets led to increased functionality and application of thin materials in the new field of kirigami (paper cutting), the addition of adhesion leads to the new field of kuttsukugami (from Japanese: sticky+paper. Translation thanks to Prof. Dan King of Hokkaido University). Kuttsukugami also has the possibility of being more useful than traditional origami or kirigami. One major advantage is that adhesion is a surface force. This means that as films are scaled down from sub-millimeter thickness to micro- and nono-meter thickness the likelihood that structures will remain in a stable configuration goes up. This also affects the size of the racquet shape used to create analogous folds in these structures. As the film thickness decreases, the minimum length that needs to bend and self-adhere to created a stable fold also goes down, as was explored in the previous chapter.[44, 133] Practically, this allows for more and more complexity to be built into smaller and smaller films. Again, as described in previous chapters, capillary origami and surface treatments of the film and substrate offer a non-destructive mechanism for accomplishing multi-step assembly of these structures.

In this chapter the possibilities of Kuttsukugami are explored. Several topics are introduced that each represent separate and unique aspects of the adhesive folding system, but can work together to create complex and useful structures. First, the racquet fold is explored. This is the basic fold of adhesive systems, allowing structures to be created from plastic or elastic sheets without the need for permanent deformations. Racquet folds also create less strain, so wires can be incorporated into the sheets. The survivability of copper wires in a racquet fold system are experimentally tested and compared to the same wires in creased systems. Circuits are designed that take advantage of the ability of wires on sheets to be folded into many stable configurations. Next, shapes are introduced that can be easily made from flat sheets and adhesion. Some familiar shapes such as the Möbius strip and the scroll are studied. The interplay between the adhesion holding these shapes in a closed state and the elastic bending energy acting to release these shapes into a flat state is tested experimentally. An explanation of this relation gives insight into the possible uses for these shapes, and what is needed to switch between the two states. A wide variety of new shapes are created from simple thin strips. One of these shapes is a virtual developable cone (d-cone), that shares many of the same characteristics with a classical d-cone that may be observed in a sheet of paper that is bent in two perpendicular directions. However, this virtual d-cone does not actually permanently deform the material, instead forming this area off of the sheet.
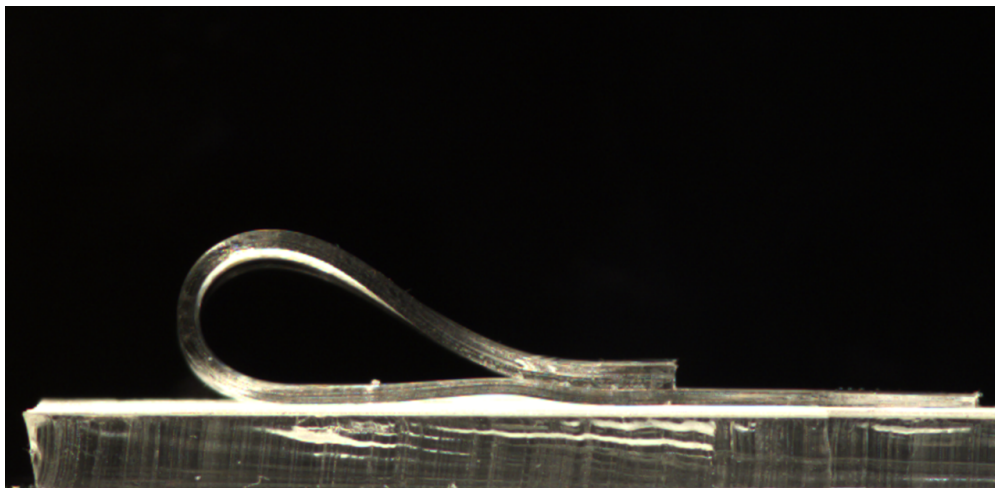
Figure 4.6. A racquet shape formed from PDMS folded onto and adhered to itself. This shape is stable because an equilibrium has been reached where the bending forces are balanced by the adhesive forces.

Finally, systems for encapsulation are discussed. These systems are of great importance at all scales. Examples can be seen in food delivery systems incorporating pasta as the encapsulating film, all the way down to microscopic drug delivery systems that must be able to encapsulate therapeutics and travel through the blood stream.[22, 5, 40] Methods for the precise release of cargo in these systems are also discussed.

4.2. Racquet Folds

A major advantage of the use of an adhesive to create three dimensional structures from sheet is the ability to use elastomeric sheets. These sheets resist permanent deformations, and will relax back to their original state when a driving force is removed, meaning that they are highly reusable. Elastomeric sheets are an ideal material for applications that experience a lot of bending and stretching, since these materials will take longer to fatigue and break than more rigid materials. However, an effect of this elasticity is that the creases commonly used in origami will no longer function. A bend created and pressed into a thin sheet of rubber or gel will not be fixed in place by the plastic deformation in the sheet like one would see with a paper sheet. A rubber sheet bent onto itself as in Fig. 4.6 may stay in place if it is allowed to adhere to itself. This shape is what is known as the "racquet" shape: a sheet or film bent 180° and placed into contact with itself. The racquet shape has been studied mathematically through use of the elastica, and is observed experimentally in carbon nanotube folding [102, 81, 82, 27, 26, 138, 44, 21, 1] and in capillary
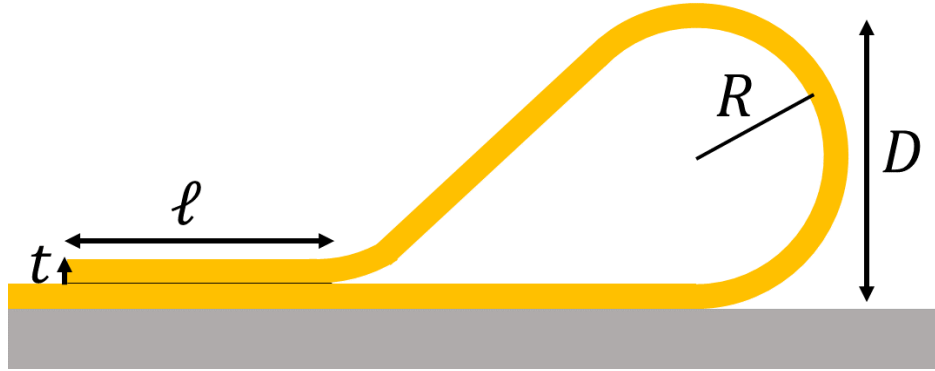
Figure 4.7. A side view of a racquet shape formed by bending an adhesive sheet of thickness t onto itself. This shape will naturally adopt a configuration where the bending force is balanced by the adhesive force, resulting in a radius of curvature (R) and a maximum height of the racquet bend (D). A minimum length of adhesion (ℓ) is required to maintain a stable racquet shape. The width of the sheet (b) is not seen, but is into the page.

origami systems.[93, 12, 70, 133] This shape is also much less destructive to the material because the strain encountered in the racquet is much less extreme than what is needed to create plastic deformations in origami folds. A simple calculation can be done to prove this point comparing a sheet of thickness 0.05 mm that is creased (interior radius of zero) to the same sheet bent into a racquet formation (interior radius of 2.68 mm). The strains encountered in the bent parts of the sheet are calculated with Eqn. 1.1, and result in $\epsilon = 1$ for the outer radius of the creased example and $\epsilon = 0.09$ for the outer radius of the racquet folded example. A difference in strain of an order of magnitude! The damage to the sheet from creating extreme strains in folds acts over time to weaken and destroy the sheet, making applications that rely on using a crease as a hinge likely to fail over repeated use. These factors make racquet bends a promising answer for systems that frequently actuate and bend around a single point.

Depending on the film's material properties and the adhesion values, the racquet shape may remain stable in this configuration or peel from themselves and open to a flat state. The schematic in Fig. 4.7 defines several geometric features of a typical racquet fold. The stability of a racquet is determined by the balance between the force acting to straighten the bend in the racquet of radius R and the adhesive force between the two parts of the sheet in contact (contact area:$A = \ell b$ where b is the width of the sheet into the page).[44] A stability solution relating the length of film that needs to be in contact with itself to the thickness of the film is found through experimentation and is given in the previous chapter of this work and in the paper by Twohig and Croll.[133] A model

for the length of film needed to create stable racquets (L_{crit}) is also given as:

$$L_{crit} = \alpha \sqrt{\frac{B}{\gamma}}. \tag{4.1}$$

Where α is a numerical prefactor determined by the model used, B is the bending modulus of the material ($B = \frac{Et^3}{12(1-\nu^2)}$), and γ is the work of adhesion of the film to itself. Our research found that the prefactor for determining the stability of elastic racquets was $\alpha = 3.8$, or 3.8 times the elastocapillary length was needed to create a stable racquet.

A model of a stable racquet shape was introduced by Glassmaker and Hui through use of a two-dimensional elastica.[44] The most easily measurable quantity covered in this paper is the maximum height of the racquet, D in Fig. 4.7. This maximum height is given by Glassmaker and Hui's model as:

$$D = \frac{\eta(\mu)}{\sqrt{Q}}, \tag{4.2}$$

where

$$Q = \frac{\gamma}{B}, \tag{4.3}$$

and $\eta(\mu)$ is a numerical result of their model which equates to $\eta(\mu) = 0.94$ when using $\mu = 0.01$ in Eqn. 4.4

$$\eta(\mu) \approx exp(-0.05810 - 0.16937 \ln \mu - 0.02846(\ln \mu)^2 - 0.00146(\ln \mu)^3). \tag{4.4}$$

Where μ is defined as the ratio of the work of adhesion of the interface destroyed by the peeling of the film from the substrate to the interface holding the racquet together. This gives a model for the expected racquet height in a system with known material properties. It should also be noted that the height of a racquet is approximately equal to double its radius of curvature, so $D = 2R$ was used for calculations.

Experiments were created to test the model of Eqn. 4.2. This experiment was conducted by creating strips of PDMS of various ratios. These ratios were 10:1, 30:1, and 40:1 prepolymer to crosslinker. The thicknesses of these samples were measured, then they were placed on a low adhesion substrate and bent 180° and into contact with themselves. After several minutes, the racquet shape was photographed in profile, producing a typical image as shown in Fig. 4.6. The height of the racquet was measured from the substrate to the top of the bend, as given by D in

Fig. 4.7. The racquet was then pressed completely closed (interior radius of near zero) and released, to ensure that the elastic forces of the film would be driving peeling and increasing the racquet radius. This allowed the racquet to approach an equilibrium value from both sides, showing the possible spread in results. After several minutes, a profile picture was taken. This was recorded as a separate height. These height values were plotted against the thickness of each film in Fig. 4.8. Model lines from Eqn. 4.2 and 4.3 were also plotted against the experimental data in Fig. 4.8. The use $\mu = 0.01$, leading to $\eta(\mu) = 0.94$ for each calculation. This number was chosen as the substrate used for experiments created $0.5 - 3\%$ surface area contact between the films and substrates, while the film-film adhesion was assumed to be $\approx 100\%$. The use of these substrates led to an effective adhesion to the film (γ') of $\gamma' = k\gamma$, where k is the percentage of contact between the film and substrate and γ is the typical adhesion value. A Poisson ratio of $\nu = 0.5$ was assumed for all PDMS ratios. Eqn. 1.15 and the values in the following table were used to compute the lines. No fit parameters were used to adjust these lines.

The data in Fig. 4.8 shows several trends. The 10:1 data (black circles) shows a relatively tight rising trend in the data closely following the dark blue model line. Meaning that thicker films lead to larger radius racquet structures. The data for 10:1 PDMS falls around the line predicted by the model. There is a slight discrepancy between the data and the model, which falls well within the error reported by Glassmaker and Hui. They report that the model predicts values that are "a factor of two to three too small."[44] This is also confirmed by our own research, which found a similar discrepancy. The model lines predicted for 30:1 PDMS (light blue) similarly undershoot their experimental values by a factor of 2 or 3. The model line for 40:1 PDMS (orange) seems to only fit the thinnest samples. Even with the correction from Glassmaker and Hui, the model diverges from actual, observed values. Some contributing factors to the model not aligning with thin film data includes that the approximations used in many of the elastica models assume zero thickness materials, and were designed for graphene films. This model also does not account for the affect of

Table 4.1. Constants for PDMS used to compute the model lines in Fig. 4.8.[36, 133]

Ratio	$E[Pa]$	$\gamma[\frac{N}{m}]$
10:1	1.69×10^6 Pa	0.124
30:1	1.1×10^5 Pa	0.15
40:1	1.3×10^4 Pa	1
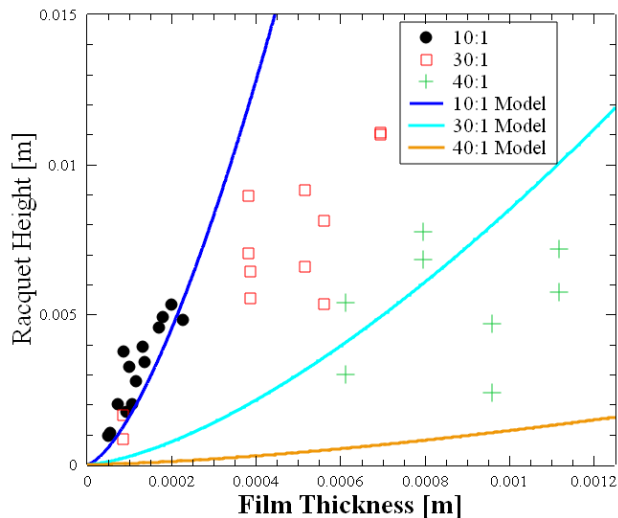
Figure 4.8. Plot of racquet heights (D in Fig. 4.7) versus the thickness of the film. These racquets were made from PDMS using 10:1 (black circles) prepolymer/binder, 30:1 prepolymer/binder (hollow red squares), and 40:1 prepolymer/binder (green crosses). Higher ratios of prepolymer to binder create films that have lower modulus and higher adhesion values. This is demonstrated in the plot with thicker films having relatively low racquet height values for the higher ratio mixtures. The blue line is the calculated model for the height of 10:1 PDMS, the light blue line is the calculated model for the height of 30:1 PDMS, and the orange line is the calculated model for the height of 40:1 PDMS.

the weight of the film. This can usually be neglected for the thin films used throughout this work (approximately 0.5 mm), since the bending of the sheet and the surface properties dominate over these regimes. However, for the thickest films represented in Fig. 4.8 there may be an effect of the weight of these films leading to lower maximum height measurements. The increased weight coupled with the high-adhesion and low-modulus films created from the 40:1 PDMS recipe all act to skew the results of these thick films. The 30:1 data (hollow red squares) follows a similar trend to the 10:1 data, but there is much more noise in the data. This could be due to the higher adhesion or the lower modulus of the material causing peel fronts to become "stuck" at a location that is near, but not at the equilibrium value. Larger bending forces can often push past these stick-slip locations. The 40:1 data continues the trend of greater noise in the data, and also a smaller relation between the thickness of the film and the maximum height of the racquet. Again, this drop could be due to the weight of the sheet favoring smaller racquets, or stick-slip mechanics not allowing movement of the peel front in such a low modulus material.

This data confirms that as the thickness of the film is decreased so does the effective radius of racquets that can be created from that film. A model was used to predict the height of racquets and was tested against experimental data. Experiments showed that there was good agreement between the prediction and trend of the measured values for films of thickness below 0.0005 m. Using Eqn. 4.2 as a guide when designing bend will allow the user to plan the maximum radius of curvature allowed for each application into the system, since the adhesive racquet will relax to this size. This makes the incorporation of electronic, for example, into systems more streamlined. If a designer knows the maximum strain allowed for an electrical component, or perhaps a curvature that the wire can be repeatedly bent and not fail, it becomes a trivial task to design a thin system that will not exceed those paramaters. The film's modulus, thickness, and adhesion values each offer different ways to manipulate the racquet radius that are well understood with most common materials.

4.3. Foldable Electronics

The drive for making smaller electronics is a major impetus for the study of thin films and how they can be assembled into complex systems. Currently, this research has led to the creation of tiny switches and hinges that can act to create or close circuits.[63] Nanowires can be placed onto thin sheets that can be assembled into permanent structures through traditional origami processes.[7] A problem arises when these origami structures need to actuate along a fold line many times. Any metal wires running through these creases will fatigue over time and eventually lead to a break. Metal wires have a relatively low strain of failure, so the extreme strain from an origami crease leads to rapid failure of the wire. Processes have been developed that work around this drawback, such as the wire not being attached to the part of the hinge that is creased or the wire being attached to the film in a sinusoidal pattern or the use of liquid metal wires.[37, 63, 132] This way when a strain is applied to the film, the wires can straighten to accommodate the higher overall increase in length. These solutions can work in specific situations to accommodate specific strains, but are not very adaptable and require a large amount of pre-planning of circuits and bend locations to be robust. The use of elastic sheets to create folds and structures creates a much lower strain on wires placed onto the films due to the racquet shape limiting peak curvature. Sheets that are pushed past this equilibrium racquet shape will relax back to a lower strain shape, ensuring that the wire does not stay in a highly strained state. This means that the wires will not fatigue and fail as easily through

107

repeated movement and that complex structures and circuits can be assembled without the need for workarounds to be built into the system to protect the wires.

Incorporating adhesion into thin film electronics not only allows for the possibility of new stable shapes to be created, but also for more configurations and circuits to be created from a single sheet. Leads printed onto the surface of a thin film can act as switches connecting different circuits merely through bending the film and adhering it to different positions connected to wires and form a circuit. A simple example of these possibilities is given in Fig. 4.9 where wires and leads are printed onto both sides of a thin adhesive film. Bending the film in one direction connects the negative lead to the terminal on the front of the sheet, thereby connecting a series circuit and illuminating the light bulbs (Fig. 4.9a). If this same sheet bent in the opposite direction, a parallel circuit is made by connecting the leads on the back of the sheet (Fig. 4.9b). Other circuits and configurations could be made through the use of more complicated folding schemes, such as folding the top right corner of the front of the sheet (Fig. 4.9a) forward so that it connects to the middle or bottom lead on the left side of the front of the sheet, producing a series circuit of 2 or 1 light bulbs, respectively.

Building complexity into these systems means that there is the possibility for huge reconfigurability of a single sheet with wires and electrical components built into the film. A sheet could act as a breadboard of sorts that would activate certain circuits when folded into specific configurations. For example, a device could be made that demonstrates the series and parallel circuit affects on light bulbs previously mentioned. Another use would be toys that light up in specific ways when folded into that configuration: an origami truck with working headlights and tail lights that light up when properly folded, a boat with lights on the bow, stern, and sail, a paper airplane with a tiny electric propeller and wing lights, a fox or bison with eyes that light up, and many other creations (even some that may not include lights at all-they are just the easiest to imagine). One could even imagine an application where a belt or Möbius strip is created with conductive wires all along its surface. This could be used to provide power to the very pulleys that the belt is wrapped around without the need for brushes or other devices to transfer electricity to spinning objects. The possibilities of reconfigurable electronics in thin elastic sheets have barely begun to be explored and could lead to many advancements from upcoming research. In this section we explore the baseline characteristics of thin, but traditional, copper wires on the surface of thin sheets. The effects of repeated bending into a racquet formation versus repeated creasing into an origami fold are tested with respect to the
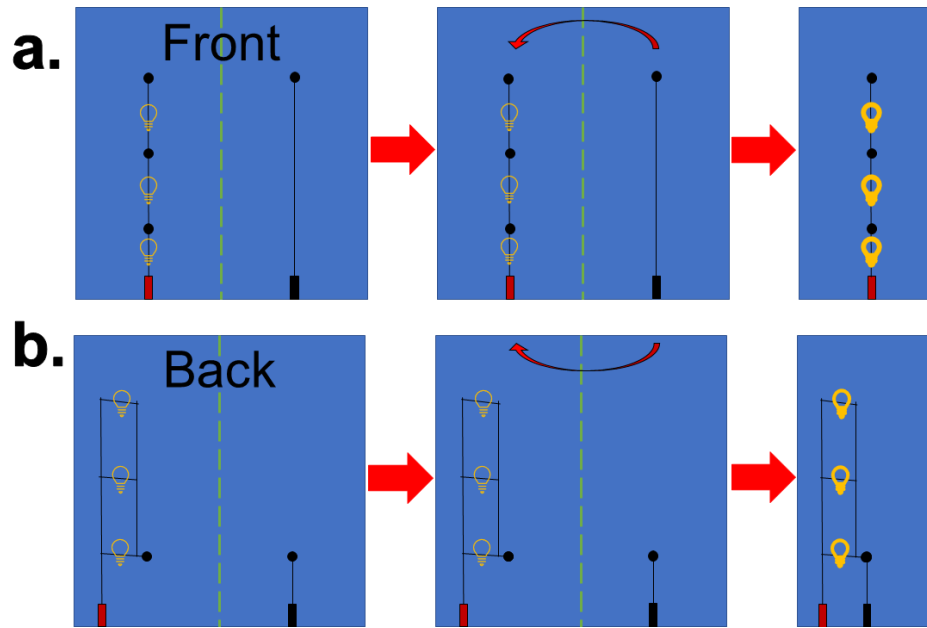
Figure 4.9. Circuit diagram for a series and parallel circuit printed onto a thin film. Green dotted lines are planned folds. Light bulbs represent lights or some other component of the circuit. Black lines represent wires. Black circles represent leads on the surface of the sheet and are assumed allow current to flow when adhered to another lead. Red and black rectangles represent positive and negative leads which may be wires protruding from the film and to a power supply. a.) Series circuit printed on the front of the sheet. When the sheet is folded, the lead on the top right side of the sheet connects to the top lead on the left side of the sheet. This creates a circuit where the three light bulbs are all in series. b.) Parallel circuit printed onto the back of the sheet. When the sheet is folded, the lead on the bottom right side of the sheet connects to the lead on the left side of the sheet. This creates a circuit where the three light bulbs are all in parallel with one another.

continuity of the wire. Designs incorporating wire circuits, such as those mentioned in Fig. 4.9, can incorporate these racquet bends and become more robust, actuating circuits with a much longer lifetime than circuits made where wires traverse traditional origami creases. This will allow any origami shape that can be constructed with racquet folds, such as the shapes in Figs. 4.3b and 4.2b, to safely incorporate circuits on their surface.

4.3.1. Experimental Comparison of Creasing and Racquet Bending

Experimental data was collected comparing the continuity of copper wires attached to a thin sheet of polyimide (provided by Prof. Mike Bartlett of Virginia Polytechnic Institute and State University) under various bending and creasing experiments. The sheets were 0.05 mm thick with a 0.04 mm thick and 1 mm wide copper wire attached to their surface, and were cut into strips 50 mm long. The sheets would plastically deform under large strain, but would not tear
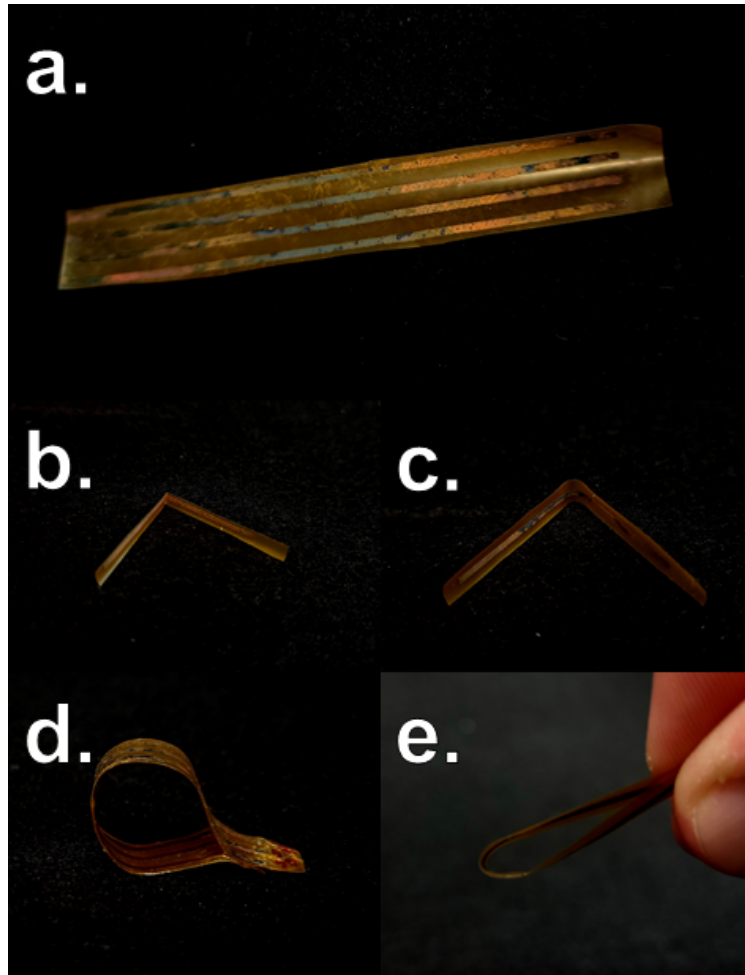
Figure 4.10. Thin film-wire composites. a.) A sheet of polyimide with four thin copper wires attached to its surface. b.) Film-wire composite creased and permanently deformed using an origami fold. c.) Film-wire composite bent around a cylinder of radius 2.68 mm. Deformed, but the wires are not damaged. d.) Racquet fold formed by applying an adhesive to the inside surface of the film-wire composite, then attaching the two ends of the strip together. e.) Bend produced by bending around the scoopula barrel. Radius of curvature is smaller than the racquet fold.

or fracture during the tests. Each strip had a lead cleaned of oxidation with a file and then an alligator clip was attached to each end of the wire. A current and voltage were applied to the wire with a GW GPS-1850D power supply. The current I was measured from the power supply, and the voltage V was measured with an Extech Instruments multimeter at the two ends of the wire. These were used to find the resistance R of the wire using $R = \frac{V}{I}$ Measurements were made before any bending or creasing happened, and then after every bend and crease up to 10 cycles. After this, larger numbers of cycles between measurements were used and recorded. Any strips that were still showing connection after 500 cycles were deemed stable. Fig. 4.11 shows the resistance calculated
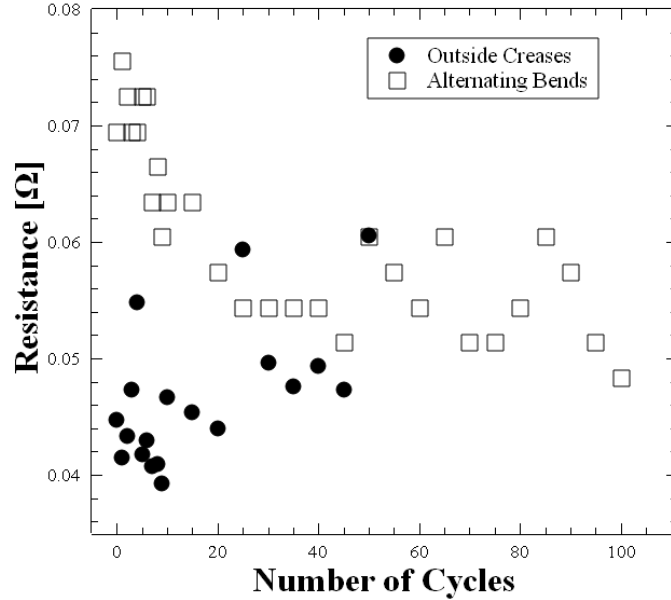
Figure 4.11. Plot of the resistance calculated in the wires versus the number of creasing/bending cycles completed. The bent wire shows an initial drop in resistance, smoothing out to an equilibrium value. The creased wire shows the opposite trend of rising resistance, but approaches the same value. The creased wire broke before 50 cycles were completed.

vs. the number of cycles completed for creases where the wire is on the outside of the film (black circles) and for alternating bends around a scoopula barrel (hollow squares). This plot covers the first 100 bends for each sample, or until the wire broke, whichever came first.

Traditional origami creases were tested for their damage to wires by bending the strip at its middle and pressing this bend into a fold between the pages of a hardcover book for about 5 seconds. The strip was then straightened and measurements were taken. The cycle was then repeated until the current across the straightened strip was zero, or 500 cycles had been achieved. The number of cycles before breaking the wire were averaged and are reported in Fig. 4.12. This was repeated for creases that had the wire on the inside of the fold, outside of the fold, and alternating sides with three wires for each test. This test was repeated with bends instead of creases by wrapping the strips around the cylindrical barrel of a pen (diameter=9.6 mm) and a scoopula (diameter=2.68 mm). The pen barrel was used with the wire on the outside of the bend to recreate a likely situation where adhesive is applied to the sheet on the side without wires. The scoopula was used with alternating bends, as this was seen as the most destructive situation from the crease tests. Both of these tests

111
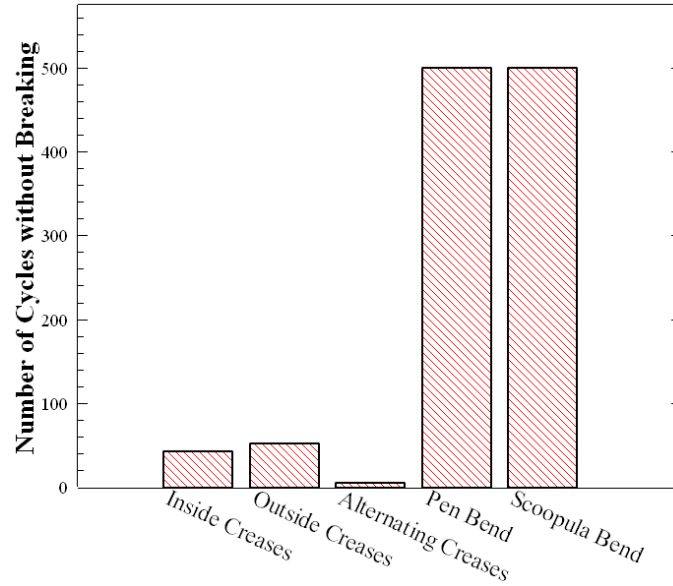
Figure 4.12. Graph showing the number of bending/creasing cycles completed before a break was noticed. The wires that were creased (in any configuration) broke much earlier than the wires that were bent around a cylinder. All of the creased experiments broke before 50 cycles, while the bent wires did not show signs of damage through 500 cycles.

ran to the limit of 500 bends without a noticeable drop in the current across the wire, and this is shown in the results of Fig. 4.12.

Fig. 4.11 shows data from two experiments of cycling bends/creases and straightening. Overall, there is not a great deal of change in the resistance of either wire as cycles are repeated. Both wires start at an initial resistance and drift about 0.015 Ω towards a similar value of around 0.055 Ω. The bent sample starts at a higher resistance and drops, while the creased sample starts at a lower resistance and rises to approach the value. The creased sample breaks between 45 and 50 cycles of creasing and straightening. leading up to this breakage, there is no obvious indication of the wear in the resistance data. The alternating bends sample was unharmed through the 100 cycles shown in Fig. 4.11, and further to at least 500 cycles, as shown in Fig. 4.12.

Fig. 4.12 shows that bending the sheets and wires into a 180° bend is a much less destructive method than creating a traditional origami crease. This is shown even though the wire's substrate material is a plastically deformable material similar to paper. The test conducted with alternating inside and outside creases was the most destructive of the creased samples, with the wire failing around 5 folds in each of the tests. The inside folding situation destroyed the wire connectivity before 50 cycles. The outside folded situation destroyed the wire connectivity around 50 cycles.

The number of cycles to failure was not recorded in the first 500 cycles for either of the bending tests conducted, and each of the bending samples showed no signs of fatigue or near failure. These tests demonstrate that the racquet shape is a much less destructive shape for the connectivity of wire circuits that traverse the bend. The wires remain connected through at least an order of magnitude more cycles when the strips are bent instead of creased. A similar rise in the survivability of these bendable structures could be expected when incorporated into systems that get repeated and cyclic use.

It should also be noted that in tests where adhesive was applied to the sheet and then the sheet was bent onto itself, the stable racquet radius that was observed was similar to the radius of the pen barrel. One would expect similar results to the bending experiments if the strips would have adhesive applied and were cycled between a racquet and straight configuration.

4.4. Shapes from Adhesive Sheets

Many of the shapes that can be made through the use of kuttsukugami can be created through other means, like traditional origami. However, the number of steps required to create a stable loop or cylinder using only classical origami techniques of folding and bending is astronomical when compared to the one-step process of bending a film into contact with itself using kuttsukugami techniques, akin to an analogue to digital transition. Other shapes can be made with well-known manufacturing processes, like loops or cylinders or even heart or bent shapes. Often this is done by joining together many different members into a single structure. This is where the major advantage of kuttsukugami assembly becomes apparent. Structures can be made by manipulating a flat sheet, which is readily scalable to microscopic scales. Thus, kuttsukugami methods allow for the creation or assembly of many useful structures from well understood materials and relatively simple processes. Additionally, some shapes remain impossible to create from a flat sheet without adhesion, such as a Möbius strip. Again this shape can be assembled with just two or three steps: the sheet is bent, then twisted, then adhered to itself. Kuttsukugami often gives either a simple path to create useful shapes, or a solution of how to create a previously impossible structure. In this section we describe many structures created by the kuttsukugami method.

Any torroidal shape is difficult to create using only origami, but becomes much easier to create through the use of adhesion. The cylinder, loop, and Möbius strip have been mentioned.

113
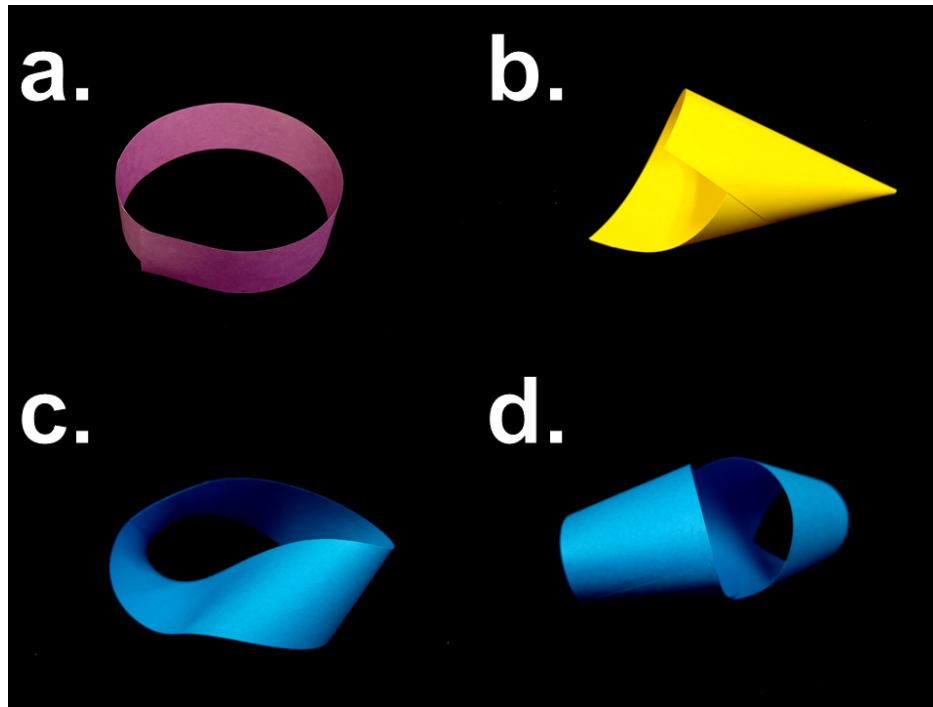
Figure 4.13. a.) Cylinder constructed by bending a strip of paper onto itself and adhering the ends together. b.) Cone constructed from a sheet of paper twisted around an edge and adhered to itself. c.) Möbius strip constructed by bending a strip of paper onto itself and then twisting one of the ends 180° before adhering them together. d.) Double-twist strip constructed by bending a strip of paper onto itself and then twisting one of the ends 360° before adhering them together.

The cone is another useful structure that is easily assembled from a bendable sheet with adhesion, among many more common shapes (Fig. 4.13).

Certain shapes can be assembled with traditional origami, but are improved through the use of adhesion. A paper airplane is easily assembled from a sheet of paper only (Fig. 4.14a), but one piece of tape securing the backbone of the airplane closed makes the entire structure more stable (Fig. 4.14b)(and more aesthetic in my opinion). Addition of creases into the curved adhesion guidelines opens the possibility of creating even more shapes. A box is a shape that can be relatively easily assembled through origami, but through a mixture of folding and adhesion can assembled into a significantly more stable shape. Boxes and cartons used in industrial and everyday applications are assembled in this manner, combining origami and adhesion to create strong containers from paper or cardboard.

The combination of adhesion, origami, and cutting of the sheet allows for the creation of yet more new structures. These structures can be assembled to act as a spring, or to hold
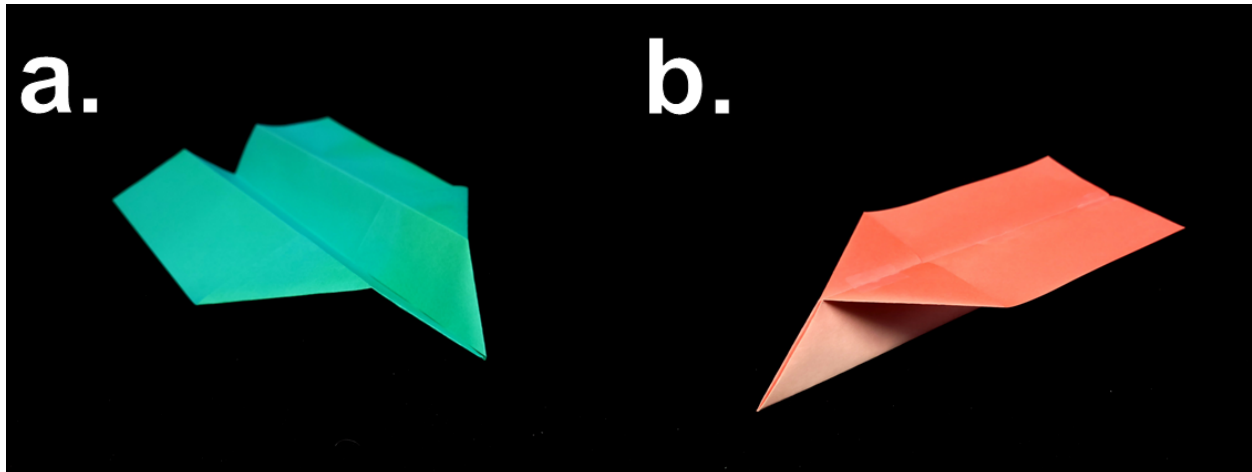
Figure 4.14. a.) Paper airplane constructed using traditional origami methods. Flops to a relaxed state when not held in a closed state. b.) Paper airplane constructed with traditional origami methods, then adhesive tape applied to keep the airplane in a rigid state. Backbone remains in a completely folded state.

certain components in a strained state, providing some structural stability. The post-it note "chain" represents one possibility seen in Fig. 4.15a. Each sheet has a thin strip of adhesive that bonds it to the sheet below. That sheet is bonded to the next sheet down, but at the opposite end from the previous adhesive strip. Pulling on one end of the post-it chain creates a repeating pattern where the adhesive parts of the system are parallel to one another, and perpendicular the the direction of the applied force. Applications that come to mind include artistic shelving and ladders, as well as possible conveyer belt configurations. This system offers the advantage that it can be easily packed into a shape that is the exact footprint of each sheet and only as tall as the sum of the sheet's thicknesses. The post-it chain is made from separate sheets of paper, or is constructed from a single sheet of paper origami-creased at regular intervals and adhered to itself near each crease, as opposed to the racquet bends discussed earlier (Fig. 4.15b).

Structures can also be assembled to maintain an overall shape of a larger structure. The heart is a familiar example of a shape that can be made this way. A loop is created, and creased in two positions on opposite sides of the loop. Then adhesion is used to hold the two sides of the loop together near one of the creases (Fig. 4.15c). Applying the adhesive on the inside of the loop near the crease creates more of a fish shape (Fig. 4.15d). Creating a loop with many creases that have adhesive applied near each crease can be used to create clover-like shapes (Fig. 4.15e), or star shapes (Fig. 4.15f); depending on if the adhesive is applied to the inside or outside of the loop.

115
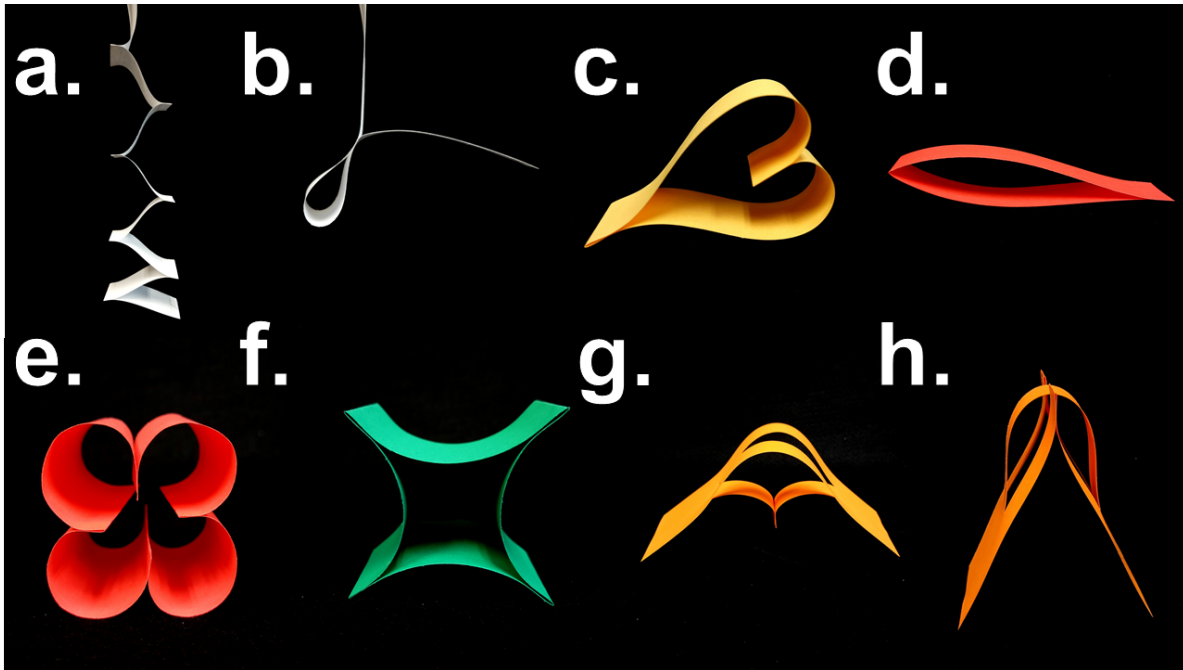
Figure 4.15. a.) Post-it chain constructed from a single sheet creased at regular intervals and adhered to itself on opposite sides of each crease. b.) Racquet bend adhered to itself. This shape could also be substituted into the post-it chain for the sharp creases in materials that cannot hold permanent creases, such as elastomers. c.) Heart shape created from a strip with a crease. The two ends of the strip were adhered together, pointing into the shape-forming a heart. d.) A fish shape constructed in a similar way to the heart, except that the two ends are adhered to one another pointing outward from the shape. e.) A clover shape constructed from a single sheet creased at regular intervals. Adhered to itself at the ends of the sheet and around each crease, each pointing inward, towards the shape. f.) A star shape constructed from a single sheet creased at regular intervals. Adhered to itself at the ends of the sheet and around each crease, each pointing outward, away from the shape. g.) Bridge shape constructed by cutting two slits into a strip and creasing the center portion. The center portion was adhered to itself around the crease. Remains in a stable bridge shape. h.) Tall bridge shape constructed by cutting two slits into a strip and creasing the outer portions. The outer portions were adhered to themselves around the creases. Remains in a stable bridge shape, but is more easily deformed than the previous shape.

Pairing the clovers and stars together create crude gear systems that can fit together in a tooth-and-groove like formation. Larger versions of this design can even switch between configurations, making the deployment of an array of these shapes into a system highly reconfigurable. Two designs for "bridges" are created from a strip that has two parallel cuts running along much of its length (Fig. 4.15g and h). Creasing and adhering different parts of this strip together allow for segments to be held in tension, resisting loads placed on different parts of the system by bending the smaller radius portions of the sheet that are held in a balance with the other portions of the sheet. Each of these specific shapes could have actual applications when structures are made from adhesive

sheets, and especially when the thinnest films are used to scale down technology to microscopic scales. These simple shapes made during the research of this and earlier projects represents just the surface of possible useful shapes that could be created in such a way.

4.4.1. Möbius Strip

The Möbius strip is one a widely known shape in the mathematical literature. It resides in the happy medium as a shape that is easily visualized and created, while also having interesting and often surprising properties. For example, most will cite that a Möbius strip is a single surface wrapped upon itself, so a straight line drawn along the surface will eventually meet itself. This is accomplished by taking a long and flat sheet and bending it 180°, then twisting one end 180°, and adhering the two ends of the strip together. A constructed Möbius strip is pictured in Fig. 4.16. The most widely seen use for a Möbius strip is as the belt on a conveyer belt or belt drive system as historically used in grain mills, saw mills, threshing machines, and many other uses where a large flat belt is driven from a flywheel or belt pulley. The inside-out twisting of the strip means that as the belt moves over the pulleys, there will not always be an "outside" or "inside" side of the strip. This is said to spread out the wear on the strip evenly and add to the longevity of the belt as opposed to a regular loop.[54] However, most of the popularity of the Möbius strip is due to the mathematical curiosity surrounding this interesting shape. Of interest to the thin film community is the discussion that has arisen regarding the total elastic bending energy stored in a Möbius strip.[8] This may seem like a simple question, but the unique shape of a Möbius strip gives rise to some complications.[77, 116] First, the width and length of the sheet used to create the Möbius strip dictate its final shape. If the width is too large compared to the total length, then a true Möbius strip will not even be possible. At the limiting width, the shape created will be more like a flat and hollow triangle. Second, there is not one large bend to calculate, like with a loop. There is a bend and a twist, so following one surface through a 360° rotation will leave the observer right where they started on a Möbius strip, except now on the outside of the shape. Also, the actual material properties do not appear to determine the shape for most Möbius strips. As long as the overall length is not huge compared to the width, and the film is relatively stiff and won't collapse, the shapes will be determined by the ratio of width to length. The thickness and modulus of the film do not relate to the overall shape of the Möbius strip, assuming that the bond holding the strip together is unbreakable. Since the modulus and thickness of the film do still factor into the overall
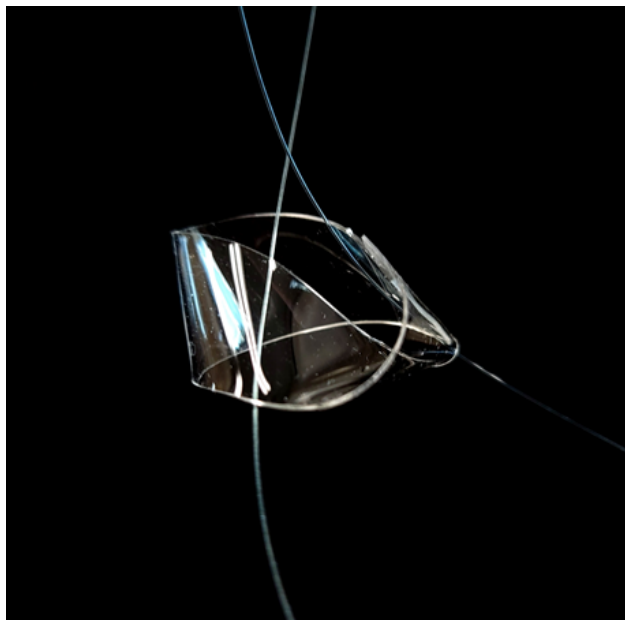
Figure 4.16. A Möbius Strip created by bending, twisting, and adhering a film of 10:1 polydimethyl-siloxane onto itself.

energy stored in the bends of the Möbius strip, there will be a point at which the elastic energy is too large for the adhesive to hold and the Möbius strip will peel from itself and relax to a flat film.

As an experimental approach to produce results that may point towards an answer for the total elastic energy stored in a Möbius strip, an setup was devised to find the total adhesive energy needed to hold a Möbius strip together. This experiment was conducted using well characterized 10:1 PDMS films that were measured for thickness, length, and width. The films were then bent and twisted into a Möbius strip configuration and adhered to themselves. The length of the overlapping region was measured, then the Möbius strip was allowed to relax. If the adhesive energy was less than the total elastic energy in the Möbius strip, then the film would break open and relax to its flat state. If this outcome occurred, the process was repeated with a larger overlap region. If the Möbius strip did not detach from itself after five minutes, it was recorded as stable. Stable strips were also disassembled and then reassembled with a smaller overlap.

The data for one of Möbius strip experimental runs using a strip of 10:1 PDMS, and changing the adhered length, is presented in Fig. 4.17. This plot demonstrates the relation between the effective strip length versus the area of adhesion between the strip and itself. Black circles represent stable configurations, and the red cross represents the configuration that was unstable and collapsed.

118

The effective strip length is the total flat strip length minus the length of the overlapped (adhered) region. The area of adhesion is the width of the film times the length of the adhered region. Fig. 4.17 shows that as the area of adhesion decreases the effective length increases, and eventually the Möbius strip breaks and relaxes to a flat state. This sample had a total length of 40.17 mm, a width of 6.96 mm, and a thickness of 0.227 mm. The effective length was calculated as the total length minus the length of overlap of the ends of the strip. The area of adhesion was calculated as the strip width times the overlap length. Knowing the area of adhesion and the G_c value for 10:1 PDMS adhered to itself ($\gamma = 0.124\frac{N}{m}$), a calculation can be made for the total adhesive energy of the last stable configuration and for the unstable configuration. The final stable configuration had an adhesive energy of 1.72 μNm, and the unstable strip had an energy of 1.07 μNm. Since the effective length of the strip changes with the area of adhesion, it can is difficult to pinpoint the exact elastic energy that is balanced by the adhesive energy, but these measurements give a good limiting value. Comparing this to the elastic energy stored in a PDMS loop with the same thickness and width predicts a radius of approximately 30 cm. This implies that the twist in the strip holds a large amount of energy, therefore increasing the loop size that would be equivalent to the Möbius strip.

According to Mahadevan and Keller (1993) the energy stored in a Möbius strip can be calculated by an equation built from the energies of bent and twisted elastic rods.[77] This leads to the energy expression $U = \frac{Eab^3}{\ell}5.69\pi^2$, where a is half the width of the film and b is half the thickness of the film and ℓ is the effective length of the film. The constant 5.69 is found numerically and includes a Poisson ratio of $\nu = 0.5$. Using this equation and the dimensions of the film used to create the data for Fig. 4.17 we arrive at an energy value of $U = 12.6$ μNm for the last stable configuration, and $U = 12.4$ μNm for the configuration that was unstable. These values correspond to the earlier reported adhesion values of 1.72 μNm and 1.07 μNm, respectively. Dividing the adhesive energies by the bending energies gives values of 0.14 and 0.08 for the stable and unstable configurations, respectively. This suggests that the critical adhesion to bending stability ratio is around 0.1 for this experiment.

The calculated bending energies are about an order of magnitude larger than the energy of the adhesion holding the strip together, suggesting that there are effects unaccounted for in the adhesion model and/or in the Möbius strip model. One such affect could be from the peeling of the
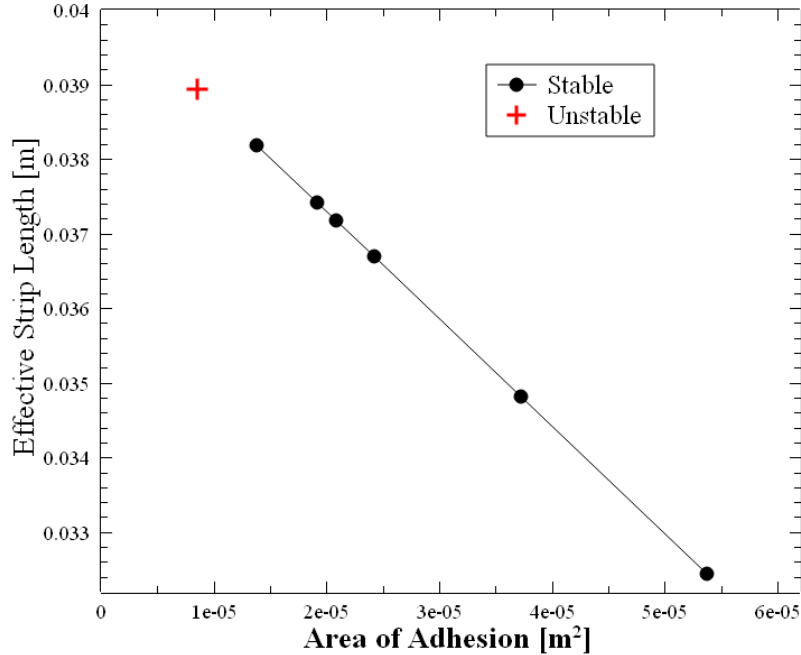
Figure 4.17. A plot of the effective strip length versus the area of adhesion between the strip and itself for a 10:1 PDMS Möbius strip. Black circles represent stable configurations, and the red cross represents the configuration that was unstable and collapsed.

two ends of the strip not occurring in the idealized 90° peel configuration that is often used to find adhesion values. Peeling at a lower angle often increases the force required to separate the surfaces and could contribute to this discrepancy.[55] The experimental design of overlapping the film may also be a contributing factor. The overlapped region is twice as thick as the rest of the strip, and therefore eight times as hard to bend. This will naturally push the double-thickness region to a region of the Möbius strip that is experiencing less strain. This would mean that the adhesive overlap region would not be experiencing the effect of the entire bending energy of the Möbius strip, but only a fraction of the total.

4.4.2. Virtual D-Cones

A developable cone (d-cone) is an area of a bent sheet where several differing curvatures meet to create an area of extreme deformation.[18] The easiest way to make a d-cone is to fold a piece of paper in half, then fold the bent piece of paper it in half again the opposite direction that it was initially folded. This is pictured in the double fold experiments (Fig. 3.13) described earlier in this work. In sheets that permanently deform, the area of the d-cone is often completely

120
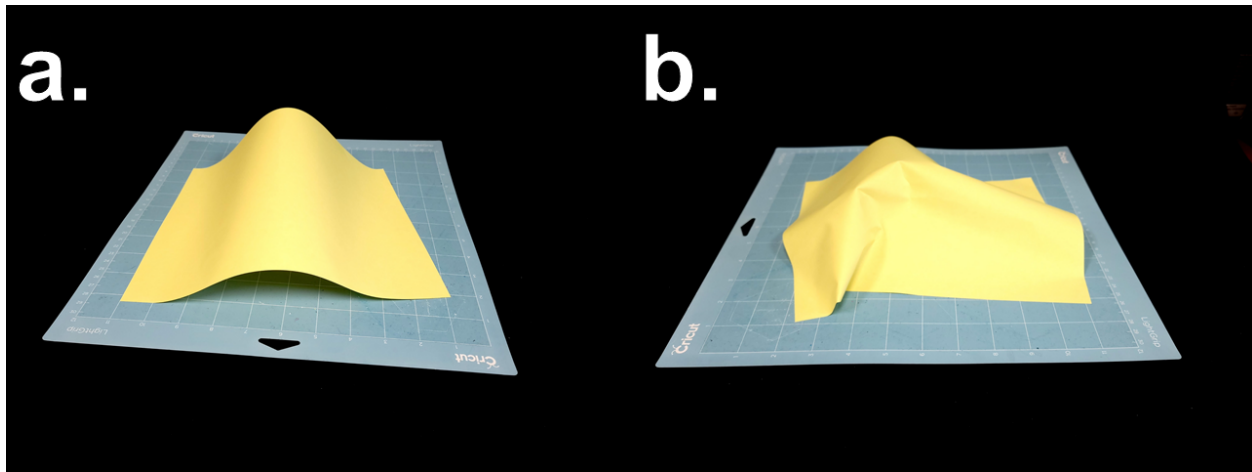
Figure 4.18. a.) A virtual d-cone made from paper attached to an adhesive substrate. The left and right sides of the sheet are not attached to the substrate parallel to one another, creating a change in the curvature between the front and back. The back has a much higher radius of curvature than the front. b.) A paper sheet attached to an adhesive substrate in a way such that the d-cone is within the sheet.

destroyed leaving a hole or rip as evidence of this deformation. Elastic sheets can also be used to create d-cones, but usually do not show permanent deformations from these extreme local strains.

The d-cone can act as a mechanical memory. Once a d-cone is created, that area of the sheet is destroyed locally and costs very little energy to deform again. Future bends in the area of the destroyed sheet will gravitate to the location of the d-cone. Shifting or adjusting other parts of the curved sheet will often use the d-cone as a pivot for these movements. Movement of a d-cone can be forced under certain conditions, resulting in a line of destroyed sheet for every point that had been occupied by the d-cone. This is a very high energy process and can be a contributing factor in the structural stability of shapes containing d-cones.[16, 15]

Adhesive sheets can be used to create "virtual d-cones." The simplest version of a virtual d-cone is created by securing a one side of a sheet to a solid substrate. The rest of the sheet is bent and the opposite side of the sheet is adhered to the substrate so that opposing sides of the sheet are not parallel with one another. This configuration is seen in Fig. 4.18a, where the bent sheet has smooth curves even though the curvature changes between the left and right and the front and back of the sheet. If the sheet were extended, it could only maintain this shape if a d-cone were formed. A real d-cone is formed from a similar setup when the left side of the sheet is adhered to the substrate, then the front is adhered. The right side of the sheet is adhered, again in a direction

121

that is not parallel to the left side of the sheet. This creates a destructive d-cone on the surface of the shape, which often leads to further destructive deformations, as seen in Fig. 4.18b. We further note, the cone shape of Fig. 4.13b is another shape created with a virtual d-cone.

A virtual d-cone offers some of the advantages of a regular d-cone without the major drawback of the need to destroy a section of the sheet (or invest the energy needed to create a d-cone). Once a virtual d-cone is created, it also acts as a pivot around which deformations of the sheet can adjust. The irreversible process of creating a d-cone in permanently deformable sheets is replaced with the reversible process of peeling and adhering the sheet to a substrate, or even to itself. The ability to change the position of a d-cone without any permanent effects in the sheet again point to the usefulness and multitude of reconfigurability of thin systems when adhesion is incorporated.

4.4.3. Scrolls

A thin sheet with adhesive applied to at least one side can be rolled into a much smaller package known as a scroll. Depending on the adhesive and material properties, a scroll can remain stable in a rolled-up configuration or release and unfurl to a flat configuration. The use of switchable adhesives can allow a system that is stable rolled-up to switch to an unstable state which will then unroll to a flat state.[29] Scrolls from thin sheets exist in various forms in the modern world from paper rolls, to metal rolls, to the coiled springs or rolled capacitors in many devices.[56, 41, 65, 109, 13] However, most of these applications need a container to keep the structure from unfurling itself. Adhesive scrolls also exist, for example in Fruit Roll-Ups™. The ability to switch between the stable and unstable scroll state is a key to useful applications of scrolled sheets and films. It should also be stressed that ability to scale down these systems greatly expands the possible applications in technology and medical uses.

The use of scrolls as encapsulates is an enexplored possibility for thin systems, but could offer a built-in feedback loop for release of a chemical. Consider an adhesive that dissolves in acidic solution. This adhesive could be applied to an elastomeric sheet, mixed with a basic powder, and then rolled into a scroll. In neutral solution the scroll is stable, but if the solution becomes acidic-the scroll will release the adhesive and unravel. This releases basic powder, which balances the pH of the system and stops the unraveling of the scroll. This device could feedback and act to balance the pH of a system for a length of time without sophisticated control. A similar system could be designed for drug delivery, where an adhesive is sensitive to a bodily function or illness. A proof-of-concept
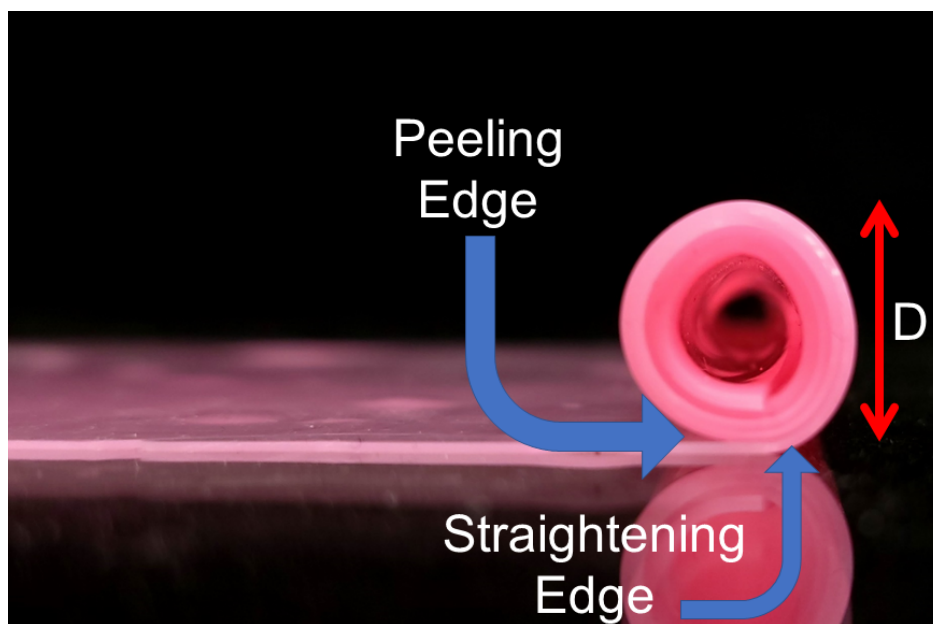
Figure 4.19. Diagram of a scroll made from a thin film (polyvinylsiloxane for visibility). An unstable scroll will have a higher bending cost than the adhesion is able to counteract, so it will unroll. The straightening edge of the scroll at the bottom right corner is the part of the film relaxing through unrolling. The film-film peel front is located where the top of the flat portion of the film meets the scroll. The height of the scroll was measured, and used to find an outer radius of the scroll.

system was designed and tested by Dr. Andrew Croll and family consisting of a thin (and sticky) Jell-O™ sheet scrolled around sodium bicarbonate. This scroll was dropped into a vinegar solution where it unfurled and released the sodium bicarbonate payload and produced a large amount of fizzing. The reaction of the sodium bicarbonate with the vinegar also may have helped to speed the unfurling of the Jell-O™.

While spirals, scrolls, and coils of sheets and films have received attention in the literature, the affect of adhesion between layers of the structure has often been neglected or ignored.[71, 110, 100, 11] Theoretical models and experiments designed to explore the shapes that are created when a film is coiled upon itself are often constrained by a rigid outer structure, removing any chance of the scroll spontaneously unrolling. Knowledge of the equilibrium between the adhesive forces of the system and the bending forces is vital for the creation of structures that are designed to switch between stable and unstable coils for specific purposes.

The stability of elastomeric scrolls was experimentally explored using polydimethylsiloxane (PDMS) films. PDMS was used because of the material's highly studied and understood material and adhesive properties and the ability to change these properties by varying the prepolymer to

123
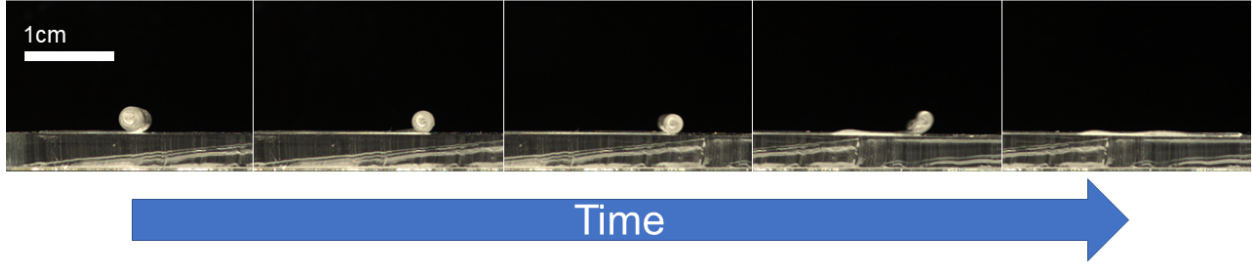
Figure 4.20. Sequence of a thin 30:1 polydimethylsiloxane scroll unrolling. The time between each frame is approximately 10-30 seconds.

binder recipe.[36, 133, 25, 34, 79, 53] Thin strips of PDMS were rolled into scrolls and imaged in profile (Fig. 4.19). Stable scrolls would remain in this configuration, similar to the first frame of Fig. 4.20. Scrolls that were unstable would progress through the rest of the frames in Fig. 4.20 until the sheet had completely unrolled and returned to a flat state. Pictures were taken of the system at regular intervals to determine the stability of the system. Scrolls that were stable were allowed to rest for several minutes, then were unrolled manually a small amount and allowed to relax. This was repeated until the scrolls reached an unstable configuration where they spontaneously unrolled. The length, width, thickness, and unrolled length of the film were recorded. The height of the scroll was also recorded, and was approximated to be double the radius of the outermost layer of the scroll.

An unstable scroll needs to unroll by shedding the outside layers first. Since the outside layers of a scroll have a larger radius of curvature than the inner layers, as unrolling progresses, the ratio of local strain to local adhesion for each segment of the scroll increases for the innermost layers. Since the adhesive forces remain unchanged, the energy balance tips in favor of the bending dominating the interaction the closer one gets to the center of a scroll. This continues until the very center of the scroll is reached, where the radius of curvature of the film is near equal to its thickness. The radius of each layer is smaller than the layer immediately outside of it by $R_n \approx R - nt$, where n is the number of layers counted from the outside $\rightarrow$ in and $n = 0$ is the outside layer. R is the outermost radius of the scroll ($D = 2R$ in Fig. 4.19). In the case of hollow scrolls, the adhesive and elastic contributions from this missing coiled film between the theoretical start point and the actual innermost point of the film are removed from the calculations. When unrolling is initiated by the outermost segment (the bottom right part of the scroll in Fig. 4.19) straightening and causing

124

the scroll to roll and peel from the opposite side of film-film contact, adhesion and bending are no longer in equilibrium. Unrolling will continue until the scroll is completely flat (or an area of higher adhesion/lower stiffness is encountered).

Naturally, the balance that determines the stability of adhesive elastic scrolls is between the bending energy and the adhesion energy. Eqns. 1.16 and 1.27 allow us to determine the energues of each of these two components for a scroll. The bending energy of the outermost layer of a scroll is $U_{bending} = bB\kappa^2L$ where $\kappa = \frac{1}{R} = \frac{2}{D}$, B is the bending modulus (Eqn. 1.15), and $L = 2\pi R$. The adhesive energy is $U_{adhesive} = b\gamma L$ where again $L = 2\pi R$. These two equations lead to a balance of $b\gamma(2\pi R) = bB\frac{4}{D^2}(2\pi R)$, which solves to an observable scroll height that signifies the crossover between stable and unstable scrolls:

$$R = \frac{D}{2} = \sqrt{\frac{B}{\gamma}}. \tag{4.5}$$

This solution is the elastocapillary length (Eqn. 1.37), and accounts for the contributions of the outermost layers of the scroll working against one another to either unroll the scroll or have it remain in place.

Data from these stability experiments was compiled to illustrate how the stability of the scrolls is related to the thickness of the films and the radius of the outermost layer of the scroll in Fig. 4.21. The radius of the outermost layer was found through an approximate method of dividing the height of the scroll in half. The hollow red squares represent configurations where the scroll did not unroll when released. Black circles represent configurations that spontaneously unrolled to a flat state when they were released. The line represents the elastocapillary length (Eqn. 4.5) of the PDMS films in contact with themselves. The elastocapillary length is a simple relation that takes into account the effect of the stiffness of a film and the adhesion or capillary forces acting on the film. This line was produced from known material properties of 10:1 PDMS ($E = 1.69 \times 10^6$ Pa, $\gamma = 0.124\frac{N}{m}$, $\nu = 0.5$) and is a good fit for the data near the instability.[36, 133] No unstable configurations are seen in the area above the fit line. Films that are closer to the elastocapillary length seem to become more stable. No results were observed for stable systems with outer radii that were not near the elastocapillary length, suggesting that films created above the elastocapillary fit would also be stable. There does, however, appear to be a small drift from the elastocapillary fit to where the actual crossover is observed in this data set. The line appears at a slightly lower
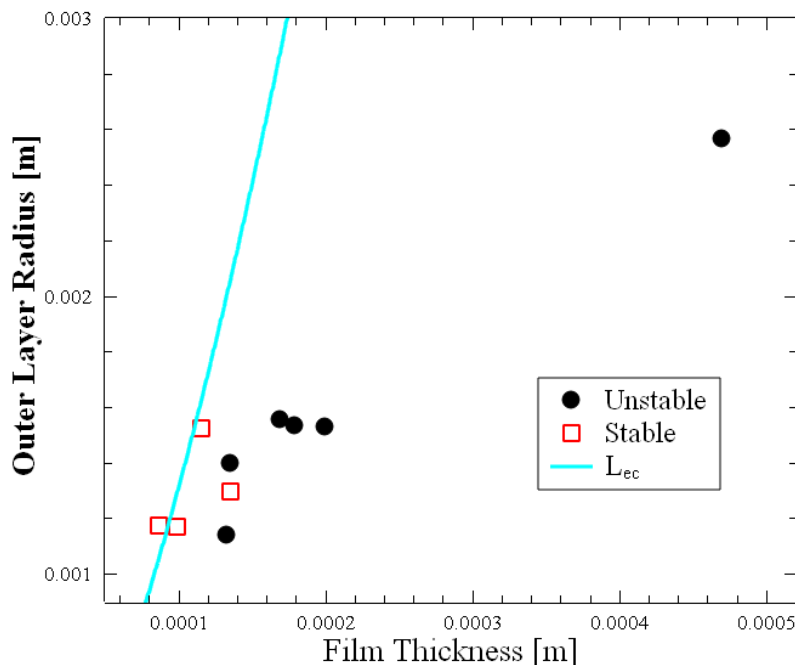
Figure 4.21. Plot illustrating the stability of thin film scrolls in terms of the outer radius of the scroll and the thickness of the films. Stable configurations that did not spontaneously unroll are represented by hollow red squares. Unstable configurations that spontaneously unrolled to a flat state are represented by black circles. The blue fit line represents the elastocapillary length for 10:1 PDMS films.

thickness than where it may be expected from experimental data. This indicates that either the effective modulus of the scroll system is smaller than that of 10:1 PDMS, or the effective adhesion is larger in the scroll system. Both of these factors could also be affected because of the disjointed geometry of this system, with the peel front on an opposite side of the object as the straightening region. This shift could also be from the bending energy of interior layers of the scroll. The model that equates to the elastocapillary length assumes that the internal adhesion and bending are balanced at every interface. This may not be the case, as internal layers may contribute to the straightening forces of the outer layers, or could act to stretch outer layers. A fit parameter could be added to the model predicted by Eqn. 4.5 to improve the accuracy of the model, but at this time more study is required to determine if a prefactor is necessary. The noise observed in the apparent overlap of the stability region could be due to stick-slip mechanisms, films may stop unrolling or be unable to initiate unrolling because of some small surface defence. Arrested unrolling could also be observed in scrolls whose weight was large compared to the stiffness of the film, so care was taken to use relatively short films (several cm in length).

4.5. Encapsulation

The most widely encountered use of adhesive thin films in everyday life comes in the form of food delivery systems. These encapsulation systems are designed either to keep food safe until the packaging is removed, and the food is eaten/prepared or to be eaten while still encapsulating the food-acting as a direct delivery system. Packaging where the food is removed includes tea bag packaging, milk cartons, and butcher paper for wrapping meat. These types of packaging serve to keep the food within the package, create a barrier between the food and the outside world, and protect from minor mechanical damage. The paper wrap for meat is the simplest of these packages, often created by wrapping the food in paper and applying a single piece of tape to keep the package closed. Tea bag packaging consists of a single sheet that is folded over a tea bag and adhered or crimped to itself around the edges as a seal. The initial shape is similar to the racquet shape that has been described throughout this work, with the exception that the outside perimeter of the shape is adhered at a with a much higher adhesive force than the force observed to allow for the creation of the racquet bend. The milk carton is a more rigid paper sheet creased and adhered to itself in a more complicated manner, and represents a shape that is made through the use of adhesion, but one that would be difficult to create using racquet folds.

A more interesting application of films as encapsulants for food is seen in the wide variety of pasta shapes that are meant to contain food and be edible.[4] Common shapes include ravioli (Fig. 4.22a), tortellini (Fig. 4.22b), and sacchetti. Ravioli is often made with a thin sheet of pasta having food placed in the middle of the sheet. A different, similar sized sheet is then place on top. The top and bottom sheets are adhered together with either the application of water or an egg-wash around the outside of the encapsulated food. This binds the two sheets together, until they are cooked. Tortellini and sacchetti are made from a single sheet. A square sheet is layed flat and food is placed in its center. The next step for tortellini is to fold from a corner to the opposite corner and use a liquid to adhere the perimeter of the shape. The corners touching the hypotenuse are then brought together and the shape is cooked. Sacchetti is a similar process, except all of the corners of the sheet are bent upwards and adhered together, covering the food. Other food delivery systems are constructed in similar ways from sheets other than pasta, such as egg rolls, spring rolls, sushi,
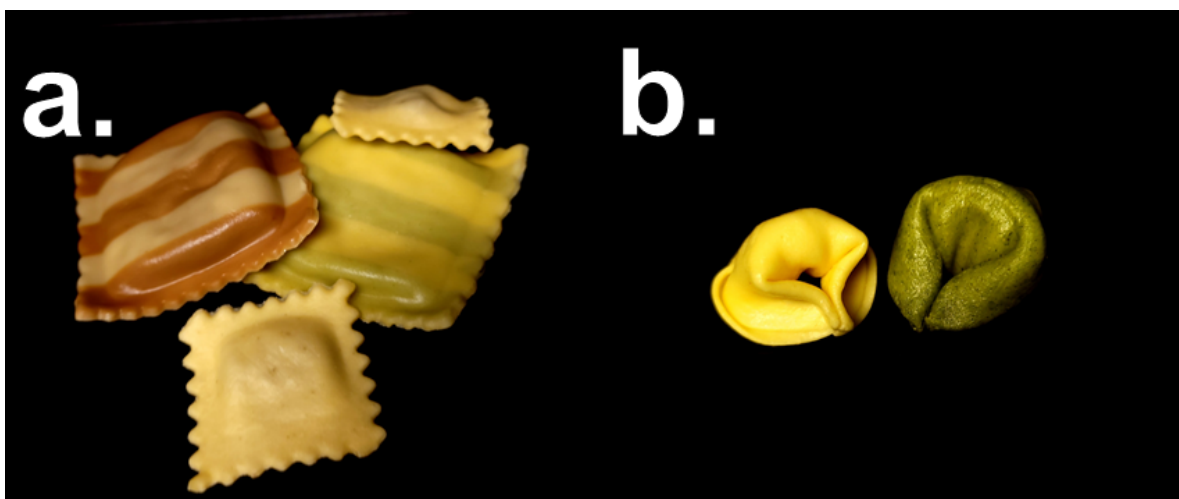
Figure 4.22. Common encapsulation systems that use pasta to encapsulate food. a.) Ravioli made by trapping food between two thin sheets of pasta. The pasta is adhered around the perimeter until cooking permanently binds the two sheets together. b.) Tortellini made form a circular sheet of pasta folded over food cargo, then edges brought together and adhered.

rolled pastries, galette (Fig. 4.4), and rangoon. These foods also rely on an adhesive to be formed between the layers of film that holds the shape together until it can be cooked.

Thin pasta sheets are very low modulus and easily stretchable, but have low adhesion values. They are also easily torn if large strains are applied. Over the years, people have developed methods of working with these sheets that can directly be applied to creating encapsulation systems from other thin materials that share these characteristics, including the application of an adhesive to an otherwise nonadhesive surface. Very thin sheets fit these characteristics very well. The thinnest sheets require that care must be taken to not stretch or twist too much to avoid ripping or permanently deforming these sheets. PDMS can have similar characteristics, especially the higher prepolymer ratios. The main difference being that these PDMS samples will also have high adhesion. This makes these sheets harder to work with, but also makes any shapes created more stable.

Scaling pasta-inspired encapsulation systems down to microscopic sizes could help to create robust systems of drug delivery within a body. These systems must completely cover and protect a therapeutic drug from releasing in the body until they have reached their destination.[22, 5, 40] Then the drugs must be fully released in a reliable way. This can be achieved through the use of a switchable adhesive tailored to be sensitive to the area of release, or to a certain stimuli.[69, 29] Ideal
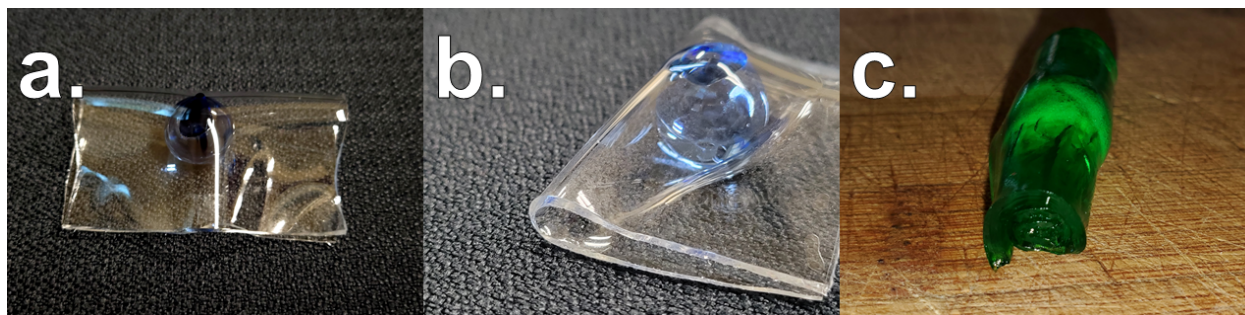
Figure 4.23. a.) A 10:1 PDMS film folded over a glass sphere. The sheet contacts and adheres to itself at most points, but racquet formations leave open areas near the fold. b.) Close-up view of the racquet formed at the edges of these encapsulations. c.) A Jell-O™sheet encapsulating sodium bicarbonate in a scroll formation. Picture taken by Andrew Croll and family while conducting thin film encapsulation experiments (used with permission).[28]

shapes for delivery include thin film scrolls and square sheets folded into a racquet configuration. Both of these shapes will naturally relax to a flat state if the adhesive between the sheets is removed. The scroll will unroll and gradually release its cargo as the adhesive is removed. While the folded racquet will release cargo in one large movement.

Food delivery systems can also be created using edible materials that are similar to the materials used in this research. Jell-O™ is an edible hydrogel that is similar to very sticky PDMS. Jell-O™ can be made into thin sheets, bent, and adhered to itself. This allows Jell-O™ to be used as a test bed for new food delivery options. Dehydrated fruit leather can also be used as a film, but is much stiffer than Jell-O™ and may fracture if bent into a small radius racquet. A food that uses an edible material similar to Jell-O™ and fruit leather is Gushers™-fruit filled snacks.

Preliminary experiments into the efficacy of the thin film delivery systems were conducted using PDMS films to cover a glass sphere (Fig. 4.23a). These tests revealed that no matter how thin or adhesive the film was, there would still be a hollow racquet tube along the edge of a folded sheet (Fig. 4.23b). This means that any cargo in this fold would slowly leak from the sides. Solutions can be devised to try to completely seal a cargo with an elastic sheet (the sacchetti shape is a candidate), but the requirement of these pasta shapes is that there is always an area that needs to plastically deform to completely seal a cargo in persists. A plastically deformable sheet is required to completely seal in cargo using a racquet bend. However, the use of a plug to seal the ends of a racquet is also possible. This plug would then either need to dissolve or detach from the system when cargo release was desired.

The test conducted by Andrew Croll and family, mentioned in Section 4.4.3, filled a Jell-O™ scroll with cargo and released it into a liquid (Fig. 4.23c). The Jell-O™ scroll effectively encapsulated the cargo until it began to react with the liquid. As the scroll unrolled, more and more of the cargo was released. Refinement of this system could tailor the speed of unrolling to release the cargo at a specific rate. Alternatively, these same ideas may be used as a literal drug delivery system for picky pets. A nasty tasting pill is wrapped in a thin sheet of tasty food, such as cheese, bacon, or ham. An adhesive, like honey, is applied to the system to keep it closed (and cover medicine smell) until it is immersed in liquid. The dog eats the roll and it releases the medicine in the stomach. As long as the packaging is not too large, the pet will not notice the treatment.

Adhesive thin film systems offer a great opportunity as delivery systems. Packaging and encapsulation systems can be created on the macroscopic scale for food delivery and down to the microscopic scales needed for drug delivery into a body. Adhesive systems can replace the containers for drug delivery that use capillary origami to hold thin films in place[22, 5, 40], eliminating the problems associated with releasing a capillary drop while immersed in a capillary environment. Adhesives can hold these containers in place whether or not the cargo is present, and can be designed to release under specific conditions. Adhesive systems can also be relatively easily created at any scale from flat rectangular sheets and adhesives. Eliminating the need to micromachine shapes and holes into a timed release system removes much of the difficulty associated with manufacturing large numbers of encapsulating structures, thereby streamlining production.

4.6. Conclusion and Future Work

Kuttsukugami has the potential to change the field of thin film assembly and implementation in much the same way that the original introduction of origami techniques and later kirigami techniques did. In much the same way many of the simple designs and uses for adhesive sheets have existed in one form or another for quite a while. However, through the identification of what makes the manipulation and assembly of complex structures from thin adhesive sheets possible, we have begun the process of creating more and more complex designs and a wide variety of uses for these structures. This process is also inherently scalable to microscopic sizes, so any advancements made in the discovery of shapes or systems can be readily implemented to applications that require the smallest components possible.

The racquet fold has been presented as an alternative to the destructive creases used in paper origami for applications that cannot survive such sharp bends, such as bendable electronics. The survivability of wires bent into a racquet loop and an origami crease were compared and showed that the bent wire survived at least an order of magnitude more bend and straighten cycles than a creased wire. The racquet bend was also demonstrated to be the necessary bend to create origami structures using elastic sheets and films. The need to hold a plastic crease is not necessary if racquet bends can be produced with adhesion.

A wide variety of shapes and systems were created from adhering sheets to themselves. Some of these shapes were familiar, such as the cylinder, the Möbius strip, and the cone. These were assembled in a simple manner that required just a few steps. Other structures were created by incorporating origami creases or adhesion of separate sheets such as the post-it chain, the bridges, the clover, heart, and star. Scrolls and Möbius Strips were studied experimentally and mathematically to determine stability conditions for these shapes when made of thin films. The virtual d-cone was explored. This is a shape that has existed, but has not really been noticed for study or use. This shape exists due to the adhesion of a bendable sheet to a rigid substrate. Encapsulation systems were studied that can hold a cargo safely until the cargo reaches its desired destination. Pasta shapes were used as inspiration for the creation of a racquet-folded encapsulation system. Scrolled encapsulation systems were also created for the gradual delivery of cargo as the scroll unrolls itself. All of these shapes were, again, simple to create requiring at most a few steps and can have many useful applications on both the macroscopic and microscopic scale.

Moving forward, each topic mentioned in this chapter will need further study. The surface has only been scratched with the research presented here. Structures and designs should be made with different sheets and films that are plastic, glassy, gel, and elastomeric. The use of applied and switchable adhesives should be studied with shapes and bends that can release and then be brought back to their original state by some repeatable stimulus. The research into Möbius strips and scrolls should be expanded for more mixtures of PDMS and other materials as well. Rigorous mathematical models can also be developed to explain the results presented here. The Möbius strip is of particular interest, since the stability results could be used to point to the most valid of a handful of theories regarding curvature of and the elastic energy stored in a Möbius strip.

Figure 4.24. Cornucopia of shapes made from thin sheets and adhesion.

Research will also be conducted on miniaturizing the structures created through kuttsukugami. The effects of high surface forces on super thin materials could emerge as either an advantage or curse when scaling structures to smaller and smaller scales. Physically moving the films and precisely placing them into contact with one another will also require further study. At a certain scale, everyday tools no longer work for interacting with thin films. Capillary origami and substrate adhesion can help at smaller scales, but for truly tiny objects the effectiveness of these methods will need to be tested. A great deal of imagination will also need to be employed to create completely new structures and applications that can solve problems in different ways. Like when capillary origami was seen as a way to construct and deliver drugs to within a body, opening the door to kuttsukugami will yield surprising results far outside the realm of what is currently thought possible.

Figure 4.25. Origami zoo of many of the shapes created during my work. Folds, bends, crumples, adhesive joints, racquets, and loops all came together to create new and interesting shapes.

REFERENCES

[1] J. Aljedani, M. J. Chen, and B. J. Cox. Multi-layer graphene folds supported on a substrate: a variational model. *Mater. Res. Express*, 8:015002, 2021.

[2] B. Andreotti, O. Bäumchen, F. Boulogne, K. E. Daniels, E. R. Dufresne, H. Perrin, T. Salez, J. H. Snoeijer, and R. W. Style. Solid capillarity: when and how does surface tension deform soft solids? *Soft Matter*, 12(12):2993–2996, 2016.

[3] A. Antkowiak, B. Audoly, C. Josserand, S. Neukirch, and M. Rivetti. Instant fabrication and selection of folded structures using drop impact. *Proceedings of the National Academy of Sciences*, 108(26):10400–10404, 2011.

[4] C Antognelli. The manufacture and applications of pasta as a food and as a food ingredient: a review. *International Journal of Food Science & Technology*, 15(2):125–145, 1980.

[5] A. Azam, K. E. Laflin, M. Jamal, R. Fernandes, and D. H. Gracias. Self-folding micropatterned polymeric containers. *Biomedical microdevices*, 13(1):51–58, 2011.

[6] J. Bae, N. P. Bende, A. A. Evans, J. H. Na, C. D. Santangelo, and R. C Hayward. Programmable and reversible assembly of soft capillary multipoles. *Materials Horizons*, 4(2):228–235, 2017.

[7] D. Baran, D. Corzo, and G. T. Blazquez. Flexible electronics: Status, challenges and opportunities. *Frontiers in Electronics*, 1:2, 2020.

[8] S. Bartels and P. Hornung. Bending paper and the möbius strip. In *The Mechanics of Ribbons and Möbius Bands*, pages 113–136. Springer, 2016.

[9] J. Bico, B. Roman, L. Moulin, and A Boudaoud. Elastocapillary coalescence in wet hair. *Nature*, 432(7018):690–690, 2004.

[10] B. Bircan, M. Z. Miskin, R. J. Lang, M. C. Cao, K. J. Dorsey, M. G. Salim, W. Wang, D. A. Muller, P. L. McEuen, and I. Cohen. Bidirectional self-folding with atomic layer deposition nanofilms for microscale origami. *Nano Letters*, 20(7):4850–4856, 2020. PMID: 32525319.

[11] S. F. Braga, V. R. Coluci, S. B. Legoas, R. Giro, D. S. Galvão, and R. H. Baughman. Structure and dynamics of carbon nanoscrolls. *Nano letters*, 4(5):881–884, 2004.

[12] N. D. Brubaker. Two-dimensional capillary origami with inextensibility and free triple-contact points. *SIAM Journal on Applied Mathematics*, 79(2):572–593, 2019.

[13] P. A. Butyrin, G. G. Gusev, D. V. Mikheev, and F. N. Shakirzianov. Coil capacitor for an inductive–capacitive converter. *Bulletin of the Russian Academy of Sciences: Physics*, 82(8):918–921, 2018.

[14] F. T. Carson and V. Worthington. Stiffness of paper. *Journal of Research of the National Bureau of Standards*, 49(6), 1952.

[15] E. Cerda, S. Chaieb, F. Melo, and L. Mahadevan. Conical dislocations in crumpling. *Nature*, 401(6748):46–49, 1999.

[16] E. Cerda and L. Mahadevan. Conical surfaces and crescent singularities in crumpled sheets. *Physical Review Letters*, 80(11):2358, 1998.

[17] E. Cerda and L. Mahadevan. Geometry and physics of wrinkling. *Phys. Rev. Lett.*, 90:074302, Feb 2003.

[18] S. Chaïeb, F. Melo, and J. C Géminard. Experimental study of developable cones. *Physical review letters*, 80(11):2354, 1998.

[19] S. Chen, J. Chen, X. Zhang, Z. Y. Li, and J. Li. Kirigami/origami: unfolding the new regime of advanced 3d microfabrication/nanofabrication with "folding". *Light: Science & Applications*, 9(1):1–19, 2020.

[20] T. Chen, O. R. Bilal, R. Lang, C. Daraio, and K. Shea. Autonomous deployment of a solar panel using elastic origami and distributed shape-memory-polymer actuators. *Physical Review Applied*, 11(6):064069, 2019.

[21] X. Chen, L. Zhang, Y. Zhao, X. Wang, and C Ke. Graphene folding on flat substrates. *Journal of Applied Physics*, 116(16):164301, 2014.

[22] J. H. Cho and D. H. Gracias. Self-assembly of lithographically patterned nanoparticles. *Nano letters*, 9(12):4049–4052, 2009.

[23] J. H. Cho, M. D. Keung, N. Verellen, L. Lagae, V. Moshchalkov, P. Van Dorpe, and D. H. Gracias. Nanoscale origami for 3d optics. *Small*, 7(14):1943–1948, 2011.

[24] S. J. Cho, K. H. Choi, J. T. Yoo, J. H. Kim, Y. H. Lee, S. J. Chun, S. B. Park, D. H. Choi, Q. Wu, S. Y. Lee, et al. Hetero-nanonet rechargeable paper batteries: toward ultrahigh energy density and origami foldability. *Advanced Functional Materials*, 25(38):6029–6040, 2015.

[25] Dow Chemical Company. Technical data sheet sylgard 184 silicone elastomer. Technical Report 11-3184-01 C, 2017.

[26] B. J. Cox, D. Baowan, W. Bacsa, and J. B Hill. Relating elasticity and graphene folding conformation. *RSC Adv.*, 5:57515, 2015.

[27] S. Cranford, D. Sen, and M. J. Buehler. Meso-origami: Folding multilayer graphene sheets. *Applied Physics Letters*, 95(12):123121, 2009.

[28] A. B. Croll and Family. Picture was provided from pictures of experiments conducted with jello sheets, 2021.

[29] A. B. Croll, N. Hosseini, and M. D. Bartlett. Switchable adhesives for multifunctional interfaces. *Advanced Materials Technologies*, 4(8):1900193, 2019.

[30] B. Davidovitch and D. Vella. Partial wetting of thin solid sheets under tension. *Soft Matter*, 14:4913–4934, 2018.

[31] P. G. De Gennes, F. Brochard-Wyart, and D. Quéré. *Capillarity and wetting phenomena: drops, bubbles, pearls, waves.* Springer Science & Business Media, 2013.

[32] S Deboeuf, E Katzav, A Boudaoud, D. Bonn, and M. Adda-Bedia. Comparitive study of crumpling and folding of thin sheets. *Phys. Rev. Lett.*, 110:104301, 2013.

[33] D. A. Dillard, B. Mukherjee, P. Karnal, R. C. Batra, and J Frechette. A review of winkler's foundation and its profound influence on adhesion and soft matter applications. *Soft Matter*, 14:3669–3683, 2018.

[34] K. Efimenko, W. E. Wallace, and J. Genzer. Surface modification of sylgard-184 poly (dimethyl siloxane) networks by ultraviolet and ultraviolet/ozone treatment. *Journal of colloid and interface science*, 254(2):306–315, 2002.

[35] T. Elder, D. Rozairo, and A. B Croll. Origami inspired mechanics: measuring modulus and force recovery with bent polymer films. *Macromolecules*, 52(2):690–699, 2019.

[36] T. Elder, T. Twohig, H. Singh, and A. B Croll. Adhesion of a tape loop. *Soft Matter*, 2020.

[37] R. Etherington. Biostamp temporary tattoo electronic circuits by mc10. *Last Update: March 28th*, 2013.

[38] L. Euler. *The Rational Mechanics of Flexible Or Elastic Bodies 1638-1788: Introduction to Vol. X and XI.* Springer Science & Business Media, 1980.

[39] C. W. Extrand and Y. Kumagai. Contact angles and hysteresis on soft surfaces. *Journal of colloid and interface science*, 184(1):191–200, 1996.

[40] R. Fernandes and D. H. Gracias. Self-folding polymeric containers for encapsulation and delivery of drugs. *Advanced drug delivery reviews*, 64(14):1579–1589, 2012.

[41] H. Fuhrmann, J. Ostrowski, and J. Mood. Rolled film capacitor, May 25 2010. US Patent 7,724,495.

[42] N. R. Geraldi, F. F. Ouali, R. H. Morris, G. McHale, and M. I. Newton. Capillary origami and superhydrophobic membrane surfaces. *Applied Physics Letters*, 102(21):214104, 2013.

[43] M. Gerbault. At what stress level is the central indian ocean lithosphere buckling? *Earth and Planetary Science Letters*, 178(1-2):165–181, 2000.

[44] N. J. Glassmaker and C. Y. Hui. Elastica solution for a nanotube formed by self-adhesion of a folded thin film. *Journal of applied physics*, 96(6):3429–3434, 2004.

[45] D. H. Gracias, V. Kavthekar, J. C. Love, K. E. Paul, and G. M. Whitesides. Fabrication of micrometer-scale, patterned polyhedra by self-assembly. *Advanced Materials*, 14(3):235–238, 2002.

[46] J. Huang, M. Juszkiewicz, W. H. De Jeu, E. Cerda, T. Emrick, N. Menon, and T. P. Russell. Capillary wrinkling of floating thin polymer films. *Science*, 317(5838):650–653, 2007.

[47] C. Y. Hui and A. Jagota. Deformation near a liquid contact line on an elastic substrate. *Proc. R. Soc. A*, 470:20140085, 2014.

[48] W. Jayawardana and CCWJ Photography. Foods that wathsala made that include adhesion. `https://www.instagram.com/ccwjkitchen/`, 2021.

[49] W. Jayawardana and CCWJ Photography. Foods that wathsala made that include adhesion. `https://www.facebook.com/pg/ccwjphotography/photos/?ref=page_internal&tab=album&album_id=182793803547394`, 2021.

[50] S. J. Jeon and R. C Hayward. Simultaneous control of gaussian curvature and buckling direction by swelling of asymmetric trilayer hydrogel hybrids. *Soft Matter*, 16(3):688–694, 2020.

[51] E. R. Jerison, Y. Xu, L. A. Wilen, and E. R. Dufresne. Deformation of an elastic substrate by a three-phase contact line. *Phys. Rev. Lett.*, 106(18):186103, 2011.

[52] M. Johnson, Y. Chen, S. Hovet, S. Xu, B. Wood, H. Ren, J. Tokuda, and Z. T. H. Tse. Fabricating biomedical origami: A state-of-the-art review. *International journal of computer assisted radiology and surgery*, 12(11):2023–2032, 2017.

[53] I. D. Johnston, D. K. McCluskey, C. K. L. Tan, and M. C Tracey. Mechanical characterization of bulk sylgard 184 for microfluidics and microengineering. *Journal of Micromechanics and Microengineering*, 24(3):035017, 2014.

[54] J. L. Kapp. Woven endless belt of a spliceless and mobius strip construction, November 16 1976. US Patent 3,991,631.

[55] K. Kendall. Thin-film peeling-the elastic term. *Journal of Physics D: Applied Physics*, 8(13):1449, 1975.

[56] E. Kishi, O. Shinohara, and H. Ishikawa. Toilet paper roll, April 15 1975. US Patent 3,877,576.

[57] D. Kumar, J. D. Paulsen, Russell T. P., and N. Mennon. Optimal wrapping of liquid droplets with ultrathin sheets. *Science*, 359:775–778, 2018.

[58] K. Kuribayashi, K. Tsuchiya, Z. You, D. Tomus, M. Umemoto, T. Ito, and M. Sasaki. Self-deployable origami stent grafts as a biomedical application of ni-rich tini shape memory alloy foil. *Materials Science and Engineering: A*, 419(1-2):131–137, 2006.

[59] K. S. Kwok, Q. Huang, M. Mastrangeli, and D. H. Gracias. Self-folding using capillary forces. *Advanced Materials Interfaces*, 7(5):1901677, 2020.

[60] R. J. Lang. Origami and geometric constructions. *Self Published (1996 2003)*, 1996.

[61] R. J. Lang. The science of origami. *Physics world*, 20(2):30, 2007.

[62] C. Lee and S. D. King. Dynamic buckling of subducting slabs reconciles geological and geophysical observations. *Earth and Planetary Science Letters*, 312(3-4):360–370, 2011.

[63] A. Legrain, J. W. Berenschot, N. R. Tas, and L. Abelmann. Capillary origami of micro-machined micro-objects: Bi-layer conductive hinges. *Microelectronic engineering*, 140:60–66, 2015.

[64] A. Legrain, T. G. Janson, J. W. Berenschot, L. Abelmann, and N. R. Tas. Controllable elastocapillary folding of three-dimensional micro-objects by through-wafer filling. *Journal of applied physics*, 115(21):214905, 2014.

[65] W. L. Lehner and M. L. Lincoln. Rolled capacitor structure, June 18 1963. US Patent 3,094,651.

[66] T. G. Leong, P. A. Lester, T. L. Koh, E. K. Call, and D. H. Gracias. Surface tension-driven self-folding polyhedra. *Langmuir*, 23(17):8747–8751, 2007.

[67] S. Li, D. M. Vogt, D. Rus, and R. J. Wood. Fluid-driven origami-inspired artificial muscles. *Proceedings of the National academy of Sciences*, 114(50):13132–13137, 2017.

[68] Y. Li, R. Chen, and R. J. Baker. A fast fabricating electro-wetting platform to implement large droplet manipulation. In *2014 IEEE 57th International Midwest Symposium on Circuits and Systems (MWSCAS)*, pages 326–329. IEEE, 2014.

[69] J. Liu, Y. Gong, and G. Cao. Chemical mediated elasto-capillarity of elastic sheets. *Soft matter*, 13(44):8048–8054, 2017.

[70] J. Liu and J. H. Lee. Self-folding of a slender microbeam and thin film: An elastica model. *Journal of Mechanics of Materials and Structures*, 8(2):169–183, 2013.

[71] Z. Liu, J. Gao, G. Zhang, Y. Cheng, and Y. W. Zhang. From two-dimensional nano-sheets to roll-up structures: expanding the family of nanoscroll. *Nanotechnology*, 28(38):385704, 2017.

[72] D. W. Lloyd, W. J. Shanahan, and M. Konopasek. The folding of heavy fabric sheets. *International Journal of Mechanical Sciences*, 20(8):521–527, 1978.

[73] A. E. H. Love. Xvi. the small free vibrations and deformation of a thin elastic shell. *Philosophical Transactions of the Royal Society of London.(A.)*, (179):491–546, 1888.

[74] Q. Lu, M. Arroyo, and R. Huang. Elastic bending modulus of monolayer graphene. *Journal of Physics D: Applied Physics*, 42(10):102002, 2009.

[75] N. G. Ly. A model for fabric buckling in shear. *Textile Research Journal*, 55(12):744–749, 1985.

[76] G. L. Mack, J. K. Davis, and F. E. Bartell. The boundary tension of gallium. *The Journal of Physical Chemistry*, 45(5):846–851, 1941.

[77] L. Mahadevan and J. B Keller. The shape of a möbius band. *Proceedings of the Royal Society of London. Series A: Mathematical and Physical Sciences*, 440(1908):149–162, 1993.

[78] A. Malczyk and H. D. Adomeit. The airbag folding pattern as a means for injury reduction of out-of-position occupants. *SAE transactions*, pages 2890–2906, 1995.

[79] A. Mata, A. J. Fleischman, and S. Roy. Characterization of polydimethylsiloxane (pdms) properties for biomedical micro/nanosystems. *Biomedical microdevices*, 7(4):281–293, 2005.

[80] D. Maugis and M. Barquins. Fracture mechanics and adherence of viscoelastic solids. In *Adhesion and adsorption of polymers*, pages 203–277. Springer, 1980.

[81] X. Meng, M. Li, Z. Kang, X. Zhang, and J. Xiao. Mechanics of self-folding of single-layer graphene. *Journal of Physics D: Applied Physics*, 46(5):055308, 2013.

[82] X. H. Meng, M. Li, Z. Kang, and J. L. Xiao. Folding of multi-layer graphene sheets induced by van der waals interaction. *Acta Mechanica Sinica*, 30(3):410–417, 2014.

[83] J. C. Meyer, A. K. Geim, M. I. Katsnelson, K. S. Novoselov, T. J. Booth, and S. Roth. The structure of suspended graphene sheets. *Nature*, 446(7131):60–63, 2007.

[84] M. Z. Miskin, K. J. Dorsey, B. Bircan, Y. Han, D. A. Muller, P. L. McEuen, and I. Cohen. Graphene-based bimorphs for micron-sized, autonomous origami machines. *Proceedings of the National Academy of Sciences*, 115(3):466–470, 2018.

[85] P. H. Mott and C. M. Roland. Limits to poisson's ratio in isotropic materials. *Physical review B*, 80(13):132104, 2009.

[86] J. H. Na, N. P. Bende, J. Bae, C. D. Santangelo, and R. C Hayward. Grayscale gel lithography for programmed buckling of non-euclidean hydrogel plates. *Soft Matter*, 12(22):4985–4990, 2016.

[87] N. Nadermann, C. Y. Hui, and A. Jagota. Solid surface tension measured by a liquid drop under a solid film. *Proc. Nat. Acad. Sci.*, 110:10541–10545, 2013.

[88] D. Palomba, G. E. Vazquez, and M. F. Díaz. Prediction of elongation at break for linear polymers. *Chemometrics and Intelligent Laboratory Systems*, 139:121–131, 2014.

[89] J. D. Paulsen, V. Démery, C. D. Santangelo, Russell T. P., B. Davidovitch, and N. Mennon. Optimal wrapping of liquid droplets with ultrathin sheets. *Nat. Mat.*, 14:1206–1209, 2015.

[90] J. D. Paulsen, V. Démery, K. B. Toga, Z. Qiu, T. P. Russell, B. Davidovitch, and N. Menon. Geometry-driven folding of a floating annular sheet. *Phys. Rev. Lett.*, 118(4):048004, 2017.

[91] J. D. Paulsen, E. Hohlfeld, H. King, J. Huang, Z. Qiu, T. P. Russell, N. Menon, D. Vella, and B Davidovitch. Curvature-induced stiffness and the spatial variation of wavelength in wrinkled sheets. *Proc. Nat. Acad. Sci.*, 113(5):1144–1149, 2016.

[92] E. A. Peraza-Hernandez, D. J. Hartl, R. J. Malak Jr, and D. C Lagoudas. Origami-inspired active structures: a synthesis and review. *Smart Materials and Structures*, 23(9):094001, 2014.

[93] C. Py, P. Reverdy, L. Doppler, J. Bico, B. Roman, and C. N. Baroud. Capillary origami: spontaneous wrapping of a droplet with an elastic sheet. *Physical review letters*, 98(15):156103, 2007.

[94] C. Py, P. Reverdy, L. Doppler, J. Bico, B. Roman, and C. N. Baroud. Capillarity induced folding of elastic sheets. *Euro. Phys. J. Spec. Top.*, 166(1):67–71, 2009.

[95] C. L. Randall, E. Gultepe, and D. H. Gracias. Self-folding devices and materials for biomedical applications. *Trends in biotechnology*, 30(3):138–146, 2012.

[96] M. F. Reynolds, K. L. McGill, M. A. Wang, H. Gao, F. Mujid, K. Kang, J. Park, M. Z. Miskin, I. Cohen, and P. L. McEuen. Capillary origami with atomically thin membranes. *Nano Letters*, 19(9):6221–6226, 2019. PMID: 31430164.

[97] M. F. Reynolds, K. L. McGill, M. A. Wang, H. Gao, F. Mujid, K. Kang, J. Park, M. Z. Miskin, I. Cohen, and P. L. McEuen. Capillary origami with atomically thin membranes. *Nano Letters*, 19(9):6221–6226, 2019.

[98] J. Rogers, Y. Huang, O. G. Schmidt, and D. H. Gracias. Origami mems and nems. *MRS Bulletin*, 41:123–129, 2016.

[99] B Romanowicz. The thickness of tectonic plates. *Science*, 324(5926):474–476, 2009.

[100] V. Romero, T. A. Witten, and E. Cerda. Multiple coiling of an elastic sheet in a tube. *Proceedings of the Royal Society A: Mathematical, Physical and Engineering Sciences*, 464(2099):2847–2866, 2008.

[101] J. P. Schaffer. *The science and design of engineering materials*. Irwin Professional Publishing, 1999.

[102] O. G. Schmidt and K. Eberl. Thin solid films roll up into nanotubes. *Nature*, 410(6825):168–168, 2001.

[103] R. D. Schroll, M. Adda-Bedia, E. Cerda, J. Huang, N. Menon, T. P. Russell, K. B. Toga, D. Vella, and B Davidovitch. capillary deformations of bendable films. *Phys. Rev. Lett.*, 111:014301, 2013.

[104] K. Schulgasser. The in-plane poisson ratio of paper. *Fibre Science and Technology*, 19(4):297–309, 1983.

[105] R. D. Schulman and K. Dalnoki-Veress. Liquid droplets on a highly deformable membrane. *Phys. Rev. Lett.*, 115:206101, 2015.

[106] R. D. Schulman and K. Dalnoki-Veress. Liquid droplets on a highly deformable membrane. *Physical review letters*, 115(20):206101, 2015.

[107] R. D. Schulman, R. Ledesma-Alonso, T. Salez, Raphaël, and K. Dalnoki-Veress. Liquid droplets act as "compass needles" for the stresses in a deformable membrane. *Phys. Rev. Lett.*, 118:198002, 2015.

[108] R. D. Schulman, M. Trejo, T. Salez, Raphaël, and K. Dalnoki-Veress. Surface energy of strained amorphous solids. *Nat. Comm.*, 9:982, 2018.

[109] R. Sharma, C. C. B. Bufon, D. Grimm, R. Sommer, A. Wollatz, J. Schadewald, D. J. Thurmer, P. F. Siles, M. Bauer, and O. G. Schmidt. Large-area rolled-up nanomembrane capacitor arrays for electrostatic energy storage. *Advanced Energy Materials*, 4(9):1301631, 2014.

[110] X. Shi, N. M. Pugno, and H. Gao. Mechanics of carbon nanoscrolls: a review. *Acta Mechanica Solida Sinica*, 23(6):484–497, 2010.

[111] C. R. Shreenithee and P. Prabhasankar. Effect of different shapes on the quality, microstructure, sensory and nutritional characteristics of yellow pea flour incorporated pasta. *Journal of Food Measurement and Characterization*, 7(4):166–176, 2013.

[112] K. R. Shull. Contact mechanics and the adhesion of soft solids. *Materials Science and Engineering: R: Reports*, 36(1):1–45, 2002.

[113] F. Song, L. Ma, J. Fan, Q. Chen, G. Lei, and B. Q. Li. Electro-wetting of a nanoscale water droplet on a polar solid surface in electric fields. *Physical Chemistry Chemical Physics*, 20(17):11987–11993, 2018.

[114] Z. Song, T. Ma, R. Tang, Q. Cheng, X. Wang, D. Krishnaraju, R. Panat, C. K. Chan, H. Yu, and H. Jiang. Origami lithium-ion batteries. *Nature communications*, 5(1):1–6, 2014.

[115] F. H. Spedding and K. Gschneidner. Crc handbook of chemistry and physics. 1972.

[116] E. L. Starostin and G. H. M. Van Der Heijden. The shape of a möbius strip. *Nature materials*, 6(8):563–567, 2007.

[117] R. W. Style, R. Boltyanskiy, Y. Che, J. S. Wettlaufer, L. A. Wilen, and E. R. Dufresne. Universal deformation of soft substrates near a contact line and the direct measurement of solid surface stresses. *Phys. Rev. Lett.*, 110(6):066103, 2013.

[118] R. W. Style, R. Boltyanskiy, Y. Che, J. S. Wettlaufer, L. A. Wilen, and E. R. Dufresne. Universal deformation of soft substrates near a contact line and the direct measurement of solid surface stresses. *Physical review letters*, 110(6):066103, 2013.

[119] R. W. Style and E. R. Dufresne. Static wetting on deformable substrates, from liquids to soft solids. *Soft Matter*, 8(27):7177–7184, 2012.

[120] R. Tang, H. Huang, H. Tu, H. Liang, M. Liang, Z. Song, Y. Xu, H. Jiang, and H. Yu. Origami-enabled deformable silicon solar cells. *Applied Physics Letters*, 104(8):083501, 2014.

[121] Y. Tao, Y. C. Lee, H. Liu, X. Zhang, J. Cui, C. Mondoa, M. Babaei, J. Santillan, G. Wang, D. Luo, et al. Morphing pasta and beyond. *Science Advances*, 7(19):eabf4098, 2021.

[122] A. Terfort, N. Bowden, and G. M. Whitesides. Three-dimensional self-assembly of millimetre-scale components. *Nature*, 386:162–164, 1997.

[123] G. W. Timco and R. M. W. Frederking. Compressive strength of sea ice sheets. *Cold Regions Science and Technology*, 17(3):227–240, 1990.

[124] G. W. Timco and R. M. W. Frederking. Seasonal compressive strength of beaufort sea ice sheets. In *Ice-Structure Interaction*, pages 267–282. Springer, 1991.

[125] G. W. Timco and W. F. Weeks. A. review of the engineering properties of sea ice. *Cold regions science and technology*, 60(2):107–129, 2010.

[126] S. Timoshenko. P, and goodier, jn theory of elasticity, 1970.

[127] S. Timoshenko. *History of strength of materials: with a brief account of the history of theory of elasticity and theory of structures.* Courier Corporation, 1983.

[128] S. Timoshenko and S. Woinowsky-Krieger. *Theory of Plates and Shells.* McGraw Hill, 1959.

[129] K. B. Toga, J. Huang, K. Cunningham, T. P. Russell, and N. Menon. A drop on a floating sheet: boundary conditions, topography and formation of wrinkles. *Soft Matter*, 9(34):8289–8296, 2013.

[130] J. Tryding. In-plane fracture of paper. *Division of Structural Mechanics, Lund Institute of Technology*, 1996.

[131] N. Turner, B. Goodwine, and M. Sen. A review of origami applications in mechanical engineering. *Proceedings of the Institution of Mechanical Engineers, Part C: Journal of Mechanical Engineering Science*, 230(14):2345–2362, 2016.

[132] R. Tutika, A. B. M. Tahidul Haque, and M. D. Bartlett. Self-healing liquid metal composite for reconfigurable and recyclable soft electronics. *Communications Materials*, 2(1):1–8, 2021.

[133] T. Twohig and A. B Croll. Adhesion directed capillary origami. *Soft Matter*, 2021.

[134] T. Twohig, S. May, and A. B Croll. Microscopic details of a fluid/thin film triple line. *Soft matter*, 14(36):7492–7499, 2018.

[135] W. Wu and Z. You. A solution for folding rigid tall shopping bags. *Proceedings of the Royal Society A: Mathematical, Physical and Engineering Sciences*, 467(2133):2561–2574, 2011.

[136] H. Yasuda, Y. Miyazawa, E. G. Charalampidis, C. Chong, P. G. Kevrekidis, and J. Yang. Origami-based impact mitigation via rarefaction solitary wave creation. *Science advances*, 5(5):eaau2835, 2019.

[137] T. Young. Iii. an essay on the cohesion of fluids. *Philosophical transactions of the royal society of London*, (95):65–87, 1805.

[138] W. Zhou, Y. Huang, B. Liu, K. C. Hwang, J. M. Zuo, M. J. Buehler, and H. Gao. Self-folding of single-and multiwall carbon nanotubes. *Applied Physics Letters*, 90(7):073107, 2007.